

WISSENSCHAFTLICH-TECHNISCHE BERICHTE

FZR-275

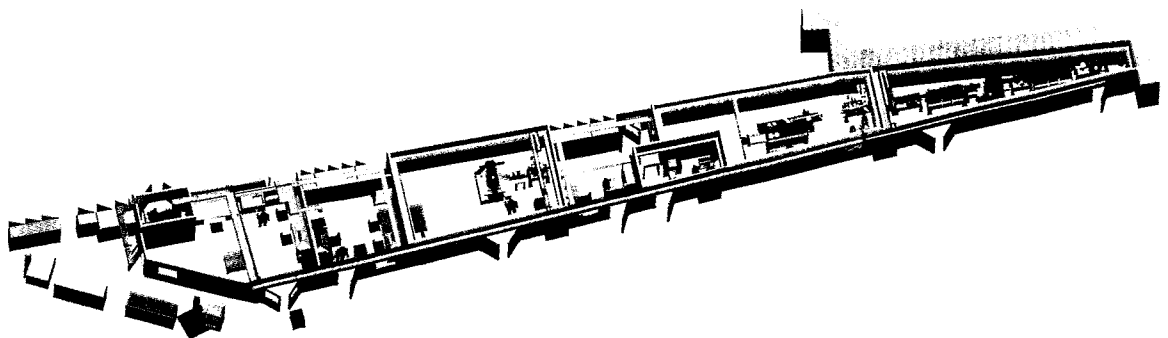
September 1999

ISSN 1437-322X



Project-Group ESRF-Beamline (ROBL-CRG)

Archiv-Ex.:



Report

January 1998 - June 1999

Cover picture:

Bird's eye view of the ROssendorf BeamLine (ROBL) at the European Synchrotron Radiation Facility (ESRF) in Grenoble, France. The facility consists of the X-ray optics hutch (right), the hutch for radiochemistry experiments (middle) and the hutch for materials research (left). Additional control cabins are located behind each experimental hutch.

Forschungszentrum Rossendorf e. V.

Postfach 51 01 19

D-01314 Dresden

Bundesrepublik Deutschland

Telefon +49 (3 51) 2 60 31 22

Telefax +49 (3 51) 2 60 34 38

E-Mail w.matz@fz-rossendorf.de

Internet <http://www.fz-rossendorf.de/FWE/>

FORSCHUNGSZENTRUM ROSSENDORF

WISSENSCHAFTLICH-TECHNISCHE BERICHTE



FZR-275

September 1999

**Project - Group ESRF-Beamline
(ROBL-CRG)**

Report

January 1998 - June 1999

Editor: W. Matz

Preface

During the last years the Forschungszentrum Rossendorf has built its own synchrotron radiation beamline called ROBL (= ROssendorf BeamLine) at the European Synchrotron Radiation Facility (ESRF) in Grenoble, France. ROBL is one of ten CRG-beamlines (CRG = collaborating research group). This implies that ROBL is fully financed by the FZR during the investment phase as well as in the current operation phase. The inauguration of ROBL took place on June 8, 1998. Since the fall of 1998 ROBL is running with scheduled experiments.

ROBL has two experimental end-stations operating alternatively, using the same X-ray optics. One station is the Radiochemistry Hutch (RCH) and the other the Materials Research Hutch (MRH). A more detailed description of the equipment is given in the first contribution of this report.

ROBL was built and is operated by the Project Group ESRF-Beamline of the FZR. This group consists of scientists, engineers and technicians of the Institute of Ion Beam Physics and Materials Research, the Institute of Radiochemistry and the Central Department Experimental Facilities and Information Technology. The Department of Safety and Radiation Protection of the VKTA (Verein für Kernverfahrenstechnik und Analytik) gave a strong support for the development of the safety instrumentation of the RCH.

The beamtime is used by 2/3 from the FZR and collaborating institutes. The other 1/3 available beamtime is scheduled by the ESRF for peer-reviewed experiments.

This is the first activity report of ROBL. It is intended to publish every two years such a report. The report is organised in three main parts. The first part contains extended contributions on results already obtained at ROBL. The second part gives an overview about the scheduled experiments, a list of guests having visited ROBL for test experiments and some other information. Finally, the third part collects the experimental reports of the users received until end of August 1999.



Dr. W. Matz
Head of the Project Group ESRF-Beamline
Spokesman of the ROBL-CRG

Contents

	Page
Contributions	
ROBL – the ROssendorf BeamLine at the ESRF	5
Silicon implanted with carbon ions: SiC crystallite formation and strain in Si	14
Fold of a buried relief in epitaxially grown Nb layers	19
Determination of radionuclide speciation in aqueous solutions by EXAFS spectroscopy	24
Solution coordination chemistry of uranium in the binary UO_2^{2+} - SO_4^{2-} and the ternary UO_2^{2+} - SO_4^{2-} - OH^- system, a combined EXAFS and ^{17}O NMR study	31
Statistics	
Scheduled experiments at the radiochemistry end-station	37
Scheduled experiments at the materials research end-station	38
Guests at ROBL	40
Personnel of the Project-group ESRF-Beamline	41
Experimental reports	
Experimental reports from the radiochemistry end-station (No. 20_01_xxx)	43
Experimental reports from the materials research end-station (No. 20_02_xxx)	55
Experimental reports from experiments scheduled by the ESRF	76

ROBL – the ROssendorf BeamLine at the ESRF

W. Matz^{*°}, N. Schell[°], G. Bernhard⁺, F. Prokert^{*}, T. Reich⁺, J. Claußner[#], W. Oehme[#], R. Schlenk[#], S. Diemel[#], H. Funke⁺, F. Eichhorn^{*}, M. Betzl^{*}, D. Pröhl[#], U. Strauch[°], G. Hüttig⁺, H. Krug[#], W. Neumann[#], V. Brendler⁺, P. Reichel^{*}
Forschungszentrum Rossendorf e.V.

* Institute of Ion Beam Physics and Materials Research

+ Institute of Radiochemistry

Central Department Experimental Facilities and Information Technology

° Project Group ESRF-Beamline

Introduction

The ROssendorf BeamLine (ROBL) is a collaborating research group (CRG) beamline at the European Synchrotron Radiation Facility (ESRF) in Grenoble, France. The beamline was built and is operated by the Forschungszentrum Rossendorf. ROBL has been designed for performing experiments on two different experimental stations: a Radiochemistry Hutch (RCH) and a Materials Research Hutch (MRH), both operating alternatively. X-ray absorption spectroscopy and X-ray diffraction and reflectometry are the main experimental techniques used in RCH and MRH, respectively. Most of the beamtime is used by the FZR for in-house research devoted to:

- Radioecological research as scientific background for risk assessment and development of remediation strategies for areas contaminated by radionuclides. Determination of the chemical speciation of radionuclides interacting with geological material, natural and anthropogenic organics, and micro-organisms. Study of the influence of these interactions on radionuclide migration and retardation in the environment.
- Structural identification and characterisation (including texture) of modifications of surfaces and interfaces produced by ion beam techniques for applications as hard covers, sensors or in semiconductor technology. Study of interfaces in thin films and nanometer-multilayers. Structural investigations of melts and amorphous solids.

The beamline is also available to outside users to perform experiments either in collaboration with the FZR or by submitting a proposal to the ESRF: one third of the ROBL beamtime will be allocated by the ESRF for peer-reviewed experiments.

This paper gives an overview about the beamline design and describes the standard experimental equipment of both experimental stations [#].

Beamline optics

The beamline is located at the bending magnet port BM 20 of the ESRF. The overall layout of ROBL is shown in the title page of the report. The beamline optics uses horizontally a fan of 2.8 mrad of synchrotron radiation from the hard edge of the ESRF bending magnet (0.8 T range, critical energy 19.6 keV) [1]. The layout of the optics is sketched in Fig. 1. The main elements are a fixed-exit double crystal monochromator located between two mirrors. The beamline is designed for an energy range from 5 to 35 keV. The lower energy limit is given essentially by the mandatory Be-windows. The upper energy limit was chosen to allow X-ray absorption spectroscopy (XAS) experiments on all chemical elements from Ti onward, since at least one absorption edge is in the energy range 5 to 35 keV.

The two mirrors, with the same grazing angle of 2.5 mrad suppress the higher-order harmonics in the monochromatic beam, reduce the heat load on the monochromator, and provide a parallel or vertically focussed beam at the experimental stations at a fixed height.

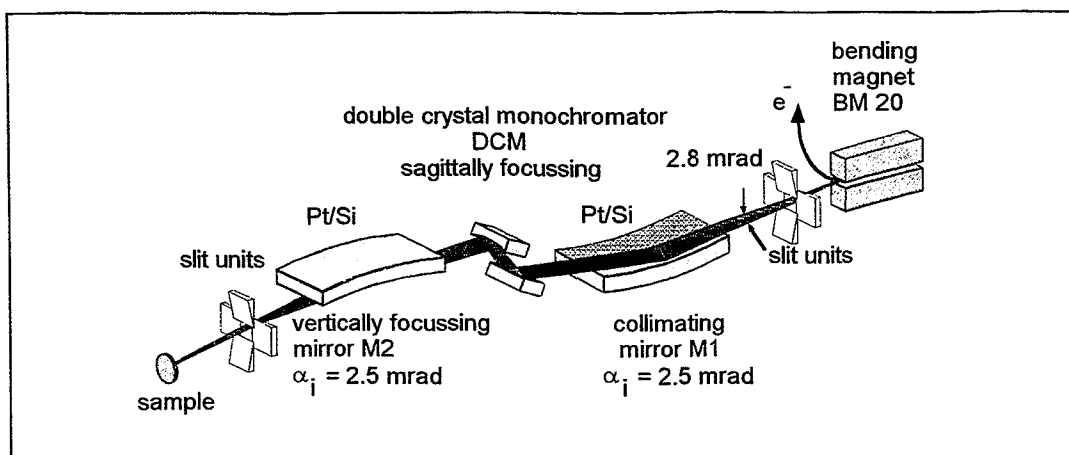


Fig. 1: Scheme of the X-ray optics of ROBL. A mirror - double crystal monochromator - mirror arrangement selects a monochromatic beam for the two experimental end-stations

The X-ray mirrors including cooling and bending mechanisms were purchased completely. The first mirror is made of a single Si crystal which is water cooled. The second mirror uses a ZERODUR substrate without cooling. Both mirrors are equipped with pneumatic benders. The first is bent with a radius of 20.8 km to collimate the incident radiation onto the first monochromator crystal. The second with an adjustable bending radius down to 8 km focuses the beam vertically to one of the two experimental end-stations. The mirror substrates were coated with two parallel stripes of silicon and platinum which are used alternatively. The harmonic suppression is better than 8×10^{-4} for all energies when using the silicon stripes. For the platinum stripes, it is of the same order of magnitude for energies above 13.5 keV.

The calculated spectral flux for the two cases is shown in Fig. 2. The intensity decrease below 10 keV, is due to the absorption of the beryllium windows.

The double crystal monochromator (DCM) provides a fixed-exit beam with a vertical offset of 18 mm. It operates with either Si(111) or Si(311) crystal sets. The mechanical construction allows to reach 25 keV using Si(111) crystals and 35 keV using Si(311) crystals. The design is mainly a commercial one. The axis of a high-precision rotation table is fed into a vacuum vessel. A crystal cage mounted on this axis carries both crystals. The first crystal is mounted with the rotation axis on the reflecting surface. The second crystal can be moved relative to the first one, parallel and perpendicular to the beam direction. The combined motion of both drives realises a fixed-exit beam. The first crystal is water cooled. The second crystal will be equipped with a bender for sagittal focussing; in the beginning it will be available only for Si(311).

For Quick-EXAFS, a pseudo channel-cut mode of the monochromator is possible by keeping fixed the position of the second crystal relative to the first one. In this mode only the Bragg angle of the DCM is changed during a scan; for energies above 14 keV the beam height variation during a 500 eV wide scan is less than 0.6 mm.

A feedback system is installed, which compensates intensity modulation during XAS scans, by fine tuning the orientation of the second crystal on the base of a signal coming from a monitor in front of the sample.

The overall energy resolution of ROBL is shown in Fig. 3. This resolution allows to study the near-edge structure at all absorption edges within the accessible energy range with a resolution better than the core hole width.

In addition to the mirrors and the monochromator, in the optics are various slit units, filters, and beam position monitors.

The motions of nearly all optical components are motorised, mostly with stepper motors, controlled by an UNIX workstation based system. Many standard ESRF software applications are used in the control programs, which utilise SPEC[®] code package [4]. The control system includes also interlock components for the vacuum, beam shutters and the cooling of components exposed to the white beam. The characteristics of the monochromatic beam are summarised in Table 1.

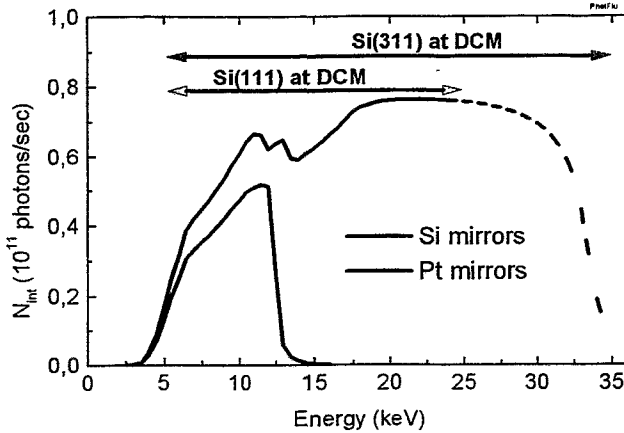


Fig. 2: Calculated flux of focussed radiation with silicon and platinum coated mirrors and silicon (111) crystals in the double crystal monochromator obtained using the SHADOW code [2,3]. The attenuation from beryllium windows of the total thickness of 1.5 mm is included. The maximum energy of 35 keV can be realised only with Si(311) monochromator crystals. Geometrical constraints of the DCM design limit the accessible energy range for Si(111) crystals to about 25 keV.

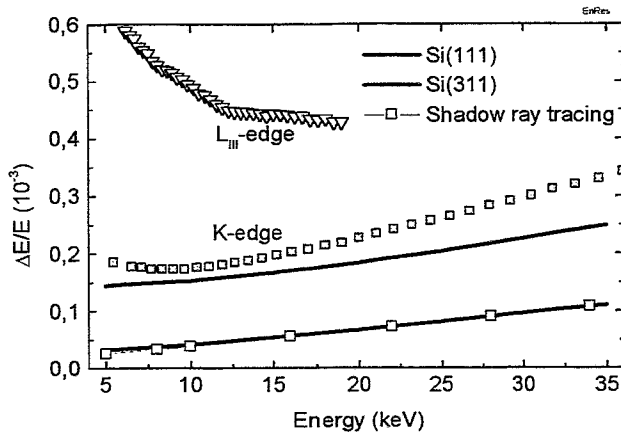


Fig. 3: Calculated energy resolution of the double crystal monochromator with silicon crystals and parallel incident beam. For comparison the natural line widths of the absorption edges of the elements are shown. Besides the analytically calculated values, results obtained with SHADOW code are included for Si(311).

Table 1: Characteristic data of monochromatic synchrotron beam

energy range	5 - 35 keV
energy range with Si-mirrors	5 - 12 keV
energy resolution with Si(111) crystals	$1.5 - 2.5 \times 10^{-4}$
energy resolution with Si(311) crystals	$0.5 - 1.0 \times 10^{-4}$
integrated flux for focussed beam (calc.)	6×10^{11} ph./s @ 20keV, 200 mA
standard beam size	20 mm (w) x 3 mm (h)
focussed beam size	< 0.5 mm x 0.5 mm

Radiochemistry end-station

The radiochemistry end-station is designed for studying radionuclides of environmental importance such as Tc, U, Th, Np, Pu, Am. X-ray absorption spectroscopy is a powerful technique to obtain information on the molecular and electronic structure of these radionuclides in solids and liquids. It is an element specific method and provides information about the oxidation state as well as the bond lengths and numbers of neighbouring atoms in the first, second and even third coordination shell of the absorber. Such knowledge is essential to understand complexation and speciation of radionuclides and also absorption processes from solutions. Actinides are known to exist in many oxidation states which are difficult to be determined by chemical or optical methods. In contrast XAS can distinguish the oxidation state from the shift of the absorption edge, providing also information if different states are present in one sample. Another advantage of XAS for radiochemical investigations is the possibility to use solid or liquid samples as well as very dilute ones (micro-mol region).

The ROBL-CRG obtained a license from the French authorities to perform XAFS experiments with the isotopes listed in Table 2. Under this license the maximum allowed activity at any given time present at ROBL is 185 MBq (5 mCi). These elements emit mostly alpha and beta particles and only weak gamma radiation. Therefore, the heart of the radiochemistry end-station is a glovebox without additional lead shielding (see Fig.4). To ensure a safe handling of the radionuclides, the entire experimental station is built as a radiochemistry laboratory according to legal safety requirements.

Table 2: List of radioactive elements which can be investigated at ROBL and the maximum amount of material to remain below the activity limit of 5 mCi

Isotope	Half-Live (years)	Amount (g)	Isotope	Half-Live (years)	Amount (g)
Np 237	2.1×10^6	6.97	Pu 239	2.4×10^4	0.08
Am 241	433	1.4×10^{-3}	Pu 242	3.75×10^5	1.27
Am 243	7370	0.025	Ra 226	1600	0.005
Po 208	2.9	8×10^{-6}	Tc 99	2.1×10^5	29.1
Po 209	103	3.01×10^{-4}	U nat	4.47×10^9	1000
Pa 231	3.28×10^4	0.106	Th nat	1.4×10^{10}	1000

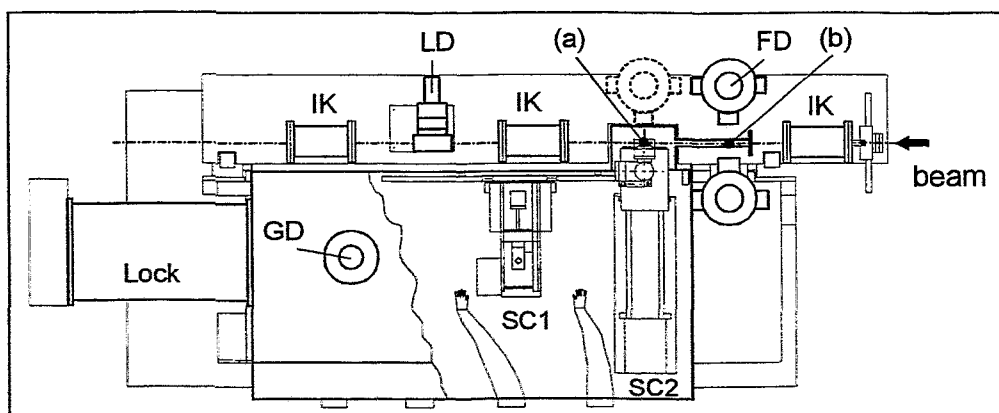


Fig. 4: Principal layout of the glovebox. (a) standard sample position for XAFS experiments; (b) sample position for fluorescence radiation detection from dilute liquid samples. The ionisation chambers (IK) are mounted on an optical bench and can also be used for non-radioactive samples while the box is moved out of the beam. FD- fluorescence detector; LD – Lytle detector; GD – gamma detector for measurement of sample activity, SC1,2 - sample changers.

The XAFS spectra can be measured both in transmission and fluorescence modes. For transmission mode the sample is placed perpendicular to the photon beam between two ionisation chambers (IK in Fig. 4). In fluorescence mode, the sample is inclined by 45° with respect to the beam and the fluorescence radiation is detected with Ge solid state detectors (FD in Fig. 4) positioned perpendicular to the beam. The radioactive samples are positioned inside the glovebox equipped with $125\ \mu\text{m}$ thick Kapton (polyimide) windows which are transparent to hard X-rays. All detectors, e.g., gas ionisation chambers and fluorescence detectors, are mounted on an optical bench outside the glovebox. This arrangement allows a direct and easy access to the detectors and avoids bringing signal cables, gas and power supply lines into the glovebox. In addition, even in the unlikely case of a contamination inside the glove box, the detectors will not be affected.

Inside the glovebox it is possible to use sample holders at different positions. Two, marked (a) and (b), are indicated in the schematic glovebox layout of Fig. 4. At position (a) a larger space is available so it is possible to mount either an automatic sample holder which provides room up to eight solid or liquid samples or a closed cycle He cryostat. The samples in position (a) can be measured both in transmission and fluorescence modes. For measurements on very dilute samples, a special single sample holder can be placed at position (a). The rotating arm of this positioning system moves the sample to position (b), between two Kapton windows and rotates it of 45° with respect to the beam: two Ge solid state detectors record simultaneously the fluorescence signals.

Since the samples are safely contained in the glove box, it is possible to change some of the sample conditions during the experiment. With the closed cycle He cryostat the sample temperature can be varied between 10 K and 295 K. It is also possible to modify the chemical conditions of liquid samples just before or during the XAFS measurements by adding non-radioactive substances like acids, bases or complexing agents.

The glovebox is mounted on a support frame which allows to move the glovebox in the horizontal direction out of the beam leaving the position of the optical bench and of the detectors unchanged. So, non-radioactive samples can be easily measured outside the glovebox by mounting them on the optical bench between the first and second ionisation chambers. For energy calibration purpose a non-radioactive reference sample can be placed between the second and third gas ionisation chamber. The reference sample is inside a fluorescence X-ray ion chamber detector (Lytle detector) to have the possibility to record the XAFS also in fluorescence mode.

When measurements take place downstream in the MRH, the box and the optical bench are moved out of the beam horizontally and vertically, respectively, and the beam path in the RCH is closed by a vacuum pipe to reduce the loss of beam intensity.

In order to guarantee a safe operation of the experiments with radioactive samples a number of safety installations was made to monitor the actual status. Basically a multi-barrier concept is realised here as usual for radiochemical work [5]. No preparation of radioactive samples is possible at the ESRF. Ready for measurement samples will be transported to the experimental end-station in certified transport containers.

To check the energy calibration of the Si(111) double crystal monochromator, the X-ray absorption near-edge structure (XANES) spectra of several metal foils in the energy range of 5 – 30 keV were measured in transmission mode. The absorption edges values found for Ti, Cr, Co, Zn, Zr, Nb, and Sb foils were compared with the values given by [6]. The data evaluation showed that the standard deviation of the Bragg angle was less than 0.002° in the entire energy range indicating an excellent linearity of the monochromator mechanics. Figure 5 displays single sweeps of K-edge XANES spectra of three representative elements. The features of the Ti and Zr K-edges are well resolved, as expected from the high resolution of the beamline, that is lower than the material core-hole lifetime.

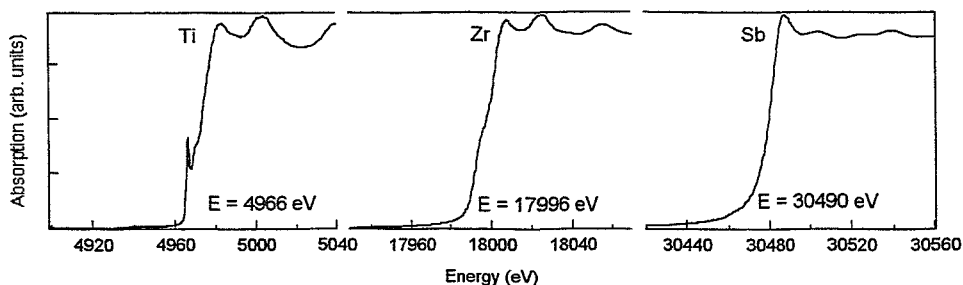


Fig. 5: K-edge XANES spectra of metallic Ti, Zr, and Sb. The energy scale was calibrated using the edge energies given in [6]. The natural line widths of the Ti, Zr, and Sb K shells are 0.94, 3.84, and 9.16 eV, respectively [7].

Materials research end-station

The materials research end-station is mainly devoted to structural studies of solids and melts by diffraction and reflectometry. The field of interest for the in-house research are crystalline phases and structural changes in thin near-surface regions of solids. Mainly samples produced or modified by ion beam techniques will be investigated. But, the diffractometer is versatile enough to allow for a wider range of applications than thin film studies. First single crystal diffraction studies have been performed [8]. A special design was made for the diffraction on melts with free surfaces.

The goniometer (Fig. 6) in the MRH is a six-circle built from standard components. The arrangement of two parallel circles each with horizontal and vertical axes, respectively, allows experiments in both scattering planes. The sample position can be equipped with an x-y-z-slide or, alternatively, with special sample environment chambers which are mounted directly on the ϕ -circle. The layout is made for a load up to 15 kg at the sample position and the χ -circle has an inner diameter of 400 mm so that even huge and heavy chambers (e.g. a high temperature chamber) can be used without difficulties. All axes are equipped with stepper motors and gear boxes which allow a minimum angular step of 0.0001° . The z-translation of the x-y-z-slide has a step width of 1 μm while the two other translations have 10 μm . Additionally, sample holders for single crystal samples and capillary sample containers are available. A high temperature chamber up to 1600°C is available.

The goniometer is fully computer controlled by a workstation and the programs are based on the SPEC[®] code [4].

Different detection systems can be mounted at the detector arm. As standard, a high load, high linearity scintillation detector is used. In front of the detector, interchangeable fixed single or soler slits can be mounted. Other detection systems are a two-dimensional CCD-camera or an energy-dispersive pin-photodiode. Optionally, a secondary monochromator unit (crystal analyser) may be mounted in front of the detector.

The resolution of a diffraction experiment depends not only on the energy resolution of the monochromator but also on the beam divergence. The experimentally achievable resolution was measured using silicon single crystals and powders. At present, radiation with the natural horizontal divergence of the synchrotron radiation beam from the source is used since the sagittal focussing option at the monochromator is not yet installed. The vertical divergence is reduced by the first collimating mirror.

Using the Si(111) monochromator and the Si mirrors, at 12 keV and a vertically parallel beam, the FWHM of a Si(004) single crystal reflection was measured to be $\Delta\theta = 0.003^\circ$ (10 arcsec). This corresponds approximately to a resolution $\Delta d/d = 1.3 \times 10^{-4}$. Vertical focussing

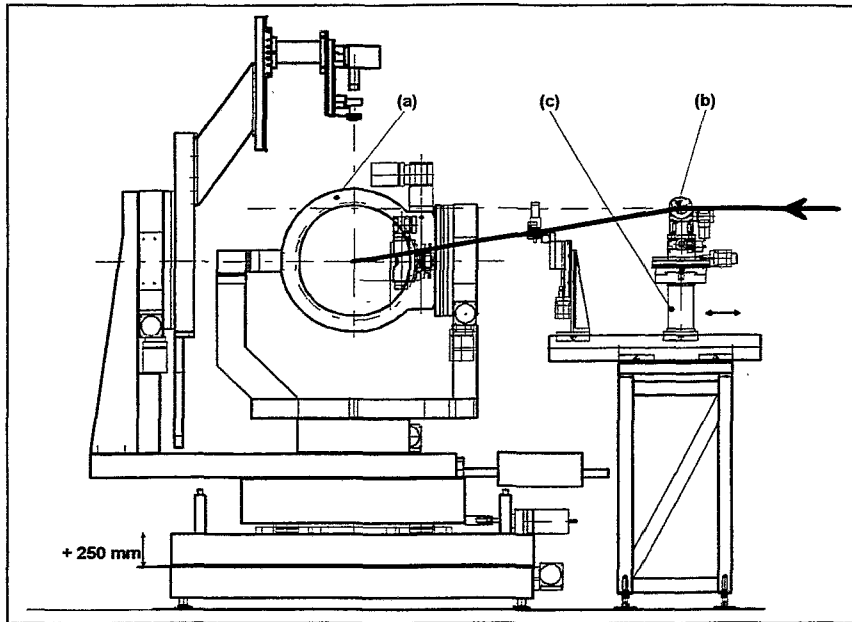


Fig. 6: Scheme of the goniometer (a) in the materials research end-station and of the deflector unit (b) for the study of melts with free surfaces. The small goniometer head with the deflecting multilayer mirror (b) can be positioned at different distances to the sample by a translation slide (c).

with the second mirror raises the FWHM up to 0.0051° but increases the incident radiation intensity significantly. It follows from these results, that ROBL's optics allows optimising the intensity by vertical focussing without significant loss in resolution for polycrystal diffraction experiments.

For powder diffraction, the instrumental contribution to the intrinsic FWHM of Bragg peak was estimated. The angular resolution in the case of Si(111) sample is entirely determined by the convolution of the incident and receiving slit apertures. The profil fitting of the measured Si(111) peak from a powder sample with a pseudo Voigt function ($F_{PSV} = \eta \cdot F_L + (1-\eta) \cdot F_G$) gives a FWHM of 0.0528° which agrees with the value of $925 \mu\text{rad} = 0.0530^\circ$ estimated from the apertures. The very small η -parameter ($\eta=0.0485$) indicates that the instrumentally determined Gaussian part dominates over the sample broadening effects expressed by the Lorentzian term.

To get the full possible resolution for powder diffraction (0.01° - 0.03°) it is possible to use a narrower receiving slit or a perfect crystal analyzer.

Typical Si-powder resolution curves $\Delta d/d$ for different energies are given in Fig. 7. These data show that the materials research end-station is also suitable for high resolution X-ray powder diffraction and for the study of line broadening effects [9].

The study of melts (or more general liquids) with free surfaces by diffraction requires an incident beam inclined to the horizontal, to hit the horizontal surface of the melt. The additional demand to tune the energy in order to make use of anomalous scattering led to the installation of a deflection unit (b) as displayed in Fig. 6. A suitable multilayer mirror of $40 \times 100 \text{ mm}^2$ is mounted on a circle with a horizontal rotation axis perpendicular to the incident beam and deflects the beam downwards. The reflecting efficiency of the deflecting multilayer mirror is 50% at 8 keV. In order to make the deflected beam to hit the sample the goniometer has a motorised height adjustment. The sample position can be set 250 mm below the primary beam from the monochromator. When changing the energy of the incident beam, the deflection angle of the mirror and the height of the sample have to be

changed. To avoid height adjustment of the huge diffractometer where the sample is mounted, the multilayer-mirror deflection unit is mounted on an additional translation stage (c). So leaving fixed the sample height the adjustment is performed by translation and rotation of the deflecting mirror alone, for an energy range of 5 keV when working at 10 keV and of 11 keV when working at 25 keV.

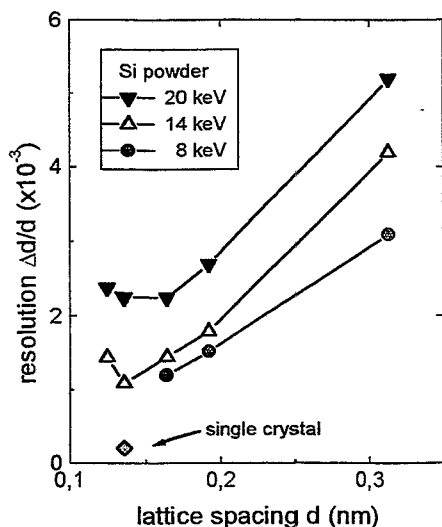


Fig. 7: Experimental resolution $\Delta d/d$ obtained on silicon powder inside a glass capillary (diameter 0.4 mm; wall thickness 0.01mm). For comparison the value from a single crystal sample is indicated. The Si(111) monochromator crystals are used.

Conclusion

The ROBL beamline with both end-stations became fully operational in fall 1998. First experiments show a reliable performance of the entire beamline and its components. This CRG beamline adds new experimental possibilities to the ESRF.

The advantages of the ROBL radiochemistry station when compared to the other synchrotron radiation beamlines are manifold: (i) the maximum allowed amount of radioactive material is 5 mCi which is higher than at most other synchrotron light sources, (ii) it is the only dedicated end-station for XAFS experiments of actinides in Europe. In addition, as to our knowledge, ROBL is the only XAFS station in the world where it is possible to manipulate the chemical and physical properties of the sample in a glove box on site and during the experiment at a third-generation high-energy synchrotron radiation source. Dedicated beamlines for the study of radioactive materials have become operational in Japan at the Photon Factory (PF) and Spring-8, but working in lower energy region [10,11]. At SSRL (USA) the maximum allowed quantity of ²³⁷Np in the experimental X-ray hut at one time must be less than 50 μ Ci. The total amount of Np material that can be shipped to and be at SSRL must be less than 500 mg (325.5 μ Ci) [12].

The materials research hut (ROBL-MRH) offers horizontal and vertical scattering planes as well as off-plane diffraction possibilities. The dedicated ESRF powder diffraction beamline (BM16) or the powder diffraction set-up of Swiss-Norwegian-Beamline (BM1) are equipped with goniometers which are restricted to one scattering plane [13-15]. For powder or polycrystalline samples we provide the same diffraction resolution and nearly the same wavelength range as the mentioned beamlines. Concerning the study of liquids with free surfaces the ROBL-MRH setup is complementary to the BM32 one, but the latter uses a silicon crystal in Laue geometry as beam deflector [16]. The arrangement at ROBL-MRH reduces the necessary movements of the goniometer and makes the arrangement of samples in chambers with small radiation windows easier.

References

- [#] The extended version of this contribution will appear in *J. Synchrotron Rad.* **6** (1999). It is also available as Technical Report FZR-256, April 1999.
- [1] ESRF Beamline handbook, Grenoble, August 1993, p. 9-10
- [2] Matz, W., Prokert, F., Schlenk, R., Claußner, J., Schell, N., Eichhorn, F. & Bernhard, G. The Rossendorf Beamline at the ESRF (Project ROBL), int. rep. FZR-158, Rossendorf 1996
- [3] Lai, B. & Cerrina, F., *Nucl. Instr. & Methods*, **A246** (1986) 337-341
- [4] Swislow, G. spec X-Ray Diffraction Software, Certified Scientific Software, POB 390640, Cambridge, Massachusetts 01239, (1996)
- [5] Funke, H. , Reich, T., Bernhard, G., Brendler, V., Claußner, J., Matz, W. , Oehme, W. , in: *Speciation, Techniques and Facilities for Radioactive Materials at Synchrotron Light Source: Workshop Proceedings, Grenoble, France, 4-6 October 1998, OECD/NEA Paris, France, 1999, (in press)*
- [6] Kraft, S., Stümpel, J., Becker, P. & Kuetgens, U. (1996), *Rev. Sci. Instrum.* **67**, 681-687
- [7] Krause, M.O. & Oliver, J.H. (1979), *J. Phys. Chem. Ref. Data* **8**, 329
- [8] see *Experimental Report 20_02_014* in the appendix
- [9] Thiele, E., Hecker, M., & Schell, N. (1999), *Proc. 6th EPDIC, Budapest, August 22-25, 1998, Materials Science Forum (in press)*
- [10] Konishi, H., Yokoya, A., Shiwaku, H., Motohashi, H., Makita, T., Kashihara, Y., Hashimoto, S., Harami, T., Sasaki, T.A., Maeta, H., Ohno, H., Maezawa, H., Asaoka, S., Kanaya, H., Ito, K. Usami, N. & Kobayashi, K. (1996), *Nucl. Instrum. Methods A* **372**, 322-332
- [11] Yokoya, A., Sekiguchi, T., Saitoh, Y., Okane, T., Nakatani, T., Shimada, T., Kobayashi, H., Takao, M., Teraoka, Y., Hayashi, Y., Sasaki, S., Miyahara, Y., Harami, T. & Sasaki, T.A. (1998), *J. Synchrotron Rad.* **5**, 10-16
- [12] Allen, P.G., Shuh, D.K., Bucher, J.J. & Edelstein, N.M. in: *Speciation, Techniques and Facilities for Radioactive Materials at Synchrotron Light Source: Workshop Proceedings, Grenoble, France, 4-6 October 1998, OECD/NEA Paris, France, 1999 , p.163-179*
- [13] Fitch, A.N., *Nucl. Instr. and Meth. in Phys. Res.* **B 97** (1995)63-69
- [14] Fitch, A.N., *Materials Science Forum* **228-231** (1996) 219-222
- [15] ESRF Beamline handbook, fourth ed., Grenoble, January 1997, p. 25-29
- [16] Dailant, J., Quinn, K., Gourier, C. & Rieutord, F., *J. Chem. Soc., Faraday Trans.*, **92** (1996) 505-513

Silicon implanted with carbon ions: SiC crystallite formation and strain in Si

F. Eichhorn, N. Schell, W. Matz, R. Kögler

Forschungszentrum Rossendorf, Institute of Ion Beam Physics and Materials Research

Carbon is a common impurity in CZ-silicon crystals. C in Si can deteriorate important device characteristics as leakage current and minority carrier lifetime, if the C concentration exceeds a threshold of about 1×10^{19} C/cm³ [1]. On the other hand an additional C ion implantation into Si reduces the transient enhanced diffusion of B dopants [2] and can improve device characteristics because of the suppression of the formation of extended defects after implantation [3]. Moreover, high energy C implantation is applied for the formation of gettering layers with high trapping efficiency against unwanted metal impurities [4]. Furthermore, SiC is well known as a wide-band gap semiconductor with high thermal and chemical stability for realizing integrated circuits for high frequency, high power and high temperature applications [5]. C implantation with stoichiometric doses at elevated temperatures (400 - 900°C) [6] or an implantation followed by annealing [5], [7] is used to synthesize buried SiC layers in Si.

The aim of this paper is to investigate the process of the formation of SiC precipitates in the Si matrix during C implantation. It is known from previous investigations that SiC formation is not a single step process [8], [9], [10]. Depending on the conditions of mixing C into Si the carbon is localized in different atomic surroundings. By implantation of C into Si the damaged and implanted region is in a non-equilibrium state and most of the C atoms occupy interstitial positions. In thermodynamic equilibrium the solubility for C in Si is only 10^{-3} to 10^{-4} at.% at 1200 to 1400°C [11] and the excess C is dissolved substitutionally or the new phase SiC is formed. The volume concentration of C and with it the strain of the Si substrate lattice varies in depth; resulting in different local conditions for nucleation and growth of Si-C complexes and SiC particles. The present study is focused on the strain in the crystalline material (Si substrate and SiC particles) due to implantation and on the first stages of forming the SiC phase in the Si lattice by using X-ray diffraction with synchrotron radiation. The new material research goniometer of the ROBL beamline at the ESRF [12] enables to follow the early stage of phase formation.

The samples were prepared by implantation of C ions with an energy of 195 keV into Si (001) wafers under perpendicular incidence, at doses varying from 5×10^{15} ions/cm² to 4×10^{17} ions/cm² and temperatures between room temperature and 800°C. A survey of the samples is given in Table 1.

Tab. 1: Sample characterization: Concentration of C, implantation temperature and ion fluence

Maximum C concentration (10 ²¹ atoms/cm ³)	Percentage of stoichiometric concentration for SiC	Implantation temperature (°C)	Ion fluence (10 ¹⁶ ions/cm ²)
0.27	0.6	room temp.	0.5
0.27	0.6	500	0.5
0.27	0.6	800	0.5
2.7	6	500	5
22	45	500	40
22	45	800	40

X-ray diffraction using synchrotron radiation was carried out on the ROBL beamline at the ESRF Grenoble [12]. In ROBL the X-ray beam is conditioned by adaptively bent Si mirrors and a Si(111) - Si(111) double crystal monochromator. The chosen wavelength was $\lambda = 0.10008$ nm.

During the implantation process in the near-surface layer the ions generate only weak distortions (damage profile). Later the ions are stopped in a deeper region (ion distribution profile), resulting in a higher content of impurity atoms (implants) with their deformation field. The damage and ion distribution profiles calculated with TRIM and a schematic representation of the regions are shown in Fig. 1. In dependence on the process temperature, the local implant concentration and the strain values determine the formation of a solid solution of C in Si, a substitutional alloy, or crystallites of SiC.

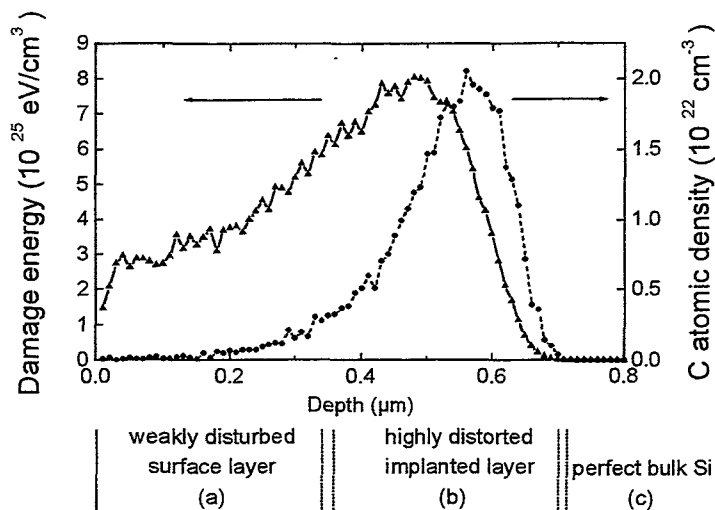


Fig. 1: Depth distribution of damage energy and C atoms after implantation of $4 \times 10^{17} \text{ cm}^{-2}$ C ions with an energy of 195 keV into Si(100) as calculated by the TRIM code (version 96.01). The regions of different strain for the simulation model are indicated.

The formation of SiC crystallites is indicated by the reflections (111), (200), (220), and (311) of the 3C-SiC phase. Other SiC polytypes were not detected in the X-ray diffraction diagram. The reflections (111), (220), (311), and (400) of the Si substrate were used to characterize the damage and strain of the Si lattice in dependence on the implanted ion dose and the thermal treatment. Both, the damage and the ion distribution profile influence the X-ray diffraction peaks from silicon due to the strain induced by them in the formerly perfect Si lattice.

Fig. 2 shows the diffraction patterns in the vicinity of the most intense 3C-SiC(111) reflection which is representative to detect the SiC formation. No signal caused by SiC crystallites smaller than 3 nm was detected after implantation with the lowest dose of 5×10^{15} ions/cm². With increasing implantation dose (5×10^{16} ions/cm² to 4×10^{17} ions/cm²) and temperature (500 °C to 800 °C) carbon related diffraction intensities occur starting with a broad distribution at the low-angle side and growing up to a crystalline peak at the expected line position.

The high resolution diffraction curves of the Si(400) reflection are given in Fig. 3. They reveal a lattice strain component perpendicular to the sample surface. The occurrence of fringes beside the interference maximum is characteristic for a layered structure. The diffraction line is a superposition of intensity modulations caused by the weakly distorted surface layer as well as by the implanted layer. The later varies in density and strain as graded transitions from the surface layer to the matrix. To get quantitative results for strain and layer thickness the measured intensity versus scattering angle is simulated by the HRXRD-code [13] with a model on the base of the damage and ion distribution profiles. The near-surface region (a) of the Si wafer is only weakly distorted by the ion damage. In the deeper region (b) near the maximum of the damage and the implant concentration the Si lattice is destroyed in a higher degree resulting in an X-ray peak shift. In the depth the bulk

material (c) diffracts X-rays as a perfect crystal. The superposition of the waves diffracted by the bulk material (c) and by the weakly distorted near-surface region (a) causes X-ray interference fringes, so far as the phase shift is only small. If these fringes are visible the lattice strain in the near-surface region can be assumed to be zero for modelling.

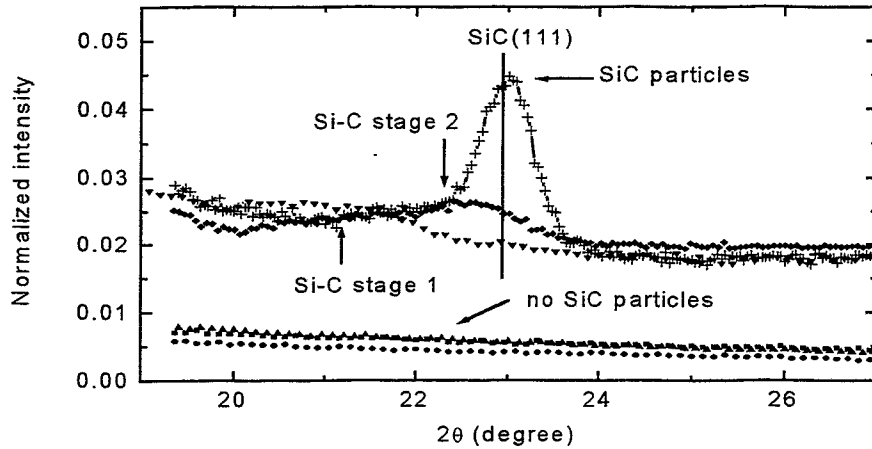


Fig. 2: Diffraction curves ($\theta:2\theta$ scans) in the vicinity of the most intense 3C-SiC(111) reflection indicating the formation of Si-C prestages and crystalline SiC particles.

Curves correspond to different implantation conditions:

- 5×10^{15} ions/cm² at room temperature, ● 5×10^{15} ions/cm² at 500°C
- ▲ 5×10^{15} ions/cm² at 800°C, ▼ 5×10^{16} ions/cm² at 500°C,
- ◆ 4×10^{17} ions/cm² at 500°C, + 4×10^{17} ions/cm² at 800°C.

The line marks the position of the SiC(111) diffraction line according to the JCPDS-PDF data. For cleanness the curves are shifted vertically in two groups.

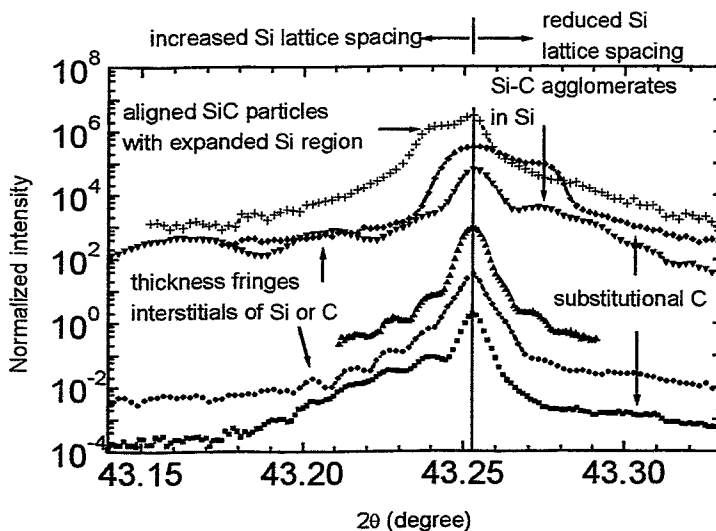


Fig. 3: Diffraction curves ($\theta:2\theta$ scans) of the Si(400) reflection revealing the lattice strain component perpendicular to the sample surface. Characteristic features and their cause are marked (Symbols as in Fig. 2). For cleanness the curves are shifted vertically by multiplying neighbouring curves by 10.

At the lowest fluence of 5×10^{15} C ions/cm² the silicon lattice is expanded due to implantation. Above the non-implanted substrate region a strained layer with a thickness in the range of 100 ... 200 nm and a strain on the order of 1×10^{-3} due to the interstitials of C

and/or Si exists as it is indicated by the extended intensity left from the substrate peak (marked by the vertical line in Fig. 3). This strained layer is located below a non-strained Si layer with a thickness of 500 nm which causes the thickness fringes. This layer thickness increases up to 560 nm with increasing implantation temperature. Again all the samples implanted with 5×10^{15} ions/cm² show very similar curves. At the high-angle tail of the Si(400) reflection a small peak is detected which indicates the existence of a Si lattice region with reduced spacing ($(\Delta d/d)_{\text{Si}} = -0.001$). At the higher implantation dose of 5×10^{16} C ions/cm² the fringe distance increases which means that the thickness of the undisturbed layer is reduced to 120 nm. Its transition to the implant layer is more smooth. At the doses 5×10^{16} ions/cm² and 4×10^{17} ions/cm² some additional peaks appear in the vicinity of the main peak.

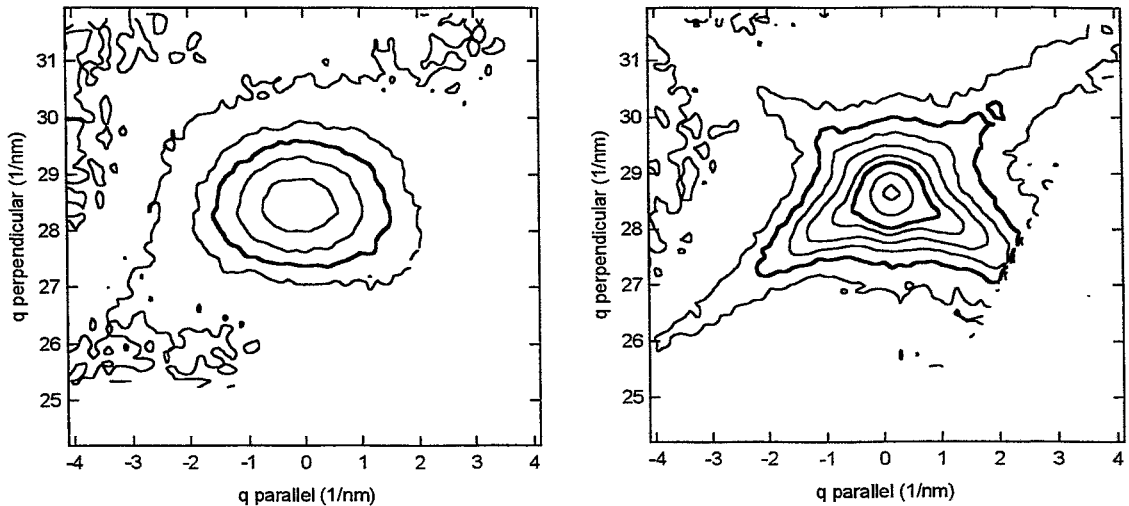


Fig. 4: Reciprocal space maps near the SiC(002) reflection for Si wafers implanted with 4×10^{17} cm⁻² C⁺ with an energy of 195 keV at 500 °C (on the left) or 800 °C (on the right), respectively. The isointensity lines are chosen in a logarithmic scale, the bulk ones corresponds to 512 counts and 2048 counts per 3 sec.

In addition, the orientation relation between the lattice of the SiC particles and the Si matrix is determined by the measurement of reciprocal space maps (RSM) of symmetric SiC(002) - Si(004) and asymmetric SiC(113) - Si (113) reflection pairs. The alignment of the cubic axes of the SiC crystallites to the Si matrix is confirmed. Fig. 4 shows the RSM near the SiC(002). The centre of the Si(004) reflection lies at $q_{\parallel}=0$ and $q_{\perp}=46.3$ nm⁻¹. For implantation at the lower temperature of 500 °C the cubic axes of the SiC crystallites are orientated with a nearly isotropic spread (FWHM $\approx 4.5^\circ$) parallel to Si [001] direction. More of SiC grows during carbon implantation at 800°C and a more complex distribution is found (right hand side of Fig. 4): The majority of crystallites is highly aligned with a spread of 2.5° isotropically distributed around [001] as shown by the symmetric top of the SiC peak, whereas the minority is anisotropically distributed around this axis with preferences into the $\langle 111 \rangle$ directions (streaks at the bottom of the SiC peak).

The experimental observations can be explained with the following processes:

1. The observed Si lattice expansion at the fluence of 5×10^{15} C ions/cm² is caused mainly by carbon interstitials and Si self-interstitials. No SiC precipitates, which X-rays detect as crystalline, were found (see Fig. 2, 3).

2. The Si lattice region with reduced spacing ($(\Delta d/d)_{\text{Si}} = -0.001$) may be caused by substitutional C with an average concentration of 1.5×10^{20} atoms/cm³ according to Vegard's rule. The corresponding peak is detected up to the dose of 5×10^{16} C ions/cm² at 500°C.

3. Very small SiC particles (pre-stages 1 and 2) with enhanced lattice spacings ($(\Delta d/d)_{\text{SiC}} = 0.07$ and $(\Delta d/d)_{\text{SiC}} = 0.02$ in comparison to the value of 3C-SiC) are found at 5×10^{16} and 4×10^{17} C ions/cm² and 500°C. They give the increased X-ray intensity detected at the low angle tail of the SiC(111) diffraction line (Fig. 2). By IR absorption studies [9] Si-C pre-stages are identified. The wavenumber of the stretching mode of Si-C bonds starts to increase before the final SiC crystallization, this is correlated with an increased atomic distance found here.

These particles cause also a small strain of $(\Delta d/d)_{\text{Si}} = -0.0004$ in the Si lattice. This is concluded from the additional intensity which arises near the central substrate peak of Si(400) at its high-angle slope (Fig. 3) in the same samples.

4. Finally, crystalline 3C-SiC particles are found for a fluence of 4×10^{17} C ions/cm² at 800°C. They are aligned to the Si host lattice in such a way that the cubic crystallographic axes of matrix and particles coincide within an accuracy of 2.5° as it was revealed by RSM studies. The 3C-SiC crystallites are surrounded by an expanded Si lattice (the peak position in Fig. 3 gives $(\Delta d/d)_{\text{Si}} = 0.0002$). The latter may be the consequence of the thermal stress by cooling down the sample from the process to room temperature due to the different coefficients of thermal expansion for Si (3.59×10^{-6} /K) and SiC (4.2 to 4.68×10^{-6} /K), respectively [14]. The SiC lattice itself is strained only negligible (see Fig. 3) if the phase formation occurs during the high-temperature implantation process. This is in contrast to strained SiC particles ($(\Delta d/d)_{\text{SiC}} \approx 0.01$) which have been reported [15] to form after thermal treatment following room temperature implantation.

Further complex X-ray studies including reciprocal space mapping and texture analysis will enlighten the mechanisms of the formation of SiC precipitates and their state in the Si host lattice.

References

- [1] I. Ban, M.C. Öztürk and E. Demirioglu, Proc. of the 11th Int. Conf. on Ion Implantation Technology, Austin, 1996, IEEE Publications 96TH8182, Piscataway, NJ, p. 740
- [2] S. Nishikawa, A. Tanaka and T. Yamaji, Appl. Phys. Lett. 60, 2270 (1992)
- [3] R. Liefting, R.C.M. Wijburg, J.S. Custer, H. Wallinga and F. Saris, IEEE Transactions on Electron. Devices Vol. 41 No.1, 50 (1994)
- [4] H. Wong, N. W. Cheung, P. K. Chu, J. Liu and J. W. Mayer, Appl. Phys. Lett. 52, 1023 (1988)
- [5] U. Preckwinkel, J. K. N. Lindner, B. Stritzker, B. Rauschenbach, Nucl. Instrum. Methods Phys. Res. B 120, 125 (1996)
- [6] A. Nejim, P. I. E. Hemment, J. Stoemenos, Appl. Phys. Lett. 66, 2646 (1995)
- [7] J. A. Borders, S. T. Picraux, W. Beezhold, Appl. Phys. Lett. 18, 509 (1971)
- [8] U. Gösele, Mat. Res. Soc. Symp. Proc. 59, 419 (1985)
- [9] M. Deguchi, M. Kitabatake, T. Hirao, N. Arai, T. Izumi, Jap. J. Appl. Phys. 31, 343 (1992)
- [10] P. Werner, S. Eichler, G. Mariani, R. Kögler, W. Skorupa, Appl. Phys. Lett. 70, 252 (1997)
- [11] T. B. Massalski, Binary Alloy Phase Diagrams, Vol.1, p. 882, ASM International, Ohio 1990
- [12] W. Matz, N. Schell, G. Bernhard, F. Prokert, T. Reich, J. Claußner, W. Oehme, R. Schlenk, S. Diemel, H. Funke, F. Eichhorn, M. Betzl, D. Pröhl, U. Strauch, G. Hüttig, H. Krug, W. Neumann, V. Brendler, P. Reichel, M.A. Denecke, H. Nitsche, J. Synchrotron Rad. 6 (1999) in press
- [13] computer code WIN-HR XRD, vers.1.02; Siemens 1994
- [14] Landolt-Börnstein, ed. by O. Madelung, Springer, New York 1982, Vol. 17
- [15] C. Serre, A. Perez-Rodriguez, A. Romano-Rodriguez, L. Calvo-Barro, J.R. Morante, J. Esteve, M.C. Acero, W. Skorupa and R. Kögler, J. Electrochem. Soc. 144 (6), 2211 (1997)

Fold of a buried relief in epitaxially grown Nb layers

T. Edelmann¹, S. Schmid¹, F. Berberich^{1,2} and N. Schell²

¹ Ludwig-Maximilians-Universität München, Sektion Physik, Lehrstuhl Prof. J. Peisl, Geschwister-Scholl-Platz 1, D – 80539 München

² Forschungszentrum Rossendorf, PF 510119, D – 01314 Dresden

Some metals, like niobium, can dissolve large amounts of hydrogen up to concentrations of one H atom per Nb atom. The hydrogen atoms are located in the niobium host lattice on tetrahedral interstitial sites and expand the lattice. The resulting long-range displacement field in the metallic host lattice causes an indirect elastic interaction between the hydrogen atoms. In a non-ideal finite crystal, surface effects play an important role. In thin layers, like the studied system of niobium on sapphire, the elastic displacements are not only influenced by the air film interface but also by the strain between film and substrate.

It is well known that for low hydrogen concentrations, thin epitaxially grown niobium films only expand perpendicular to the film plane (out-of-plane direction) [1]. During measurements in 1996 at HASYLAB we found by comparing different in-plane Bragg reflections in grazing incidence diffraction geometry (GID) that at higher concentrations the niobium lattice also expands laterally.

To measure various in-plane reflections – additionally, out-of-plane conventional Bragg diffraction and specular reflectivity data were taken – the sample had to be removed from its loading chamber and to be reinserted with a different orientation. That meant to unload the sample and thereby to change the system's morphology, rendering the subsequent data ambiguous. Therefore, it is absolutely necessary to keep the sample in a constant environment and to allow all three measuring modes (Bragg, GID, reflectivity) at the same time. To achieve those demanding conditions, a UHV chamber specially adapted for the ROBL six-circle-diffractometer was constructed (fig. 1). It allows in situ hydrogen loading without restricting the necessary diffractometer's degrees of freedom.

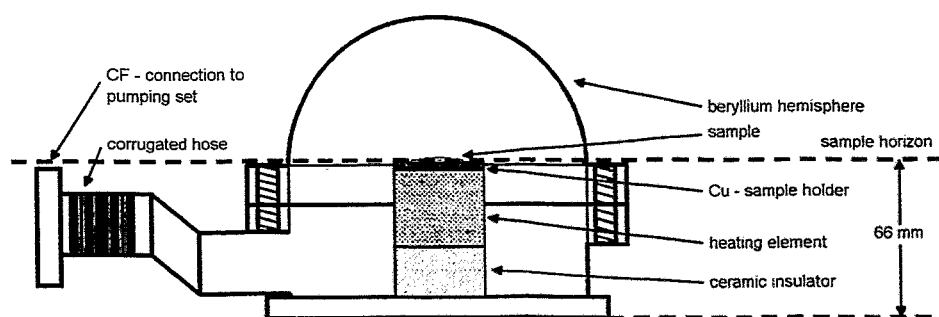


Fig. 1: In situ UHV hydrogen loading chamber „IGEL“ for the ROBL diffractometer.

The aim of the experiments at ROBL was to observe the *cross-over from one dimensional to three dimensional lattice expansion* by measuring the lattice parameters under in situ conditions and to determine the *degree of anisotropy of the lattice expansion* in dependence of the hydrogen content unambiguously.

Sample System and Experimental Method

Two samples of different Nb film thickness (220 Å and 790 Å) were examined. Both were epitaxially grown on [1120] oriented sapphire substrates (Al_2O_3) with surface areas of $10 \times 10 \text{ mm}^2$. The niobium layers were [110] oriented. Palladium cap layers of appr. 100 Å and 200 Å, resp., were protecting the niobium films against oxidation and facilitating hydrogen uptake by catalytic dissociation of the H_2 -molecules. The samples were grown by MBE (molecular beam epitaxy) at the Lehrstuhl H. Zabel at the Ruhruniversität Bochum.

The niobium films were loaded with hydrogen under in situ conditions at temperatures between 200 °C and 300 °C and at hydrogen pressures ranging from 0.1 mbar to 50 mbar. A delicate manipulation with leak and throttle valves, separating the stainless steel chamber (diameter appr. 60 mm and height 40 mm, capped with a 0.5 mm thick Be hemisphere) from the high pressure hydrogen storage container, allowed the precise control of the various experimental pressure conditions (shown below) and at the same time fulfilled stringent safety requirements.

The lattice parameter in the [110] growth direction is measured by conventional out-of-plane Bragg diffraction. The Laue fringes in (110) radial scans (due to the limited number of atomic planes in the thin films) provide information about the crystalline quality of the film perpendicular to the surface (fig. 2). Total specular reflectivity measurements ($\Theta/2\Theta$ -scans under small vertical angles) reveal the thicknesses of the palladium and the niobium layers under different hydrogen loading as well as the surface and interface roughnesses (fig. 3).

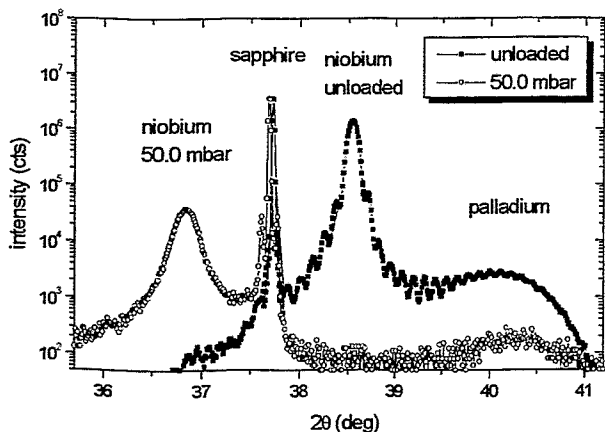


Fig. 2: Radial (110) Bragg scans for 790 Å Nb. The H induced shift – hydrogen does not dissolve into the sapphire substrate, its Bragg reflex thus serves as an angle reference – corresponds to a relative vertical lattice expansion of 4 %. In the loaded sample the Laue fringes are no longer recognizable, revealing a diminished crystal quality.

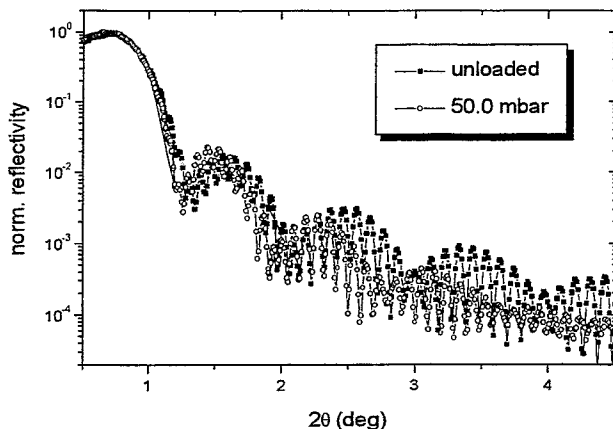


Fig. 3: Specular reflectivity for 790 Å Nb. The frequency shifts in the Kiessig oscillations (the high frequency is due to the Nb layer, the low frequency due to the Pd layer) show the changes in vertical overall thickness. The diminished amplitudes of the Kiessig oscillations reveal increased roughness.

Additional information about the changes in crystalline quality of the niobium films as well as the palladium cap layers under different hydrogen pressures can be monitored by comparing the changes in amplitudes of the Laue fringes in the Bragg scans and the Kiessig oscillations in the specular reflectivity curves (compare again figs. 2 and 3). The lateral in-plane lattice parameters and their hydrogen induced changes in the directions [110], [112] and [002] are accessible by diffraction under grazing incidence and exit angles (fig. 4).

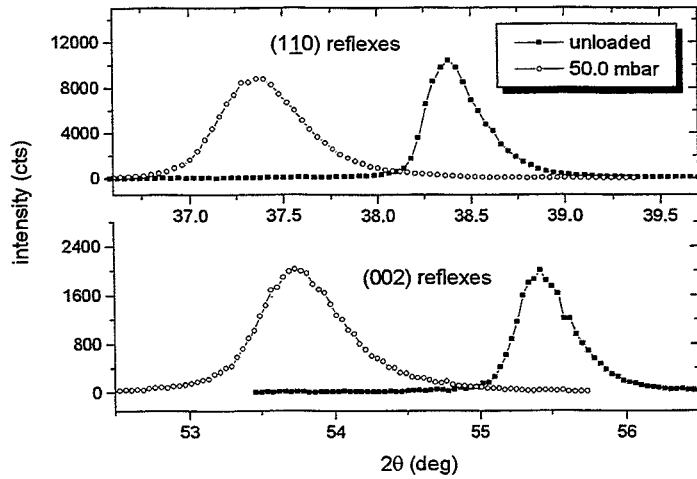


Fig. 4: Radial scans for two Bragg reflexes in GID geometry for 790 Å Nb. The lattice expansions in the two orthogonal directions [110] and [002] are 2.4 % and 2.8 %, respectively.

Anisotropic Lattice Expansion

Fig. 5 shows the relative lattice expansions in the aforementioned three orthogonal directions for the sample with 790 Å Nb thickness proving the necessity to measure under identical in situ conditions. (All three Bragg reflections were measured under the same experimental conditions before choosing a new equilibrium pressure and temperature.)

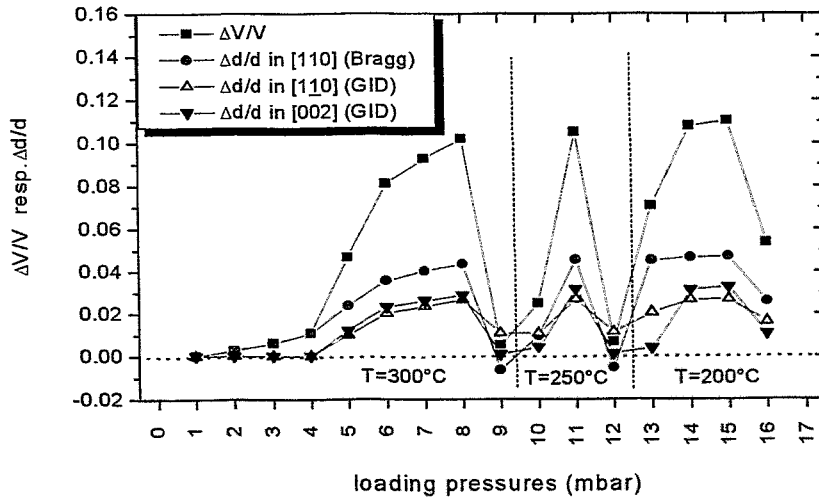


Fig. 5: Relative lattice expansions in three orthogonal directions for the sample with 790 Å Nb layer thickness (compare text).

The relative volume change $\Delta V/V$ can be calculated by the lattice expansion by

$$\frac{\Delta V}{V} = \left(1 + \frac{\Delta d}{d}\bigg|_{[110]}\right) \cdot \left(1 + \frac{\Delta d}{d}\bigg|_{[1\bar{1}0]}\right) \cdot \left(1 + \frac{\Delta d}{d}\bigg|_{[002]}\right) - 1$$

One can recognize in fig. 5 that after the first unloading¹ the Nb lattice remains contracted in its out-of-plane, i.e. growth, direction, whereas it is still expanded in the lateral [110] direction. By conservation of volume the unit cell reacts elastically: a lateral residual strain in [110] direction leads to a Poisson contraction in the perpendicular out-of-plane direction [110]. After the third loading cycle the Nb unit cell remains expanded in all three orthogonal directions due to residual hydrogen. (At 200 °C a certain amount of hydrogen remains in the sample even under evacuating; it cannot be removed totally in reasonable times.)

While X-ray diffraction shows that at a certain hydrogen concentration the niobium unit cells expand laterally, light-microscope measurements show that the Nb layer as a whole is not laterally expanding. Thus, the volume changes of the film as a whole can also be calculated by the one dimensional film thickness expansion Δt determined by specular X-ray reflectivity

$$\Delta V/V = \Delta t/t$$

Fig. 6 demonstrates the equivalence of both calculations.

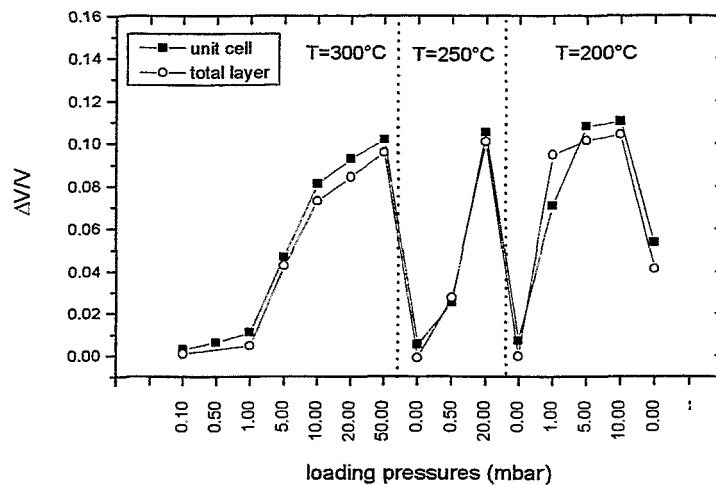


Fig. 6: Equivalence of the relative volume change calculated by the three dimensional unit cell expansion $\Delta V/V$ and the one dimensional film thickness increase $\Delta t/t$ for 790 Å Nb.

Model explanation

The lateral unit cell expansion finally leads to a gliding of parts of the niobium lattice in the direction of the surface. Thus, a disproportionally larger change of the film thickness results. Specular reflectivity shows that the roughness of the protecting palladium surface increases. An analysis of the Pd Bragg reflections proves that no hydrogen is incorporated into the palladium. However, the FWHM widths of the Pd reflections increase by more than a factor of ten. Additionally, one finds an irreversible increase of the Pd layer thickness of up to 5 Å.

These observations can be explained by a „fold of a relief“ at the niobium surface in connection with the abovementioned glide process. The „fold-process“ with its lattice imperfections, like grain boundaries and misfit dislocations, is responsible for the observed changes of the niobium layers and consequently leads to a passive destruction of the

¹ The Nb layer is unloaded by evacuating the external hydrogen atmosphere. At the experimental temperatures of 250 °C – 300 °C the hydrogen then completely diffuses out of the sample.

palladium layers. The details of this unexpected gliding process are under further investigation by our group.

We would like to mention again that the combination of a high brilliance source of an ESRF bending magnet together with a high-load versatile six-circle-diffractometer – realized at ROBL – in connection with the specially adopted in situ loading chamber were mandatory for this kind of experiment, i.e. the *simultaneous* measurement of Bragg reflections in three orthogonal directions and specular reflectivity *under identical experimental conditions* for the low scattering system niobium on sapphire.

[1] Miceli, P.F., Zabel, H., Dura, J.A., and Flynn, C.P. (1991). *Anomalous lattice expansion of metal-hydrogen thin films*. Journal of Materials Research, 6, (5), 964-968.

Determination of radionuclide speciation in aqueous solutions by EXAFS spectroscopy

T. Reich, L. Baraniak, G. Bernhard, H. Funke, G. Geipel, C. Hennig, A. Roßberg
Forschungszentrum Rossendorf e.V., Institute of Radiochemistry, Dresden, Germany

Introduction

A significant part of environmental research on radionuclides is devoted to the determination of fundamental parameters that allow to understand and to predict the migration behavior of radionuclides in the bio- and geosphere. Almost every radionuclide interaction in the environment involves aqueous systems, e.g., complex formation with dissolved organic substances, colloid formation, sorption onto mineral surfaces, interaction with microorganisms, dissolution and precipitation, and redox reactions [1].

Extended X-ray absorption fine structure (EXAFS) spectroscopy is a powerful tool for the determination of molecular-level information on the speciation of radionuclides in aqueous solutions. The speciation not only describes the type of the radionuclide and its concentration but also its oxidation state and coordination sphere. The structural parameters of the radionuclide surrounding, i.e., bond distances, coordination numbers, and type of neighboring atoms, can be determined by EXAFS spectroscopy. The X-ray absorption near-edge structure (XANES) contains information on the electronic structure and the molecular symmetry of the radionuclide.

Although EXAFS and XANES spectroscopies have demonstrated their potentials in many areas of research since the mid seventies, they were rarely used in radionuclide studies until the mid nineties. Only then it became possible at a few synchrotron light sources in the world to implement protocols and procedures allowing to handle radionuclides safely at large multi-user facilities. However, these protocols impose restrictions on the activity and type of radionuclides that can be studied and do not, usually, allow for any sample manipulation.

The Rossendorf Beamline (ROBL) is unique in that sense that it operates the first experimental station dedicated to X-ray absorption spectroscopy on radionuclides at a synchrotron light source in Europe. At ROBL it is possible to study solid and liquid radionuclide samples of the following actinides Th-nat, Pa-231, U-nat, Np-237, Pu-239, Pu-242, Am-241, Am-243 as well as Ra-226, Po-208, and Tc-99 [2]. The maximal total activity authorized to be at ROBL at any given time is 185 MBq (5 mCi). In addition to all the advantages offered by a third-generation synchrotron light source as the ESRF, the uniqueness of ROBL is also due to the possibility of sample manipulation in a specially designed glove box before or during the measurement.

The first X-ray absorption spectra of uranium sample were collected at ROBL in August 1998 followed by the first X-ray absorption fine structure (XAFS) measurements on neptunium and technetium samples in November 1998. Since the beamline was still in commissioning at that time, some of the experiments were designed to test ROBL's technical capabilities for XAFS measurements. Due to the importance of radionuclide speciation in aqueous systems mentioned above, this report will highlight some results obtained on solutions of Np, Tc, and U using XAFS spectroscopy and illustrate the type of information that can be obtained at ROBL.

Experimental

This section describes briefly sample preparation, data collection and data analysis. More details are given in the corresponding Experimental Reports at the end of this report.

For EXAFS measurements on liquid samples, 4 ml of the solution was filled in a polyethylene cuvette, which was sealed and put in a polyethylene bag. Multiple scans of the EXAFS were collected at room temperature using the Si(111) double-crystal monochromator [2, this report, p.5]. The energy scale was calibrated using the first inflection point of the absorption spectra of various metal foils. The data were analyzed according to standard procedures [3] using the software EXAFSPAK [4]. Theoretical scattering phases and amplitudes were calculated using the scattering code FEFF6 [5].

Neptunium samples

A series of aqueous solutions containing 50 mM Np in three different oxidation states was prepared by dissolving solid $\text{NpO}_2(\text{NO}_3)$ in 0.1 M HNO_3 . The isotope used was Np-237. Solution Np1 consisted of 50 mM Np(IV) in 0.1 M HNO_3 and 2 M H_2SO_4 . The sulfuric acid was added to stabilize the Np(IV) oxidation state in the solution. The composition of solutions Np2 and Np3 was 50 mM Np(V) and Np(VI), respectively, in 0.1 M HNO_3 . The different oxidation states of Np were obtained by electrochemical oxidation/reduction in a conventional H-formed electrolysis cell with a diaphragm between anode and cathode.

Technetium samples

Technetium Tc-99m is an important imaging agent in tumor diagnostic. EXAFS structural analysis of novel Tc complexes, which are synthesized by the Institute of Bioinorganic and Radiopharmaceutical Chemistry of the FZR, is the topic of intensive collaboration with the Institute of Radiochemistry [6, 7]. For Tc complexes, which do not form single crystals or do only exist in solutions, EXAFS spectroscopy is the only method that allows to obtain structural parameters of the near-neighbor surrounding of Tc. In order to evaluate the possibilities of ROBL's radiochemistry station for future EXAFS studies on Tc samples, two solutions were prepared for a first experiment with Tc-99 at ROBL. The amount of Tc in the concentrated sample with 127 mM $\text{NaTcO}_4(\text{aq})$ yielded an edge jump of ~ 1 across the Tc K-edge at 21 keV. The second sample was 100 times more dilute, i.e., the Tc concentration was 1.3 mM. This sample was measured in fluorescence mode using a quad pixel Ge fluorescence detector [8].

Uranium samples

Protocatechuic acid (PCA, 3,4-dihydroxy-benzoic acid) forms strong complexes with U(VI) and is an important wood degradation product present in waters of flooded uranium mines. The species distribution for 1 mM U(VI) and 50 mM PCA at $I = 0.1$ M was calculated under exclusion of CO_2 using the complexation constants determined by potentiometric pH titration [9] (see Fig. 1). The pH titration curves were evaluated assuming several 1:1, 1:2

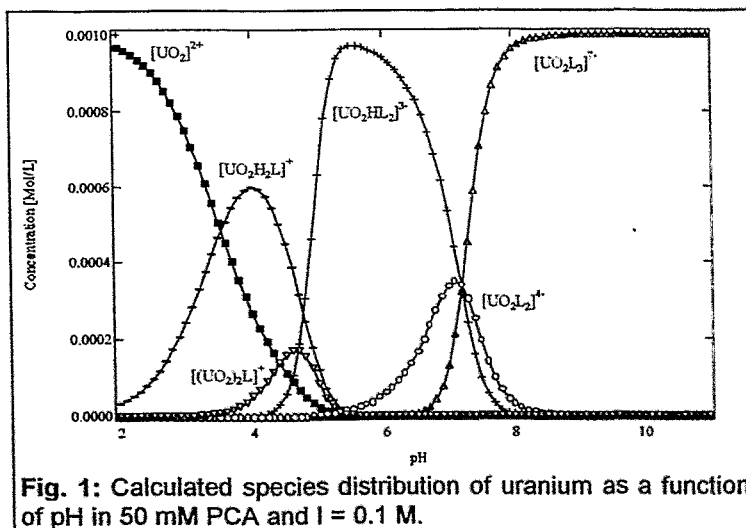


Fig. 1: Calculated species distribution of uranium as a function of pH in 50 mM PCA and $I = 0.1$ M.

and 1:3 uranyl complexes with PCA as indicated in Fig. 1. To validate these assumptions and to determine the role of the carboxylic COOH group and of the two phenolic OH groups of PCA in the complexation, seven solutions containing 1 mM $\text{UO}_2(\text{ClO}_4)_2$ and 50 mM PCA at different pH ranging from 4.30 to 6.75 were prepared under inert atmosphere for EXAFS measurements.

Results and Discussion

Np(IV), Np(V), and Np(VI) solutions

Figure 2 shows the normalized Np L(III)-edge XANES spectra of 50 mM Np solutions of the different Np oxidation states IV, V, and VI. In contrast to Np(IV), Np in its oxidation states V and VI is known to form trans dioxo cations. This is the reason why the Np L(III)-edge XANES spectra of Np(V) and Np(VI) have a similar shape, which significantly differs from that of Np(IV). As can be seen from Fig. 2, the increase in the formal oxidation state from V to VI leads to a small shift of the absorption edge by 2.5 eV toward higher energy. The observed spectral features allow to distinguish between these three different Np

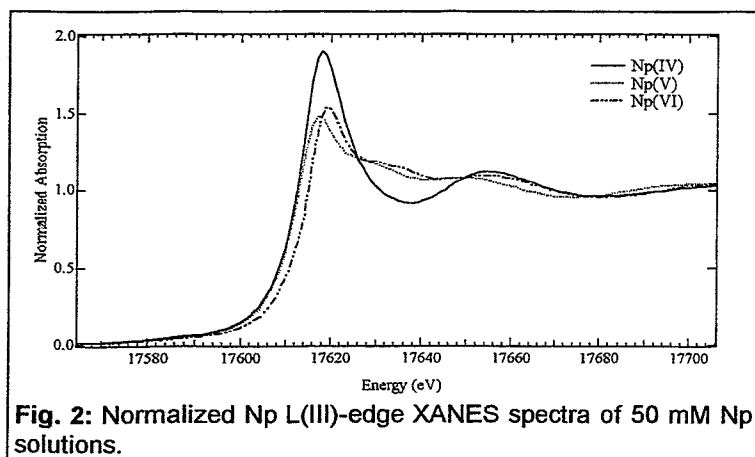


Fig. 2: Normalized Np L(III)-edge XANES spectra of 50 mM Np solutions.

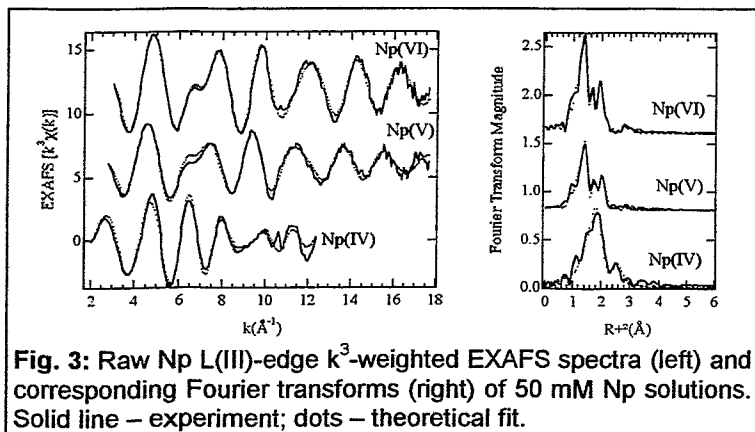


Fig. 3: Raw Np L(III)-edge k^3 -weighted EXAFS spectra (left) and corresponding Fourier transforms (right) of 50 mM Np solutions. Solid line – experiment; dots – theoretical fit.

oxidation states by Np L(III)-edge XANES spectroscopy.

In addition to the XANES spectra, information on the molecular structure is also contained in the EXAFS where it can be extracted in a quantitative way as several structural parameters. The raw EXAFS data and the best theoretical fit for solutions Np1-Np3 are shown in Fig. 3. The obtained structural parameters are given in Tab. 1. In solution Np1 Np(IV) is surrounded by 11 oxygen atoms at a distance of 2.39 Å. In the second coordination sphere we observed two sulfur atoms with a Np-S distance of 3.07 Å. This distance corresponds to a bidentate coordination of the SO_4^{2-} ion to the Np. Using the measured Np-O distance of 2.39 Å and the structural parameters of the SO_4^{2-} unit (S-O = 1.51 Å, angle O-S-O = 109° [10]), the calculated Np-S distance of 2.93 Å is in

good agreement with the measured value of 3.07 Å.

Both Np(V) and Np(VI) solutions Np2 and Np3 show the typical structural parameters of an actinyl ion. In case of Np(V), the distance to the axial oxygen atoms, O_{ax} , is 1.82 Å. In the equatorial plane the Np is surrounded by 4 water molecules with a Np- O_{eq} distance of 2.49 Å. The increase of the Np oxidation state from Np(V) to Np(VI) leads to a shortening of the axial and equatorial oxygen bonds by 0.07 Å and an increase of the number of water molecules attached to the neptunyl from four to five. The bond distances Np- O_{ax} and Np- O_{eq} of the Np(VI) solution are 1.75 Å and 2.42 Å, respectively.

The observed structural parameters for the Np-O bond distances of Np(IV) and Np(V) are in good agreement with the values reported for 5 mM Np in chlorine solution [11]. The structural parameters for Np(IV) sulfate and Np(VI) hydrate given in Tab. 1 are reported for the first time.

Tab. 1: EXAFS structural parameters for 50 mM Np solutions.

Sample	Shell	R(Å)	N	σ^2 (10^{-2} Å ²)
Np1, Np(IV)	Np-O	2.39	11.3(4)	1.18
	Np-S	3.07	2.2(3)	0.70
Np2 Np(V)	Np-O _{ax}	1.82	1.9	0.23
	Np-O _{eq}	2.49	3.6(2)	0.61
Np3 Np(VI)	Np-O _{ax}	1.75	2.0	0.15
	Np-O _{eq}	2.42	4.6(2)	0.56

Tc Model Solutions

The raw Tc K-edge k^3 -weighted EXAFS spectra of two model solutions containing 127 mM and 1.3 mM TcO_4^- are shown in Fig. 4. The spectrum of the 127 mM Tc solution was recorded in a single sweep up to $k=21$ Å⁻¹. During this sweep the counting time per data point was gradually increased from 2 to 20 sec. It follows from the best theoretical fit to the data (Fig. 4) that Tc is surrounded by 4 oxygen atoms ($N=4.1\pm 0.1$) at a distance of 1.72 ± 0.01 Å ($\sigma^2=0.0013\pm 0.0004$ Å²). The EXAFS spectrum of the 100 times more dilute $\text{NaTcO}_4(\text{aq})$ sample is also shown in Fig. 4 and represents an average of four sweeps measured in fluorescence mode. The intensity of the Tc $K\alpha$ fluorescence line was 1.2×10^5 counts/sec. The total count rate processed by the fluorescence detector was 6.4×10^5 counts/sec. Under these conditions, it was possible to analyze the Tc K-edge k^3 -weighted EXAFS spectrum of the 1.3 mM Tc solution up to $k=15$ Å⁻¹. The structural parameters obtained are the same as for the TcO_4^- ion in the concentrated solution, i.e., $N=3.9\pm 0.2$, $R=1.72\pm 0.01$ Å, and $\sigma^2=0.0016\pm 0.0003$ Å². These structural parameters agree with a previous Tc K-edge EXAFS measurement of a 200 mM $\text{NH}_4\text{TcO}_4(\text{aq})$ solution [12].

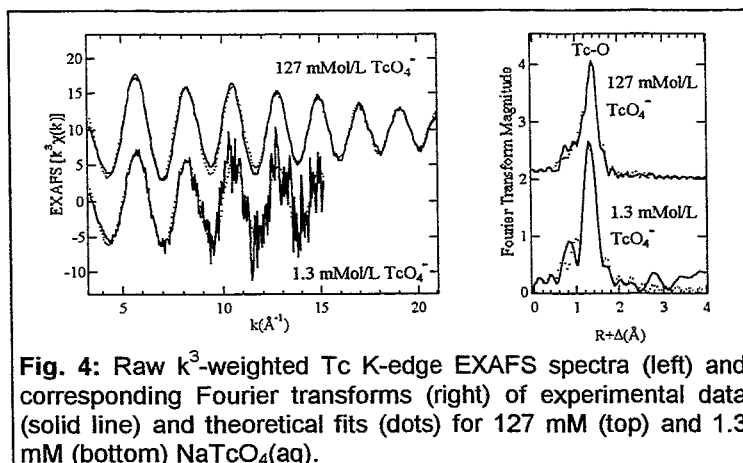


Fig. 4: Raw k^3 -weighted Tc K-edge EXAFS spectra (left) and corresponding Fourier transforms (right) of experimental data (solid line) and theoretical fits (dots) for 127 mM (top) and 1.3 mM (bottom) $\text{NaTcO}_4(\text{aq})$.

These measurements on model solutions show the capability of ROBL to record EXAFS spectra over a large energy range covering at least two orders of magnitude in metal concentration due to the high degree of beam stability, which was achieved using an additional monochromator feed-back system. The possibility to record an EXAFS spectrum over 21 Å⁻¹ as in the case of the 127 mM Tc solution, which is a record in

itself, is of great practical importance. The ability to resolve neighboring atoms as individual coordination shells, i.e., the expected smallest interatomic distance known as resolution ΔR , is given by the ratio $\Delta R=\pi/2\delta k$, where δk is the k -range of the data. For the two spectra given in Fig. 4, the expected resolution ΔR is 0.09 and 0.13 Å, respectively.

U(VI) complexation with protocatechuic acid (PCA)

Figure 5 depicts the raw U L(III)-edge k^3 -weighted EXAFS spectra and corresponding Fourier transforms of seven solutions with 1 mM U(VI) and 50 mM PCA as a function of pH ranging from 4.30 to 6.75. A significant change in the shape of the EXAFS with pH is observed in the k -range between 6 to 8 Å⁻¹. The structural parameters determined for the sample at pH 4.30 can be summarized as follows. The uranium is surrounded by two axial oxygen atoms, O_{ax} , at a distance of 1.79 ± 0.02 Å. The equatorial coordination shell consists of approximately 6 oxygen atoms, O_{eq} , with an $U-O_{eq}$ distance of 2.45 ± 0.02 Å. This long $U-O_{eq}$ distance is typical for bidentate coordination of the carboxylic group to the uranyl unit (see Fig. 6, left) [13, 14].

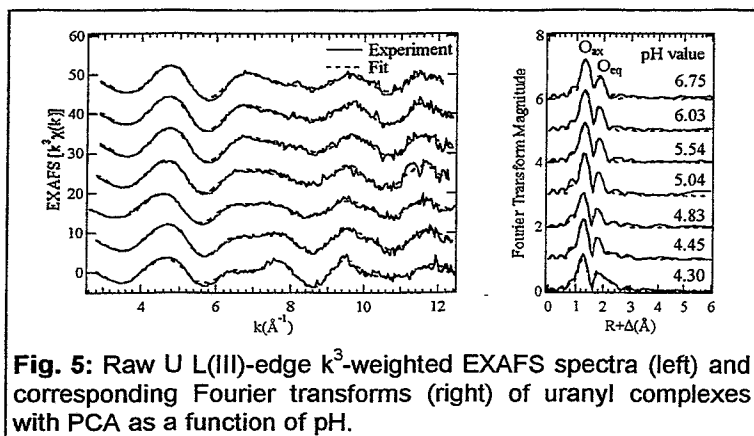


Fig. 5: Raw U L(III)-edge k^3 -weighted EXAFS spectra (left) and corresponding Fourier transforms (right) of uranyl complexes with PCA as a function of pH.

As one can see from the Fourier transforms given in Fig. 5, the $U-O_{eq}$ bond distance decreases with increasing pH. For the sample at pH 6.75, the $U-O_{eq}$ bond distance is $2.36 \pm 0.02 \text{ \AA}$, i.e., almost 0.1 \AA shorter than at pH 4.30. At high pH, the PCA ligands coordinate to the uranyl group in an o-diphenolic bonding fashion and the carboxylic group is not involved in the complex formation (see Fig. 6, right).

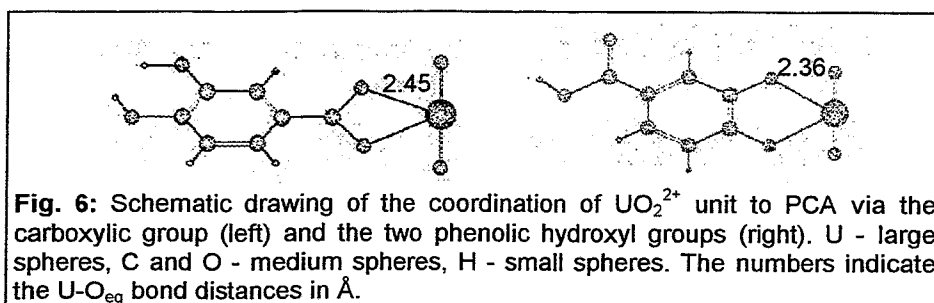


Fig. 6: Schematic drawing of the coordination of UO_2^{2+} unit to PCA via the carboxylic group (left) and the two phenolic hydroxyl groups (right). U - large spheres, C and O - medium spheres, H - small spheres. The numbers indicate the $U-O_{eq}$ bond distances in \AA .

Since the synchrotron beam probes the entire volume of the sample, the EXAFS spectrum is an average over all uranyl species present in the solution. If one assumes that the solutions at pH 4.30 and 6.75 contain only one uranyl species of different structures, it is possible to describe the EXAFS spectra at pH between 4.45 and 6.03 as a superposition of the EXAFS spectra of these two species. For pH 6.75 this assumption is supported by our previous EXAFS measurement of a sample at pH 10 where we observed similar structural parameters as at pH 6.76 [15]. The calculated contributions of the two coordination modes, i.e., bidentate-carboxylic and o-diphenolic, are shown in Fig. 7. At pH ~ 4.7 both uranyl complexes with PCA are equal in concentration. The bidentate coordination of the carboxylic COOH group dominates at pH lower than 4.7. However, above pH 4.7 the uranyl cation is predominantly coordinated by two neighboring phenolic OH groups as illustrated in

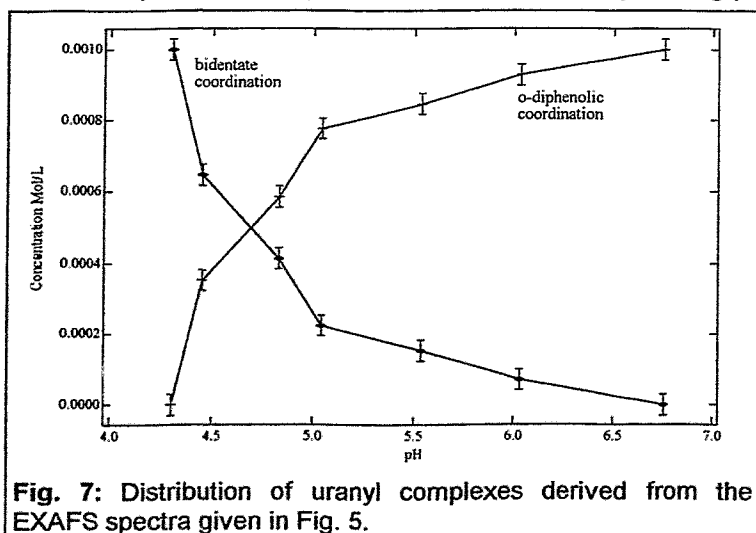


Fig. 7: Distribution of uranyl complexes derived from the EXAFS spectra given in Fig. 5.

Fig. 6. The calculated species distribution given in Fig. 1 shows also a change around pH 4.7. The concentration of the 1:1 complex $[UO_2H_2L]^+$ decreases and that of the 1:2 complex $[UO_2HL_2]^{3-}$ increases. The agreement between the calculated (Fig. 1) and measured (Fig. 7) species distributions supports the complexation models used to extract the complexation constants from the potentiometric pH titration data.

This EXAFS study of uranyl complexation demonstrates the important role EXAFS spectroscopy can play for the validation of structural models, which are needed as input parameters for the determination of complexation constants from titration experiments. The molecular-level information obtained by EXAFS is essential for the validation of models that give a macroscopic description of the complexation. EXAFS analysis can also be used to validate or to suggest surface-complexation models that describe the interaction of radionuclides at mineral-water interfaces.

Summary and Conclusions

The following conclusions can be drawn from the EXAFS and XANES studies performed on Np, Tc, and U solutions at ROBL: 1) All EXAFS spectra measured in transmission mode in the energy range of 17 - 21 keV, which have a high signal-to-noise ratio, demonstrate the excellent performance of all beamline components including the synchrotron source, the monochromator and mirrors, sample positioners, and detectors. Based on the author's experience from radionuclide experiments on second-generation synchrotron light sources, we conclude that the large k-range and data quality that can be achieved at ROBL are superior. 2) EXAFS spectroscopy is a powerful technique to obtain structural information on radionuclide species in solutions. The EXAFS study on U(VI) complexation with PCA demonstrated the interplay between EXAFS and other techniques, in this case potentiometric pH titration. The complexation constants obtained by titration are needed to calculate the species distribution in order to prepare meaningful samples for EXAFS measurements. The molecular level information, which is the result of the EXAFS analysis, can be used to validate or to modify the underlying complexation models. 3) The actinide L(III)-edge XANES spectra are sensitive to the electronic and molecular structure of the actinide complexes and can be used to determine the oxidation state of the element under study [16]. XANES spectroscopy is especially valuable in cases where other analytical techniques, like UV/Vis spectroscopy, are limited due to matrix effects. 4) One disadvantage of performing experiments at a synchrotron light source is that the samples are usually prepared at the home institute and shipped to the experimental station, which can introduce unwanted changes in the sample composition during transportation. This is especially the case for experiments with radionuclides. At ROBL it is possible to overcome this disadvantage by preparing/modifying the radioactive samples in the glove box. For example, it is difficult to stabilize the Np(III) hydrate in solution. But with an electrochemical cell positioned in the synchrotron beam, it will be possible in the future to prepare the Np(III) oxidation state and to measure the XANES and EXAFS spectra in situ. Additional experimental possibilities, which are not discussed here, are available at ROBL for time-dependent and spatially-resolved XAFS studies using the monochromator in quick-EXAFS mode and by focusing the synchrotron beam [2]. In conclusion, the radiochemistry station at ROBL provides many unique features, which will contribute significantly to a better understanding of processes that are currently of great interest in environmental radiochemistry.

References

- [1] R.J. Silva, H. Nitsche, *Radiochim. Acta*, **70/71** (1995) 377.
- [2] W. Matz, et al., *J. Synchrotron Rad.*, **6** (1999) in press.
- [3] D.C. Koningsberger, R. Prins, *X-Ray Absorption: Principles, Applications, Techniques of EXAFS, SEXAFS and XANES*. John Wiley & Sons, New York, 1988.
- [4] G.N. George, I.J. Pickering, Stanford Synchrotron Radiation Laboratory, EXAFSPAK: A Suite of Computer Programs for Analysis of X-Ray Absorption Spectra (1995).
- [5] S.I. Zabinsky, J.J. Rehr, A. Ankudinov, R.C. Albers, M.J. Eller, *Phys. Rev. B*, **52** (1995) 2995.

- [6] B. Johannsen, R. Jankowsky, B. Noll, H. Spies, T. Reich, H. Nitsche, L.M. Dinkelborg, C.S. Hilger, W. Semmler, *Appl. Radiat. Isot.*, **48** (1997) 1045.
- [7] R. Jankowsky, S. Kirsch, T. Reich, H. Spies, *J. Inorg. Biochem.*, **70** (1998) 99.
- [8] J.J. Bucher, P.G. Allen, N.M. Edelstein, D.K. Shuh, N.W. Madden, C. Cork, P. Luke, D. Pehl, D. Malone, *Rev. Sci. Instrum.*, **67** (1996) 1.
- [9] L. Baraniak, M. Schmidt, G. Bernhard, H. Nitsche, FZR Institute of Radiochemistry Annual Report 1996, (1997) 28.
- [10] A.F. Hollemann, *Lehrbuch der anorganischen Chemie*. de Gruyter, Berlin, 1995.
- [11] P.G. Allen, J.J. Bucher, D.K. Shuh, N.M. Edelstein, T. Reich, *Inorg. Chem.*, **36** (1997) 4676.
- [12] P.G. Allen, G.S. Siemering, D.K. Shuh, J.J. Bucher, N.M. Edelstein, C.A. Langton, S.B. Clark, T. Reich, M.A. Denecke, *Radiochim. Acta*, **76** (1997) 77.
- [13] M.A. Denecke, T. Reich, S. Pompe, M. Bubner, K.H. Heise, H. Nitsche, P.G. Allen, J.J. Bucher, N.M. Edelstein, D.K. Shuh, *J. Phys. IV France*, **7** (1997) C2-637.
- [14] M.A. Denecke, T. Reich, M. Bubner, S. Pompe, K.H. Heise, H. Nitsche, P.G. Allen, J.J. Bucher, N.M. Edelstein, D.K. Shuh, *J. Alloys Compounds*, **271-273** (1998) 123.
- [15] A. Roßberg, T. Reich, C. Hennig, M.A. Denecke, L. Baraniak, H. Nitsche, FZR Institute of Radiochemistry Annual Report 1997, FZR-218 (1998) 72.
- [16] S.D. Conradson, A. Al Mahamid, D.L. Clark, N.J. Hess, E.A. Hudson, M.P. Neu, P.D. Palmer, W.H. Runde, C.D. Tait, *Polyhedron*, **17** (1998) 599.

Solution coordination chemistry of uranium in the binary $\text{UO}_2^{2+}\text{-SO}_4^{2-}$ and the ternary $\text{UO}_2^{2+}\text{-SO}_4^{2-}\text{-OH}^-$ system, a combined EXAFS and ^{17}O NMR study.

H. Moll^a, T. Reich^b, C. Hennig^b, A. Rossberg^b, Z. Szabó^a, and I. Grenthe^a

^a Department of Chemistry, Inorganic Chemistry, The Royal Institute of Technology, Teknikringen 30, 10044 Stockholm, Sweden.

^b Institute of Radiochemistry, Forschungszentrum Rossendorf e.V., P.O. Box 510119, 01314 Dresden, Germany.

Introduction

UO_2^{2+} forms binary complexes $\text{UO}_2(\text{SO}_4)_n^{2-2n}$, $n = 1 - 3$ in slightly acid solution. The complexes are moderately strong, $\beta_1 \approx 50$, and different experimental techniques (potentiometry, spectrophotometric measurements, and TRLFS) have been used to determine the composition and stability of these species [1-3]. The occurrence of uranium (10^{-5} M) and sulfate (3×10^{-2} M) in some ground and surface waters indicates that uranyl sulfate species may be important for the understanding of the mobility of uranium in nature. At higher pH a number of different ternary complexes containing both hydroxide/oxide and sulfate are formed. This was first shown by Peterson [4] who determined the conditional hydrolysis constants of U(VI) in 1.5 M Na_2SO_4 , and showed that both the stoichiometry and the equilibrium constants were different from those previously found in perchlorate media. This can only be explained by the formation of ternary complexes containing coordinated sulfate. An attempt to determine the stoichiometry with respect to sulfate was first made by Grenthe and Lagerman, who studied the system at different total concentrations of sulfate and from these data proposed the stoichiometry and stability of the major ternary complexes: $(\text{UO}_2)_2(\text{OH})_2(\text{SO}_4)_2^{2-}$, $(\text{UO}_2)_3(\text{OH})_4(\text{SO}_4)_4^{4-}$, and $(\text{UO}_2)_5(\text{OH})_8(\text{SO}_4)_6^{10-}$ [5]. Equilibrium analysis used in [1-3] gives only the analytical composition and the amounts of species present in solution, these are in general in rapid equilibrium. Information about chemical structure and dynamics of the systems must be obtained using other experimental methods. The structure and dynamics of aqueous uranyl sulfato species are poorly understood. Infrared (IR) and Raman measurements gave no clear answer regarding the mode of co-ordination of sulfate, unidentate, bridging or chelating, to UO_2^{2+} [6, 7], however the authors assume that a bridging bidentate behaviour is more likely at $\text{SO}_4:\text{U}$ ratios, > 5 . In this study we have determined the structure and dynamics in the systems outlined above. Two sets of experiments have been made: determination of the mode of coordination of sulfate using U L_{III} -edge EXAFS spectroscopy; ^{17}O -NMR spectroscopy to determine the reaction dynamics in the binary and ternary system.

Experimental

EXAFS measurements. Samples were prepared by taking aliquots of the acidic $\text{UO}_2(\text{ClO}_4)_2$ stock solution to get a final uranyl concentration of 0.05 M. The sulfate concentration in the acidic test solutions (samples A - C) was adjusted using H_2SO_4 or Na_2SO_4 . The pH of sample D was adjusted with NaOH. Speciation calculations were made using known equilibrium constants and the program SOLGASWATER [8]. Solid $\text{UO}_2\text{SO}_4 \cdot 2.5\text{H}_2\text{O}$, was synthesised as described in [9] and was mixed with polyethylene and then pressing to give pellets with a diameter of 13 mm. EXAFS data were recorded at the Rossendorf Beamline (ROBL) at the ESRF in Grenoble. The transmission spectra were measured at room temperature using a cooled Si(111) double crystal monochromator of fixed-exit type ($E = 5\text{-}35$ keV). The higher harmonics were rejected by two Si and Pt coated mirrors. For energy

calibration of the sample spectra, the spectrum from a Zr foil was recorded simultaneously. The ionisation energy of the U L_{III} electron, E_0 , was arbitrarily defined as 17 185 eV. The data were treated using the WinXAS software [10]. Theoretical backscattering phase and amplitude functions, $\delta(k)$ and $F(k)$, used in data analysis were calculated for the test compound, $UO_2SO_4 \cdot 2.5H_2O$ [11], using the FEFF7 [12] program.

NMR measurements. The ^{17}O NMR spectra were measured using 10 mm sample tubes, on a Bruker AM400 spectrometer at $-5^\circ C$, unless otherwise mentioned. 5% D_2O in the test solutions were used to obtain locked mode. The probe temperature was adjusted using a Bruker Eurotherm variable temperature control unit and was measured by a calibrated Pt-100 resistance thermometer. The chemical shifts are given in ppm, using external water as a reference. The ^{17}O -NMR measurements were made using an acidic ^{17}O -enriched uranyl stock solution prepared as described previously using $H_2^{17}O$ (29% ^{17}O Campro Science) [13]. The line widths were determined by fitting a Lorentzian curve function to the measured signal using the WIN-NMR program [14].

Results and discussion

EXAFS in the UO_2^{2+} - SO_4^{2-} System. The isolated EXAFS oscillations and corresponding Fourier transforms for samples A to C and E are shown in Fig. 1. The obtained structural parameters are given in Tab. 1.

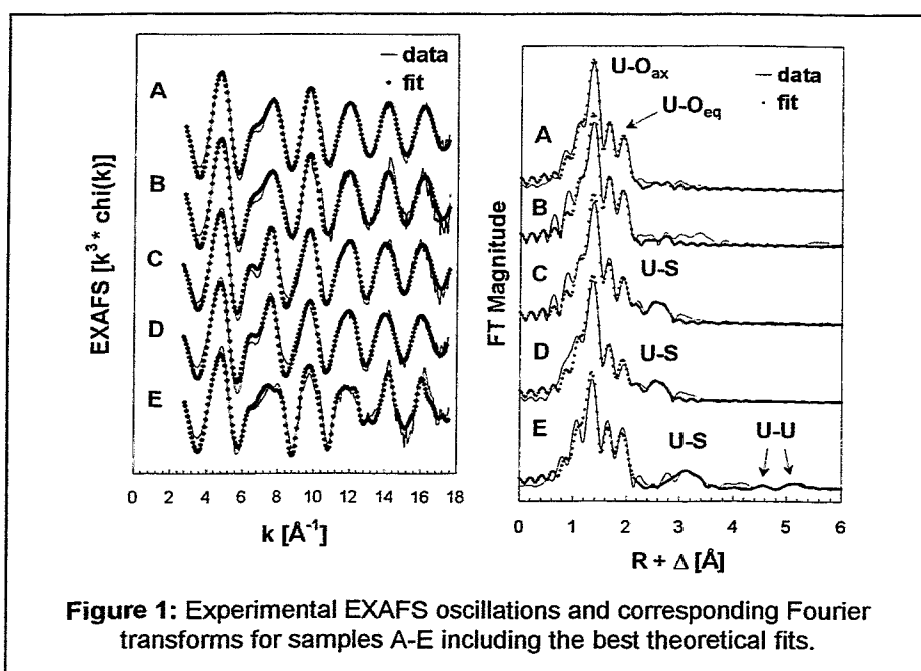


Figure 1: Experimental EXAFS oscillations and corresponding Fourier transforms for samples A-E including the best theoretical fits.

In all samples uranium is surrounded by two O_{ax} atoms at $1.77 \pm 0.01 \text{ \AA}$. Approximately five O_{eq} atoms are coordinated to the linear uranyl group at 2.39-2.43 \AA in the equatorial plane. In sample C, where $UO_2(SO_4)_2^{2-}$ is the dominant species, approximately two sulfur atoms were located at 3.11 \AA from uranium. This is in agreement with the value 3.07 \AA , reported by Blatov *et al.* in the solid $UO_2SO_4 \cdot 2CH_3CON(CH_3)_2$, where SO_4^{2-} is bidentate coordinated to UO_2^{2+} [15]. The U-S distance is longer, 3.63 \AA , if sulfate is monodentate and bridging, like in $UO_2SO_4 \cdot 2.5H_2O$. There was also evidence for U-U interactions. The U-U distance at 5.40 \AA can be clearly identified (8.2 % of the total EXAFS oscillation). The U-U distance at 4.80 \AA was included according to the crystal structure (3.8 % of the total EXAFS oscillation). In samples A and B it is difficult to localise the S backscatterer. In sample B one could

Table 1: Fit parameters to U L_{III} edge EXAFS data in the binary uranyl sulfate system (Samples A-C, and E) and the ternary uranyl hydroxide sulfate system (Sample D); ΔE_0 set at -7.0 eV. XRD values from reference [11] are in parenthesis.

Sample	Scattering Path	N	σ^2 (Å ²)	R (Å)	Residuals
A 82% UO ₂ SO ₄ (aq) 12% UO ₂ ²⁺	U-O _{ax}	1.9 ± 0.2	0.0013	1.77 ₃	11.5
	U-O _{eq}	5.0 ± 0.4	0.0084	2.41 ₂	
	U-S	1f	0.0105	3.11f	
B 50% UO ₂ SO ₄ (aq) 50% UO ₂ (SO ₄) ₂ ²⁻	U-O _{ax}	1.9 ± 0.2	0.0013	1.77 ₂	18.7
	U-O _{eq}	5.0 ± 0.4	0.0082	2.40 ₄	
	U-S	1f	0.0086	3.14 ₀	
C 12% UO ₂ SO ₄ (aq) 88% UO ₂ (SO ₄) ₂ ²⁻	U-O _{ax}	2.0 ± 0.2	0.0013	1.78 ₁	13.4
	U-O _{eq}	5.0 ± 0.4	0.0107	2.43 ₇	
	U-S	2.2 ± 0.5	0.0075	3.11 ₃	
D 10% UO ₂ (SO ₄) ₂ ²⁻ 50% (UO ₂) ₅ (OH) ₈ (SO ₄) ₆ ¹⁰⁻ 20% (UO ₂) ₃ (OH) ₄ (SO ₄) ₃ ⁴⁻ 20% (UO ₂) ₂ (OH) ₂ (SO ₄) ₂ ²⁻	U-O _{ax}	2.0 ± 0.2	0.0017	1.78 ₂	14.4
	U-O _{eq}	5.0 ± 0.4	0.0119	2.43 ₄	
	U-S	2.1 ± 0.5	0.0072	3.10 ₅	
E UO ₂ SO ₄ ·2.5H ₂ O	U-O _{ax}	1.7 ± 0.2 (2)	0.0011	1.77 ₀ (1.76 ₀)	17.5
	U-O _{eq}	4.9 ± 0.4 (5)	0.0066	2.39 ₃ (2.40 ₉)	
	U-S	1.1 ± 0.3 (1)	0.0020	3.62 ₅ (3.58 ₃)	
	U-U	0.8 ± 0.2 (1)	0.0075	4.87 ₀ (4.81 ₀)	
	U-U	0.9 ± 0.2 (1)	0.0045	5.40 (5.44 ₄)	

f: held constant during the fit.

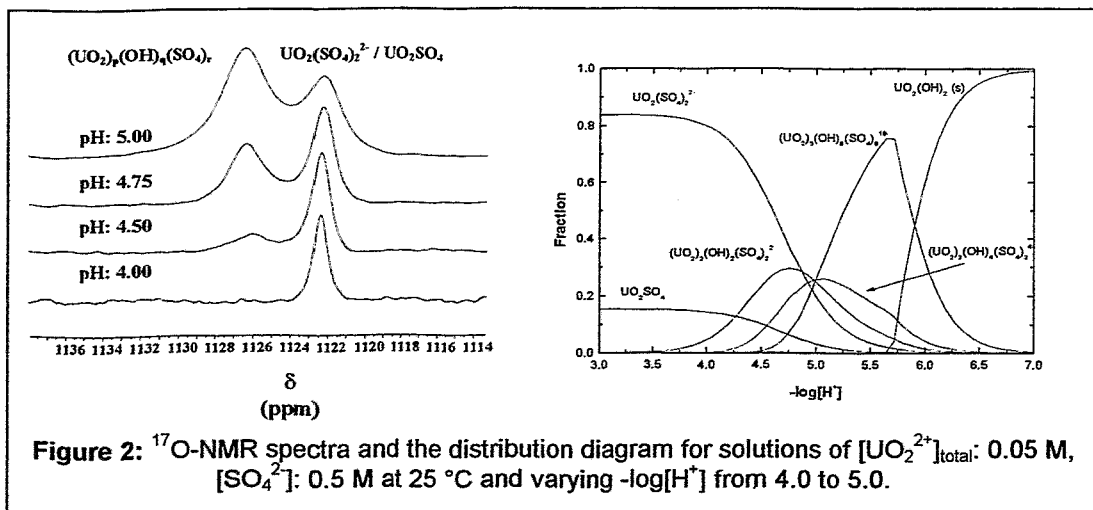
assume both a shorter U-S distance at 3.11 Å and a longer U-S distance at about 3.60 Å. We found it unlikely, considering the results from sample C, that samples A and B contained a monodentate bonded sulfate and therefore included a U-S distance fixed at 3.11 Å in the model. The short U-S distance in samples A and B are supported by the presence of a residual oscillation after subtraction the model EXAFS oscillation obtained without including the U-S shell. This remaining oscillation showed in all solutions the same pattern at a k range of 2.8 to 9.2 Å⁻¹. The resulting peak was FT filtered and the oscillation could be described using a U-S distance of 3.16 Å. However, from the results of the samples A and B alone one cannot conclude the presence of a bidentate sulfate. But by considering all information the EXAFS data indicate clearly that SO₄²⁻ is bonded in a bidentate fashion to the uranyl unit in solution.

¹⁷O-NMR studies of the UO₂²⁺-SO₄²⁻ System (for detailed information see [16]). The line width and the chemical shift increase with the sulfate concentration is a result of the formation of uranyl sulfate complexes. The only observed peak in the binary system indicates a fast exchange between the complexes on the ¹⁷O-NMR time-scale. The measured line shape can then give information about the dynamics of the system, using the matrix formalism introduced by Reeves and Shaw [17]. The chemical environment of the uranyl ion is changing by sulfate exchange which takes place via two pathways, and the pseudo first order rate constants describing the exchange between UO₂²⁺ and UO₂SO₄, $k_{1(obs)}$, and between UO₂SO₄ and UO₂(SO₄)₂²⁻, $k_{2(obs)}$, can be determined from the line width using the formalism described above. The following reactions can contribute to the pseudo first order rate constants: a) UO₂²⁺ + SO₄²⁻ ⇌ UO₂SO₄ [$k_1=(3.4±0.5) × 10^3 M^{-1}s^{-1}$], b) UO₂²⁺ + UO₂(SO₄)₂²⁻ ⇌ 2UO₂SO₄ [$k_2=(2.1±0.3) × 10^5 M^{-1}s^{-1}$], c) UO₂SO₄ + SO₄²⁻ ⇌ UO₂(SO₄)₂²⁻

$[k_3=(1.4\pm 0.2) \times 10^3 \text{ M}^{-1}\text{s}^{-1}]$, and d) $\text{U}^*\text{O}_2^{2+} + \text{UO}_2\text{SO}_4 \rightleftharpoons \text{U}^*\text{O}_2\text{SO}_4 + \text{UO}_2^{2+}$ $[k_4=(9.3\pm 0.8) \times 10^4 \text{ M}^{-1}\text{s}^{-1}]$. Similar type of reactions were observed in the case of the binary uranyl-fluoride system [18]. The mechanism consists of two steps, a faster bonding of a chelating sulfate, $k_1 = 3.4 \times 10^3 \text{ M}^{-1}\text{s}^{-1}$, to form the neutral complex UO_2SO_4 , which is followed by the coordination of a second sulfate with $k_3 = 1.4 \times 10^3 \text{ M}^{-1}\text{s}^{-1}$. These rate constants are similar to those measured for the binary uranyl-fluoride system [18]. Szabó *et al.* found a rate constant of $k_{m,n} \sim 5 \times 10^4 \text{ M}^{-1} \text{ s}^{-1}$ for the fluoride exchange reactions and suggested an intimate mechanism of the Eigen-Wilkins type. The experimental findings, $k_x \sim 7 \times 10^4 \text{ M}^{-1}\text{s}^{-1}$, indicate that the rate of complex formation is not strongly dependent on the entering ligand, F^- ($k_{m,n} \sim 5 \times 10^4 \text{ M}^{-1} \text{ s}^{-1}$ in [18]) or SO_4^{2-} , supporting an Eigen-Wilkins mechanism.

EXAFS in the $\text{UO}_2^{2+}\text{-SO}_4^{2-}\text{-OH}$ System. Figure 1 depicts a typical example for the EXAFS data measured in the ternary system. The results (Table 1, sample D) showed no significant differences from the binary uranyl sulfate system. Approximately two sulfur atoms were measured at 3.10 Å indicating that SO_4^{2-} is bonded as a chelate in the uranyl hydroxo species. We can exclude single bonded bridging, but not chelating bridging co-ordination, *c. f.* the structure proposals in Grenthe and Lagerman. Sulfate may like chromate [19] act as a bidentate bridging ligand to stabilize the polynuclear hydroxo complexes. According to the structural model of Grenthe and Lagerman and the coordination geometry of uranyl in polynuclear hydroxo complexes, it is not possible to coordinate more than 1.5 sulfates per uranyl unit. The theoretical coordination number of sulfur in sample D is between 1.2 and 1.5. The error in the coordination number using EXAFS is large, but the second number is not inconsistent with the theoretical value. Calculations using a fixed coordination number of 1.5 showed no significant changes in the results. A residual value of 14.8 was obtained compared to 14.4 when the coordination number was not fixed. No peaks corresponding to a U-U interaction between 4 and 6 Å were observed. Nevertheless, this is not an indication that the ternary species are not formed, the potentiometric measurements (see [16]) and the ^{17}O -NMR investigations clearly show the presence of polynuclear species. The measured EXAFS oscillations represents the sum of all absorber-backscatterer shell contributions. Such contributions which are out of phase, may result in the disappearance of a U-U peak. CaCO_3 is one example for such "out-of-phase" effects [20]. Thompson *et al.* found that distant contributions from U (4.9 to 5.2 Å) are weak and therefore might be difficult to detect in samples of unknown composition (see structural parameters of $\text{UO}_2\text{SO}_4 \cdot 2.5\text{H}_2\text{O}$ in Tab. 1) [21]. An other example might be the weak U-U interaction at 4.92 Å in $[(\text{UO}_2)_3(\text{CO}_3)_6]^{6-}$ [22].

^{17}O -NMR in the $\text{UO}_2^{2+}\text{-SO}_4^{2-}\text{-OH}$ System. ^{17}O -NMR was applied for the first time to obtain structural and dynamic information about this complicated system. ^{17}O -NMR spectra



measured at 0.05 M UO_2^{2+} in 2 M $NaClO_4$ + 0.5 M Na_2SO_4 and 25°C are summarized in Fig. 2.

The appearance of a second peak in addition to the peak of the binary species, which then dominates the spectra at increasing $-\log[H^+]$ is a clear indication for the formation of ternary uranyl sulfate hydroxide species, as expected from the speciation calculations. The integrals of the two peaks give information on the amount of uranium present as mononuclear and polynuclear complexes. This quantity was compared with that calculated from the equilibrium constants. The agreement between the two values was within 15%, which is within the accuracy of the two measurements. The only broad peak at 1126.2 ppm shows that it is not possible to identify the different polynuclear complexes, very likely because of the small chemical shift difference and the fast exchange between them. From the experiments we have made it is not possible to get more concrete information about the dynamics of the ternary systems. Co-ordination of sulfate to the polynuclear hydroxide complexes results in a fairly large change in the chemical shift of the "yl"-oxygens, from 1120 ppm in $(UO_2)_2(OH)_2^{2+}$ and 1124.7 ppm in $(UO_2)_3(OH)_5^+$ measured by Jung et al. [23], to 1126.2 ppm in the ternary system.

Acknowledgements

The financial support by the European Commission within the Training and Mobility of Researcher (TMR) Program under contract number ERBFMBICT972296 is greatly acknowledged. The authors are thankful for the help of Melissa A. Denecke especially with the interpretation of the EXAFS data. The EXAFS measurements were done at ROBL at the ESRF.

References

- [1] Ahrlund, S.: Acta Chem. Scand. **5**, 1151-1167 (1951).
- [2] Geipel, G., Brachmann, A., Brendler, V., Bernhard, G. and Nitsche, H.: Radiochim. Acta **75**, 199-204 (1996).
- [3] Grenthe, I., Fuger, J., Konings, R.J.M., Lemire, R.J., Muller, A.B., Nguyen-Trung Cregu, Ch., Wanner, H.: *Chemical Thermodynamics of Uranium*, NEA OECD, 1992, p. 241ff.
- [4] Peterson, A.: Acta Chem. Scand. **15**, 101-120 (1961).
- [5] Grenthe, I., Lagerman, B.: Radiochim. Acta **61**, 169-176 (1993).
- [6] Gal, M., Goggin, P.L., Mink, J.: Spectrochim. Acta **48A(1)**, 121-132 (1992).
- [7] Nguyen-Trung, C., Begun, G.M., Palmer, D.A.: Inorg. Chem. **31**, 5280-5287 (1992).
- [8] Puigdomenech, I. *Input, Sed and Pedom: Computer Programs Drawing Equilibrium Diagrams*. Trita-00K-3010, RIT, Stockholm (1983).
- [9] Cordfunke, E.H.P.: J. Inorg. Nucl. Chem. **31**, 1327-1335 (1969).
- [10] Ressler, T.: J. Synchrotron Rad. **5**, 118-122 (1998).
- [11] Putten van der, N., Loopstra, B.O., Cryst. Struct. Com. **3**, 377-380 (1974).
- [12] Zabinsky, S. I.; Rehr, J. J.; Ankudinov, A.; Albers, R. C.; Eller, M. J.: Phys. Rev. B **52(4)**, 2995-3008 (1995).
- [13] Bányai, I., Glaser, J., Micskei, K., Tóth, I., Zékány, L.: Inorg. Chem. **34**, 3785-3796 (1995).
- [14] WIN-NMR, 950901.0 ed.; Bruker-Franzen Analytik GmbH.
- [15] Blatov, V.A., Serezhkina, L.B., Serezhkin, V.N., Zhurnal Strukturnoy Khimii **31**, 131-133 (1990).
- [16] Moll, H., Reich, T., Hennig, C., Rossberg, A., Szabó, Z., Grenthe, I.: *SOLUTION COORDINATION CHEMISTRY OF URANIUM IN THE BINARY $UO_2^{2+} - SO_4^{2-}$ AND THE TERNARY $UO_2^{2+} - SO_4^{2-} - OH$ SYSTEM*, submitted to Radiochim. Acta, (1999).
- [17] Reeves, L.W., Shaw, K.N., Can. J. Chem. **48**, 3641 (1970).
- [18] Szabó, Z., Glaser, J., Grenthe, I., Inorg. Chem. **35**, 1036-2044 (1996).
- [19] Michailov, Y.N., Gorbunova, Y.E., Demetschenko, E.A., Serezhkina, L.B., Serezhkin, V.N.: Zhurnal Neorganiceskoy Khimii **43**, 1831-1833 (1998).
- [20] Denecke, M.A.: personal communication.
- [21] Thompson, H.A., Brown, G.E., Parks, G.A.: Am. Mineral. **82**, 483-496 (1997).
- [22] Allen, P.G., Bucher, J.J., Clark, D.L., Edelstein, N.M., Ekberg, S.A., Gohdes, J.W., Hudson, E.A., Kaltsoyannis, N., Lukens, W.W., Neu, M.P., Palmer, P.D., Reich, T., Shuh, D.K., Tait, C.D., Zwick, B.D.: Inorg. Chem. **34**, 4797-4807 (1995).
- [23] Jung, W.-O., Harada, M., Tomiyasu, H., Fukutomi, H.: Bull. Chem. Soc. Jpn. **61**, 3895-3900 (1988).

Scheduled Experiments at ROBL-RCH

number	title	proposers	institution	experimen- tators	shifts
20_01_001	Uranium L _{III} -edge EXAFS measurements of uranium (VI) compounds; commissioning of ROBL-RCH	Reich, Bernhard, Geipel, Nitsche, Rutsch, Funke, Hennig, Scheidegger, Dähn	FZR (FWR), PSI	Funke, Hennig, Reich, Dähn, Roßberg	81
20_01_002	Neptunium L _{III} -edge and technetium K-edge x-ray absorption spectroscopy	Reich, Bernhard, Geipel, Rossberg, Funke, Hennig	FZR (FWR)	Funke, Seifert, Künstler, Hennig, Reich, Roßberg, Strauch	48
20_01_003	EXAFS Study of Ni, Zn, and Se Sorption on clay mixtures and cement phases	Reich, Scheidegger, Dähn, Funke, Hennig	PSI, FZR (FWR)	Scheidegger, Dähn, Spieler, Reich, Hennig, Roßberg, Strauch, Funke	21
20_01_004	EXAFS study of uranium(VI) sorption on zircon and zirconia	Simoni, Catalette, Lomenech	IPN, GRECI	Simoni, Lomenech, Reich, Hennig, Roßberg	6
20_01_005	Uranium(VI) complexation in alkaline solutions	Moll, Denecke	KTH, INE	Moll, Reich, Hennig, Roßberg	6
20_01_006	Uranium (VI) EXAFS spectroscopy of organic complexes	Reich, Schmeide, Rutsch, Funke, Hennig, Roßberg	FZR (FWR), Uni Louvain	Schmeide, Pompe, Funke, Vanbegin, Froment, Hennig, Reich, Roßberg, Funke	52
20_01_007	Thorium L _{III} -edge and Ni K-edge EXAFS measurements of solutions and clay pastes	Scheidegger, Dähn, Spieler	PSI	Scheidegger, Spieler, Dähn, Hennig, Reich, Roßberg	15
20_01_008	EXAFS Study of Neptunium Hydrates	Reich, Hennig, Roßberg, Funke, Rutsch, Amayri	FZR (FWRS, FWRE)	Rutsch, Amayri, Funke, Hennig, Reich, Roßberg	8

ESRF Allocated Time for ROBL-RCH

number	title	proposers	institution	experimen- tators	shifts
CH-618	Coordination sphere of the uranyl ion in solutions of perchloric and triflic	Lützenkirchen, Barillon, Billard, Gaertner, Jung, Rossini	IreS Strasbourg	Billard, Lützenkirchen, Rossini, Hennig, Reich, Roßberg	21
CH-619	The influence of Pu local environment on the non ideality of (U,Pu)O ₂ solid solution	Ripert, Beauvy, Desgranges, Petit	CE Cadarache, CE Grenoble	Ripert, Caranoni, Desgranges, Ruello, Hennig, Reich, Roßberg	21

Scheduled Experiments at ROBL-MRH

number	title	proposers	institution	experimen- tators	shifts
20_02_001	Strain effects in Si after C implantation	F. Eichhorn	FZ Rossendorf (FWIS)	Eichhorn, Schell	10
20_02_002	Specular reflectivity on Cu/Co multilayers near absorption edges	F. Prokert	FZ Rossendorf (FWIS)	Prokert, Schell, Matz	8
20_02_003	Grain size and stress in UFG nickel	E. Thiele	TU Dresden, IPMK	Thiele, Hecker, Schell, Reichel	8
20_02_004	Anisotropic deformation of Nb films during H load	J. Peisl	LMU Munich	Edelmann, Schmidt, Berberich, Schell	16
20_02_005	Ion beam induced recrystallization of SiC	A. Höfgen, F. Eichhorn	FZ Rossendorf (FWIM, FWIS)	Schell, Eichhorn, Höfgen, Prokert, Betzl	20
20_02_006	Stress in Ni/Cu multilayers	J. Böttiger, K. Schweitz	University of Aarhus	Schweitz, Böttiger, Matz, Schell	4
20_02_007	Diffuse scattering on Co/Cu multilayers near absorption edges	F. Prokert, E. Wieser	FZ Rossendorf (FWIS, FWII)	Prokert, Schell, Matz, Betzl	10
20_02_008	Oxide nuclei formation and kinetic roughening of polycrystalline metal surfaces	A Knoll, A. Cornet, E. Smigiel	Uni Strasbourg	Knoll, Prokert, Schell	8
20_02_009 long term	Reciprocal space mapping of Si after C implantation / formation of SiC	F. Eichhorn	FZ Rossendorf (FWIS)	Eichhorn, Schell, Reichel, Betzl	15
20_02_010	Depth distribution of nitrides in Ti64 after N implantation	W. Matz, F. Berberich	FZ Rossendorf (FWIS)	Berberich, Schell	10
20_02_011	Short-range structure of bulk amorphous metallic alloys	J. Eckert, N. Mattern	IFW Dresden	Mattern, Xing, Schell	11
20_02_012	Phase formation and texture in Bi-2223/Ag superconductors	T. Fahr, N. Mattern, K. Fischer	IFW Dresden	Mattern, Fahr, Schell	3
20_02_013	Interfacial roughness in GMR multilayers	C.M. Schneider, L.v. Loyen	IFW Dresden	Hecker, Tietjen, Mattern, Schell	6
20_02_014	High-precision determination of atomic positions in 6H- and 4H-SiC crystals	A. Bauer, K. Götz, J. Kräußlich	FSU Jena	Bauer, Kräußlich, Kocher, Schell, Matz	17
20_02_015	Observation of extrinsic stacking faults in B implanted Si by CTR scattering	T.H. Metzger, J. Peisl, J. Patel	LMU Munich	Metzger, Kegel, Berberich, Schell	21

20_02_016 long term	XR-study of ion beam induced mixing effects in Co/Cu-multilayers	F. Prokert, J. Noetzel, E. Wieser	FZ Rossendorf (FWIS, FWII)	Prokert, Noetzel, Schell, Berberich	12
20_02_017	Study of self-organized dots on the surface of implanted and annealed silicon	F. Eichhorn, J. Sass, K. Mazur	FZ Rossendorf (FWIS), ITME Warsaw	Eichhorn, Schell, Berberich	18
20_02_018 long term	Comparison of the strain profile due to implantation of Si into Si wafers of (100) and (111) orientation	F. Eichhorn, R. Kögler	FZ Rossendorf (FWIS, FWIM)	Eichhorn, Schell	9
20_02_019 long term	In-situ temperature dependent measurements of phase transformations in N-ion implanted Ti-6Al-4V alloys	F. Berberich, W. Matz, E. Richter, N. Schell	FZ Rossendorf (FWIS, FWII)	Berberich, Matz, Schell	15
20_02_020	In-situ study of structural transformations of the S-phase in nitrided stainless steel during thermal cycling	W. Matz, F. Berberich, E. Richter, W. Möller	FZ Rossendorf (FWIS, FWII)	Matz, Berberich, Schell	6
20_02_021	Characterization of waveguide-structures with single-/multi-mode-guiding-layers	T. Salditt, F. Pfeiffer	LMU Munich, ILL Grenoble	Pfeiffer, Salditt, Schell	6
20_02_022	Stress relaxation in CrN layers	J. Bøttiger, P. Kringhøj, W. Matz, N. Schell	University of Aarhus	Bøttiger, Kringhøj, Schell, Berberich	6

ESRF Allocated Time for ROBL-MRH

number	title	proposers	institution	experimen- tators	shifts
HS-897	Local internal strains and stresses in coarse-grained and in ultrafine-grained Ni due to cyclic plastic deformation	E. Thiele, C. Holste	TU Dresden, IPMK	Thiele, Buque, Schell	15

Guests at ROBL

Additionally to the above mentioned experimentators for scheduled experiments, here guest are listed who came to test experiments. Informal visitors are not included.

Name	Institution
Dr. K. Richter Dr. D. Meyer	Technical University Dresden, Institute of Crystallography and Solid State Physics
Dr. J. Rinderknecht	Advanced Micro Devices (AMD) Saxony, Dresden
Prof. A. Mkrtchyan Dr. V. Mirzoyan Dr. A. Mkrtchyan	Institute of Applied Problems of Physics, National Academy of Sciences of Armenia, Yerevan
Dr. W. Wagner	Institute of Nuclear and Hadronic Physics, FZ Rossendorf
Dr. T. Halm J. Nomssi	Technical University Chemnitz, Institute of Physics
Prof. G. Bauer	Johannes-Kepler-University Linz, Austria
Dr. P. Høghøj	Institut Laue Langevin, Grenoble, France

Personnel of the Project Group ESRF-Beamline

The project group has no direct positions. The personnel comes from different institutes and departments of the FZR.

Head of the Project Group / Spokesman of the CRG:	Dr. W. Matz
Local contact at ESRF and responsible for MRH:	Dr. N. Schell
Responsible for RCH at ESRF and for radiation protection:	Dr. T. Reich

Staff at ESRF in Grenoble

Dr. Ch. Hennig (2005)	F. Berberich (2371)
Dr. N. Schell (2367)	A. Roßberg (2372)
Dr. T. Reich (2339)	U. Strauch (2372)

Postal address:

ROBL-CRG
ESRF / PLUO E 217
BP 220
F-38043 Grenoble Cedex, France

Phone: +33 4 76 88 xx xx
Fax: +33 4 76 88 25 05
e-mail: *surname@esrf.fr*

FZR - personnel working at ROBL

Institute for Ion Beam Physics and Materials Research

Dr. M. Betzl	W. Boede	A. Höfgen
Dr. F. Eichhorn	J. Kreher	J. Noetzel
Dr. W. Matz	P. Reichel	
Dr. F. Prokert		

Institute of Radiochemistry

Dr. L. Baraniak	Dr. G. Geipel	M. Rutsch
Dr. G. Bernhard	Dr. K.-H. Heise	Dr. S. Pompe
Dr. V. Brendler	G. Hüttig	Dr. K. Schmeide
Dr. H. Funke	Dr. P. Merker	S. Amayri

Institute of Bioanorganic and Radiopharmaceutical Chemistry

Dr. S. Seifert J.-U. Künstler

Central Department Experimental Facilities and Information Technology

J. Claußner	W. Neumann	T. Riedel
S. Dienel	Dr. W. Oehme	D. Boden
H. Hauck	Dr. D. Pröhl	B. Caspar
Dr. H. Krug	R. Schlenk	S. Winkelmann
		Y. Zimmermann

Experiment title: EXAFS investigations on uranyl arsenates		Experiment number: 20-01-01
Beamline: BM 20	Date of experiment: from: 19/08/98 to: 31/08/98	Date of report: 25/08/99
Shifts: 35	Local contact(s):	<i>Received at ROBL:</i> 02.09.99

Names and affiliations of applicants (* indicates experimentalists):

C. Hennig*, T. Reich*, M. Rutsch*, A. Roßberg*, H. Funke*,
G. Geipel, G. Bernhard, H. Nilsche
Forschungszentrum Rossendorf e.V., Institute of Radiochemistry, D-01314 Dresden

First EXAFS measurements were taken on the new Rossendorf Beamline (ROBL) at the European Synchrotron Radiation Facility (ESRF) in Grenoble. The monochromator, equipped with a Si(111) water cooled double-crystal system, was used in the channel-cut mode. Higher harmonics were rejected by Pt coated mirrors. U L_{III} -edge and As K-edge EXAFS spectra were collected in transmission. The Cu K-edge EXAFS spectrum was measured with a multichannel Ge fluorescence detector /1/. Two or three scans were obtained in transmission mode and 32 single accumulations were taken for the Cu K-edge fluorescence spectra. The measurements were carried out with a sample orientation of 0° and 45° to the beam direction to investigate the influence of polarization effects (not discussed here). For energy calibration of the uranium spectra we used the first inflection point of Zr at 17996eV. The samples are natural meta-zeunerite from Wheal Basset, Cornwall, and hydrogen uranyl arsenate hydrate, prepared according to the literature /2/.

Uranyl arsenates like meta-zeunerite, $\text{Cu}[\text{UO}_2\text{AsO}_4]_2 \cdot 8\text{H}_2\text{O}$, and hydrogen uranyl arsenate hydrate, $\text{H}[\text{UO}_2\text{AsO}_4] \cdot 4\text{H}_2\text{O}$, are built up by stable layers of $[\text{UO}_2]^{2+}$ and $[\text{AsO}_4]^{3-}$ units. The charge neutrality is achieved by different interlayer cations like Cu^{2+} , H^+ and H_3O^+ . We used EXAFS measurements to compare the crystal structures. The results of the curve fitting to the k^3 -weighted EXAFS data are shown in Figs. 1-2.

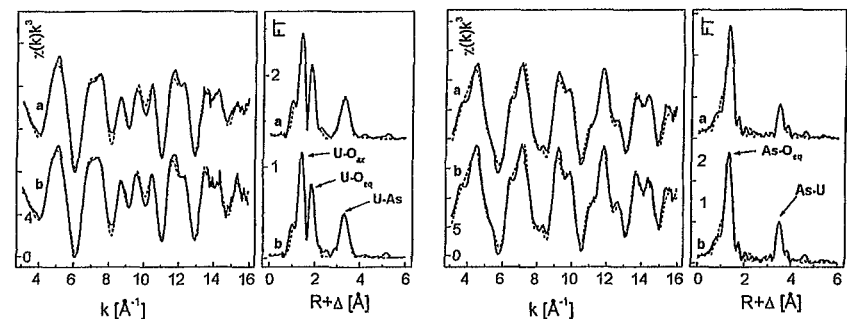


Fig. 1: U L_{III} -edge EXAFS spectra and FT of $\text{H}[\text{UO}_2\text{AsO}_4] \cdot 4\text{H}_2\text{O}$ (a), and $\text{Cu}[\text{UO}_2\text{AsO}_4]_2 \cdot 8\text{H}_2\text{O}$ (b). Fig. 2: As K-edge EXAFS spectra and FT of $\text{H}[\text{UO}_2\text{AsO}_4] \cdot 4\text{H}_2\text{O}$ (a), and $\text{Cu}[\text{UO}_2\text{AsO}_4]_2 \cdot 8\text{H}_2\text{O}$ (b)

All figures show left the k^3 -weighted EXAFS spectra and right the corresponding Fourier transforms, the solid lines are measured data, the dotted lines are the calculated values. In the U L_{III} -edge EXAFS of meta-zeunerite (Fig. 1), the first shell represent the axial oxygen atoms (O_{ax}) at a distance of 1.79\AA . The second shell correspond to the equatorial atoms with a distance of 2.28\AA and the third shell originates from the arsenic atoms with a distance of 3.67\AA . Using As as absorbing atom (Fig. 2), the As-U distance was confirmed to 3.68\AA and the As-O_{ax} distance was determined to 1.68\AA . The measurements at two near-neighbour absorber atoms allows to calculate the bond angle $\text{U-O}_{ax}\text{-As}$ to 135.34° . The interlayer Cu-O distance in meta-zeunerite was measured by Cu K-edge EXAFS to 1.95\AA . The EXAFS data of the uranyl arsenate layer on $\text{H}[\text{UO}_2\text{AsO}_4] \cdot 4\text{H}_2\text{O}$ are quite similar within the error of 0.02\AA . In conclusion, the uranyl arsenate layer structure is nearly independent from the interlayer cation arrangement. Furthermore, our investigation demonstrates the possibility to compensate the lost angle information in EXAFS using the radial distribution functions at various absorption edges.

References:

- /1/ Bucher, J.J., et al., Rev. Sci. Instrum., 67, 1, 1996
/2/ Weiss, A., et al., Z. Naturforsch., 12b, 669, 1957



ROBL-CRG

Experiment title:
Coordination Geometry of Ferrihydrite

Experiment number:
20-01-01

Beamline: BM 20
Date of experiment: from: 19/08/98 to: 31/08/98

Date of report:
25/08/99

Shifts: 6
Local contact(s):

Received at ROBL:
01.09.99

Names and affiliations of applicants (* indicates experimentalists):

C. Hennig*, T. Reich*, H. Funke*, T. Arnold
Forschungszentrum Rossendorf e.V., Institute of Radiochemistry, D-01314 Dresden

The coordination geometry in ferrihydrite was studied by EXAFS measurements at the Rossendorf Beamline (ROBL) at the European Synchrotron Radiation Facility (ESRF) in Grenoble. Iron K-edge EXAFS spectra were collected in transmission mode.

Ferrihydrite (FH) occurs during weathering processes of iron containing rocks as a metastable compound which transforms into crystalline and stable goethite (α -FeOOH) and/or hematite (α -Fe₂O₃). FH precipitates from aqueous Fe(III) solutions in particles of any nm size. Differences of peak numbers in X-ray diffraction patterns lead to a distinction between two general FH structure types: the so-called 2-line (2L-FH) and the 6-line (6L-FH) ferrihydrite. The structural and genetic relationship between 2L-FH and 6L-FH is still under discussion [1]. Therefore, we compared the EXAFS of 2L-FH and 6L-FH with hematite (Fig. 1).

In hematite, the iron is octahedrally coordinated by oxygen. The first coordination shell includes two bonding distances: Fe-O1 = 1.94 Å and Fe-O2 = 2.11 Å [2]. These bond length differences are too small to be separated by EXAFS. Ferrihydrite, in comparison, shows a very similar radial distribution function for the Fe-O distance and the coordination number. This leads to the assumption of a preferred octahedral coordination geometry in FH. But the radial distribution function for the Fe-O in FH is broadened to higher R-values, which indicates additional larger Fe-O bondings. The Fe-O octahedra in hematite are connected about 1 face ($R_{\text{Fe-Fe1}} = 2.89 \text{ \AA}$), 3 edges ($R_{\text{Fe-Fe2}} = 2.97 \text{ \AA}$), 3 corners ($R_{\text{Fe-Fe3}} = 3.36 \text{ \AA}$) and 6 corners ($R_{\text{Fe-Fe4}} = 3.70 \text{ \AA}$) [2]. This coordination gives a splitting of the second feature in the EXAFS radial distribution function of hematite into two asymmetric peaks (Fig. 1a).

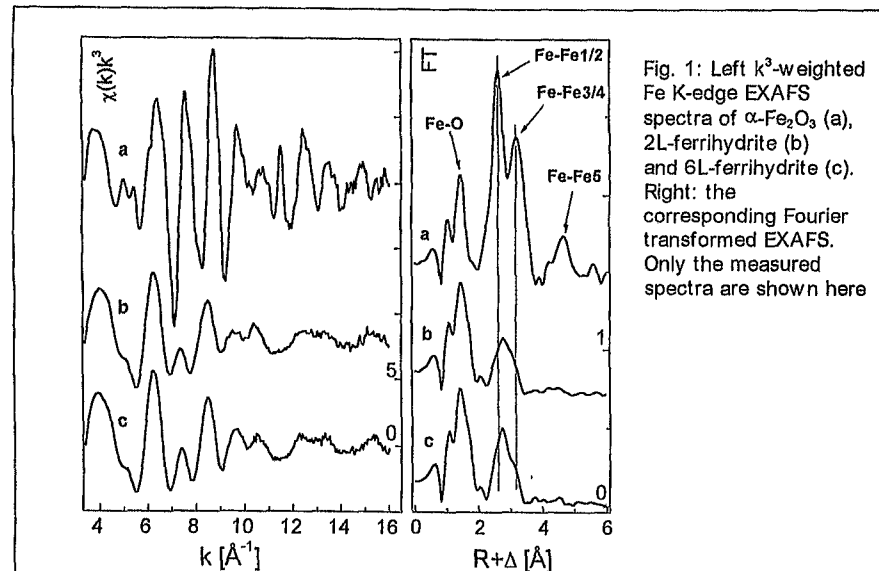


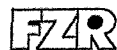
Fig. 1: Left k^3 -weighted Fe K-edge EXAFS spectra of α -Fe₂O₃ (a), 2L-ferrihydrite (b) and 6L-ferrihydrite (c). Right: the corresponding Fourier transformed EXAFS. Only the measured spectra are shown here

It is difficult to isolate these bond distances by numerical fits. However, Fourier filtering shows, that the first peak corresponds to the 2.89 Å and 2.97 Å shells and the second peak results mainly from the 3.70 Å shell including additional Fe-O distances. In contrast, the maximum of the second shell in FH is located at $R + \Delta = 2.7 \text{ \AA}$ with a shoulder at $R + \Delta = 3.0 \text{ \AA}$, which gives after phase correction Fe-Fe distances at 3.1 Å and 3.4 Å. This is in a significant difference to hematite. The lowered peak height in the EXAFS fourier transform of FH results from a short range disorder. Therefore, in connection to the broadened Fe-O Fourier transformed peak, a simple octahedral coordination geometry is not expected. In contrast to hematite, preferred bond lengths of 3.1 Å to 3.2 Å are obtained. Only small differences are found between the EXAFS spectra of 2L-FH and 6L-FH. In the spectra of the 6L-FH, the peak height of the second shell is slightly increased in comparison to the 2L-FH. This is connected to a lowering of the Debye-Waller factor. It means the structural ordering increases from 2L-FH to 6L-FH.

We thank J. Friedl/TU München for the preparation of the ferrihydrite samples.

References

- [1] Drits, V.A., et al., Clay Min., 28, 185, 1993
[2] Blake, R.L., et al., Am. Min., 51, 123, 1966



ROBL-CRG

Experiment title: First EXAFS Measurement of Neptunium Solutions at ROBL		Experiment number: 20_01_02
Beamline: BM 20	Date of experiment: from: 20/11/98 to: 29/11/98	Date of report: 24/8/99
Shifts: 27	Local contact(s): C. Hennig, T. Reich, A. Roßberg	<i>Received at ROBL:</i> 26.08.99
Names and affiliations of applicants (* indicates experimentalists): T. Reich*, G. Geipel, H. Funke*, C. Hennig*, A. Roßberg*, G. Bernhard Forschungszentrum Rossendorf e.V., Dresden, Germany Institute of Radiochemistry		

Report:**Experimental**

Two series of aqueous solutions containing 50 and 5 mMol/L neptunium in three different oxidation states were prepared for EXAFS measurements at the new Rossendorf Beamline (ROBL) at the European Synchrotron Radiation Facility (ESRF) in Grenoble, France. Solution 1 consisted of 50 mMol/L Np(IV) in 0.1 M HNO₃ and 2 M H₂SO₄. The composition of solutions 2 and 3 was 50 mMol/L Np(V) and Np(VI), respectively, in 0.1 M HNO₃. Solutions 4 – 6 were identical to solutions 1 – 3 except for the lower Np concentration of 5 mMol/L. The starting material for the sample preparation was solid NpO₂(NO₃) (AEA Technology, QSA GmbH). It was dissolved in 0.1 M HNO₃. The different oxidation states of Np were obtained by electrochemical oxidation/reduction in a conventional H-formed electrolysis cell with a diaphragm between anode and cathode. The oxidation state of neptunium and its stability with time were determined for the 5 mMol/L Np solutions by UV-Vis spectroscopy using the characteristic absorption bands of Np(IV), Np(V), and Np(VI) at 967 nm, 980 nm, and 1223 nm, respectively /1/.

For the measurements, 4 ml of the solution were filled in a polyethylene cuvette, which was sealed and put in a polyethylene bag. Multiple scans of the Np L_{III}-edge EXAFS of solutions 1 – 6 were collected in transmission mode at room temperature at ROBL using the Si(111) double-crystal monochromator in fixed-exit mode. The energy scale was calibrated using the first inflection point of the absorption spectrum of a Zr foil (17998 eV). The scattering phases and amplitudes were calculated for hypothetical clusters of NpO₄S₂, NpO₂O₄, and NpO₂O₅ using FEFF6.

Results

The raw EXAFS data and the best theoretical fit for solutions 1 – 3 are shown in Fig. 1. The obtained structural parameters are given in Tab. 1. In solution 1 Np(IV) is surrounded

by 11 oxygen atoms at a distance of 2.39 Å. In the second coordination sphere we observed two sulfur atoms with a Np-S distance of 3.07 Å. This distance corresponds to a bidentate coordination of the SO₄²⁻ ion to the Np. Using the Np-O distance of 2.39 Å and the structural parameters of the SO₄²⁻ unit (S-O = 1.51 Å, angle O-S-O = 109° /2/), the calculated Np-S distance of 2.93 Å is in good agreement with the measured value.

Both Np(V) and Np(VI) solutions 2 and 3 show the structural parameters of the actinyl ion. In case of Np(V), the distance to the axial oxygen atoms, O_{ax}, is 1.82 Å. In the equatorial plane the Np is surrounded by 4 water molecules with a Np-O_{eq} distance of 2.49 Å. The increase of the Np oxidation state from Np(V) to Np(VI) leads to a shortening of the axial and equatorial oxygen bonds by 0.07 Å and an increase of the number of water molecules attached to the neptunyl from four to five. The bond distances Np-O_{ax} and Np-O_{eq} of the Np(VI) solution are 1.75 Å and 2.42 Å, respectively.

The analysis of the 5 mMol/L Np solutions 4 – 6 gave results (not shown here) similar to the 50 mMol/L solutions. There is only a small increase of the coordination number of sulfur from 2.2 to 2.8 when going from 50 mMol/L to 5 mMol/L Np(IV).

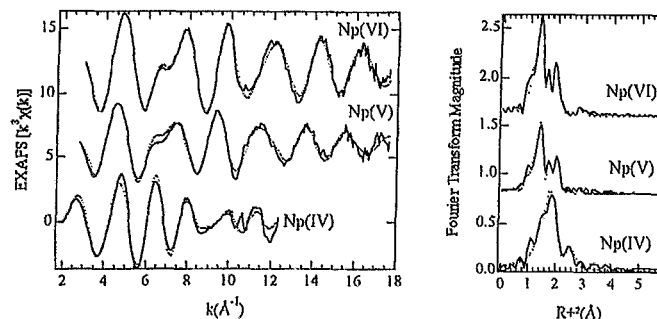
The observed structural parameters for the Np-O bond distances of Np(IV) and Np(V) are in good agreement with the values reported for 5 mMol/L Np in chlorine solution /3/. The structural parameters for Np(IV) sulfate and Np(VI) hydrate given in Tab. 1 are reported for the first time.

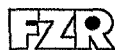
References

- /1/ Keller, C., The Chemistry of the Transuranium Elements, Verlag Chemie, Weinheim, 1971, p. 294
/2/ Hollemann, A.F., Lehrbuch der anorganischen Chemie, 101th Ed., Walter de Gruyter 1995, p. 585.
/3/ Allen, P.G., et al, Inorg. Chem. 36 (1997) 4676.

Tab. 1: EXAFS structural parameters for 50 mMol/L Np solutions.

Sample	Shell	R(Å)	N	σ ² a)
1, Np(IV)	Np-O	2.39	11.3(4)	1.18
	Np-S	3.07	2.2(3)	0.70
2 Np(V)	Np-O _{ax}	1.82	1.9	0.23
	Np-O _{eq}	2.49	3.6(2)	0.61
3 Np(VI)	Np-O _{ax}	1.75	2.0	0.15
	Np-O _{eq}	2.42	4.6(2)	0.56

a) σ² in units of 10⁻² Å²Fig. 1: Raw Np L_{III}-edge k³-weighted EXAFS spectra (left) and corresponding Fourier transforms (right) of 50 mMol/L Np solutions. Solid line – experiment; dots – theoretical fit.



ROBL-CRG

Experiment title: First XANES and EXAFS Measurements of Technetium Model Compounds at the Rossendorf Beamline ROBL		Experiment number: 20_01_02
Beamline: BM 20	Date of experiment: from: 20/11/98, 27/1/99 to: 29/11/98, 03/2/99	Date of report: 24/8/99
Shifts: 27+21	Local contact(s): C. Hennig, T. Reich, A. Roßberg	Received at ROBL: 26.8.99
Names and affiliations of applicants (* indicates experimentalists): T. Reich ^{1*} , H. Funke ^{1*} , C. Hennig ^{1*} , A. Roßberg ^{1*} , H.-J. Pietzsch ^{2*} , S. Seifert ^{2*} , J.-U. Künstler ^{2*} , G. Bernhard ¹		
Forschungszentrum Rossendorf e.V., Dresden, Germany		
1) Institute of Radiochemistry		
2) Institute of Bioinorganic and Radiopharmaceutical Chemistry		

Report:

Experimental

The structure of novel Tc complexes has been studied successfully in the framework of a collaboration between the Institute of Radiochemistry and the Institute of Bioinorganic and Radiopharmaceutical Chemistry over the last few years [1,2]. In order to evaluate the possibilities of the new Rossendorf Beamline (ROBL) for Tc EXAFS studies, we prepared four samples for a first experiment with ⁹⁹Tc at ROBL. The samples were 127 mMol/L NaTcO₄(aq), 1.3 mMol/L NaTcO₄(aq), KTcO₄(s), and TcO₂·nH₂O(s). Except for the 1.3 mMol/L Tc solution, the amount of Tc in the samples yielded an edge jump of ~1 across the Tc K absorption edge at 21 keV. These samples were measured in transmission mode using the Si(111) double-crystal monochromator in fixed-exit mode with an additional feedback system to minimize beam intensity fluctuations. The Tc K-edge EXAFS spectrum of the dilute solution was recorded using a four pixel Ge fluorescence detector. The energy scale of the XANES scans was calibrated with a Mo metal foil (Mo K edge at 20004.3 eV). For the EXAFS analysis, the first inflection point of the pre-edge absorption peak for the NaTcO₄(aq) sample was defined as 21044 eV [3].

Results and Discussion

Fig. 1 displays the raw Tc K-edge k³-weighted EXAFS spectrum of NaTcO₄(aq). The spectrum of the 127 mMol/L Tc solution was recorded in a single sweep up to k=21 Å⁻¹. During this sweep the counting time per data point was gradually increased from 2 to 20 sec. To our knowledge, this is the first Tc EXAFS spectrum of a liquid sample where it was possible to observe the fine structure of the x-ray absorption spectrum over an energy range of 1700 eV. In addition, this spectrum is an impressive demonstration of the superb quality and stability of all beamline components. It follows from the best theoretical fit to the data (Fig. 1) that Tc is surrounded by 4 oxygen atoms (N=4.1±0.1) at a distance of 1.72±0.01 Å (σ²=0.0013±0.0004 Å²). The EXAFS spectrum of the 100 times more dilute NaTcO₄(aq) sample is also shown in Fig. 1 and represents an average of four sweeps measured in fluorescence mode. The intensity of the Tc Kα fluorescence line was 1.2×10⁵ counts/sec. The total count rate processed by the fluorescence

detector was 6.4×10⁵ counts/sec. Under these conditions, it was possible to analyze the Tc K-edge k³-weighted EXAFS spectrum of the 1.3 mMol/L Tc solution up to k=15 Å⁻¹. The structural parameters obtained are the same as for the TcO₄⁻ ion in the concentrated solution, i.e., N=3.9±0.2, R=1.72±0.01 Å, and σ²=0.0016±0.0003 Å². Our structural parameters agree with a previous Tc K-edge EXAFS measurement of a 0.2 Mol/L NH₄TcO₄(aq) sample [3].

Fig. 2 displays the Tc K-edge XANES spectra of KTcO₄(s), and TcO₂·nH₂O(s). The energy of the main absorption edge defined by the first-derivative method increases from 21061.6 eV to 21065.8 eV as the Tc valence increases from IV to VII. This energy shift of 4.2 eV is in qualitative agreement with previous measurements [3]. The shape of the Tc K-edge XANES spectra reflects the symmetry of the oxygen atoms surrounding Tc. The most distinct feature of the TcO₄⁻ ion, which has T_d symmetry, is the pre-edge peak at 21050.8 eV. The XANES features can be used as a probe to determine the Tc speciation as it has been shown, for example, in cement waste forms [3].

In summary, the Tc K-edge x-ray absorption measurements on Tc model compounds showed that high-quality data can be obtained for liquids and solids at the new Rossendorf Beamline. We conclude that ROBL provides excellent experimental conditions to study the structure of solid and liquid Tc complexes with a large variety of organic and inorganic ligands covering a Tc concentration range of at least two orders of magnitude.

References:

- 1/1 Johannsen, B., et al.; Appl. Radiat. Isot. 48, 1045 (1997)
- 2/ Jankowsky, R., et al.; J. Inorg. Biochem. 70, 99 (1998)
- 3/ Allen, P.G., et al. Radiochim. Acta 76, 77 (1997) and references therein

Fig. 1: Raw k³-weighted Tc K-edge EXAFS spectra (left) and corresponding Fourier transforms (right) of experimental data (solid line) and theoretical fits (dots) for 127 mMol/L (top) and 1.3 mMol/L (bottom) NaTcO₄(aq).

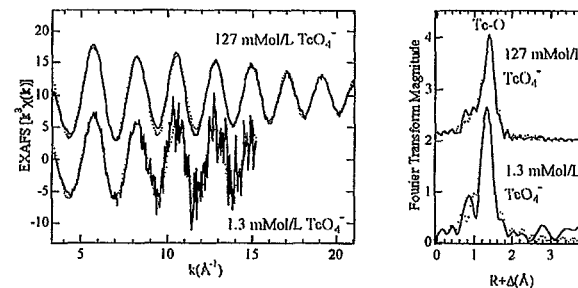
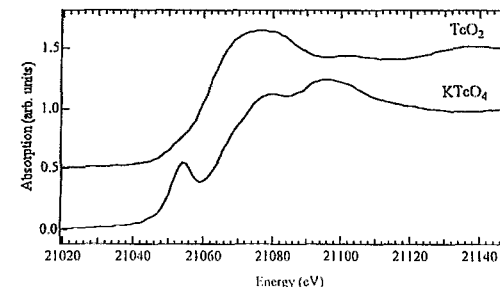
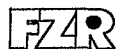


Fig. 2: Raw Tc K-edge XANES spectra of TcO₂·nH₂O(s) (top) and KTcO₄(s) (bottom).





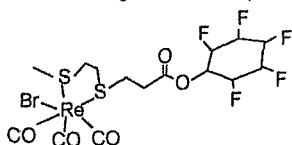
ROBL-CRG

Experiment title: EXAFS Analysis of a Rhenium(I) Carbonyl Complex		Experiment number: 20_01_02
Beamline: BM 20	Date of experiment: from: 27/01/99 to: 03/02/99	Date of report: 24/08/99
Shifts: 21	Local contact(s): Tobias Reich	<i>Received at ROBL:</i> 26.8.99
Names and affiliations of applicants (* indicates experimentalists): S. Seifert* ¹ , J.-U. Kuentler* ¹ , H. Funke* ² , A. Roßberg* ² , C. Hennig* ² , T. Reich* ² , G. Bernhard ² , B. Johannsen ¹ Forschungszentrum Rossendorf Inc. ¹ Institute of Bioinorganic and Radiopharmaceutical Chemistry ² Institute of Radiochemistry		

Report:

First EXAFS measurements of a rhenium(I) carbonyl complex were performed using the Rossendorf Beamline (ROBL). Being a collaboration between the Institute of Radiochemistry and the Institute of Bioinorganic and Radio-pharmaceutical Chemistry, this analysis serves as a stepping stone towards preparing future EXAFS experiments with ⁹⁹Tc carbonyl complexes. Rhenium and technetium carbonyl complexes of the general formula [M(CO)₃XL] (M = Re, Tc; X = Br, Cl; L = bidentate thioether or Schiff base ligand) are at present under study for the development of neutral receptor-affine complexes which are able to cross the blood-brain barrier and to bind to receptors of the central nervous system. Some of the rhenium carbonyl thioether complexes are fully characterized by X-ray analysis and other chemical methods, whose data may be used for comparison with EXAFS results.

The EXAFS spectra of the Re L_{III} and Br K-edges of the same sample were measured in transmission mode, using the Si(111) double-crystal monochromator in fixed-exit mode. The sample consists of 20 mg of the following rhenium complex:



mixed with Teflon powder as matrix material and pressed into a pellet. The EXAFS spectra were evaluated, using the program package EXAFSPAK, and the scattering code FEFF6.

To obtain a satisfactory fit result for the Re spectra, the individual scattering paths Re-C, Re-S, and Re-Br and the multiple scattering path along the carbonyl group, i.e. Re-C-O, have to be included (see Tab. 1).

The EXAFS scan of the same compound with bromine as the central atom gives a more complicated spectrum, which is dominated by the heaviest possible backscatterer rhenium. Apart from the main scattering path Br - Re, the nearly linear multiple scattering paths Br - Re - C and Br - Re - C - O yield the most important contributions to the radial distribution function. The evaluated bond length Br - Re is 2.60 Å.

Tab. 1 Comparison of bond distances obtained by EXAFS measurement and X-ray analysis data (XRD) of similar complexes ($\Delta R_{\text{EXAFS}} < 0.02 \text{ \AA}$)

Path	EXAFS			XRD ¹⁾	XRD ²⁾
	N	$\sigma^{2,3)}$	R [Å]	R [Å]	R [Å]
Re - C1	2.7	1.8	1.92	1.92	1.98
Re - C2				1.90	1.94
Re - C3				1.90	1.92
Re - Br	0.9	3.3	2.62	2.64	2.61
Re - S1	2.4	3.6	2.49	2.47	2.54
Re - S2				2.46	2.53
Re-C-O (3 legs)	2.7 ⁴⁾	3.0	3.07	3.07	no data
Re-C-O (4 legs)	2.7	3.0	3.06	3.07	

¹⁾ Re(CO)₃Br(CH₃-S-C₂H₄-S-CH₃-CCH), (2)

²⁾ Re(CO)₃Br(Cl-C₂H₄-S-C₂H₄-S-C₂H₄-Cl), (3)

³⁾ Debye Waller factors in 10⁻³ Å²

⁴⁾ The degeneracy of 2 was taken into account

Measurements of the inner coordination spheres of rhenium carbonyl complexes which differ in dithioether ligands using X-ray crystal structure methods, lead to Re - Br distances between 2.61 and 2.64 Å (1,2). The presented EXAFS results are consistent with these data.

References

- (1) Reisgys M. (1998) Rhenium- und Technetiumkomplexe mit Thioetherliganden, Thesis, TU Dresden
- (2) Alberto R., Schibli R., Angst D., Schubiger P. A., Abram U., Abram S. and Kaden Th. A. (1997) Application of technetium and rhenium carbonyl chemistry to nuclear medicine, *Transition Met. Chem.* **22**, 597-601.

	Experiment title: Determination of Ni Sorption Mechanisms on Montmorillonite	Experiment number: 20_01_003
Beamline: BM 20	Date of experiment: from: 4.2.1999 to: 11.2.1999 2.6.1999 08.06.1999	Date of report: 14.7.1999
Shifts: 24	Local contact(s): T.Reich	<i>Received at ROBL:</i> 29.7.99
Names and affiliations of applicants (* indicates experimentalists): R. Dähn, Paul Scherrer Institut, CH-5232 Villigen PSI A. Scheidegger, Paul Scherrer Institut, CH-5232 Villigen PSI P. Spieler, Paul Scherrer Institut, CH-5232 Villigen PSI		
Report: Aims of the experiment and scientific background Sorption of heavy metal ions on mineral surfaces is an important process for maintaining environmental quality. A thorough level understanding of sorption mechanisms of heavy metal sorption on mineral surfaces is therefore of fundamental importance. On smectitic clay minerals Ni(II) can sorb as surface complex on edge sites and/or interlayer sites. The aim of this study is to use EXAFS to determine sorption mechanisms of Ni on montmorillonite. Montmorillonite is an important smectitic mineral responsible for the retention of metals in the geosphere. Furthermore, the clay is used as a backfill material in the Swiss concept for a high level radioactive waste repository and thus, metal sorption on montmorillonite has been investigated in our laboratory in great details [1].		
Experiments + Results Samples were prepared in a glove box by reacting Ni and montmorillonite at pH 8.0 and at high ionic strength 0.2M Ca(NO ₃) ₂ to block cation exchange processes. The initial Ni concentrations for the samples varied from 0.03 mM to 0.92 mM Ni. After a reaction time of 1-90 days the samples were centrifuged and the wet paste was transferred into a Plexiglas sample holder. Ni K-edge fluorescence EXAFS spectra were recorded for samples containing 4 - 96 μmol/g Ni sorbed onto the montmorillonite. Figure 1 shows the dependence of different Ni concentrations sorbed onto montmorillonite after a reaction time of 90 days.		

With increasing Ni loading a characteristic shoulder at 5.3 \AA^{-1} appears in the EXAFS spectra. The corresponding radial distributions function are shown in Figure 2. The first peak represents an oxygen shell and its position and height does not depend on the Ni concentration. The second peak shifts with increasing Ni concentration to lower R values (from 2.9 \AA to 2.7 \AA) and its peak height is increasing. The dashed line characterises the position of a Ni-Ni shell in an $\alpha\text{-Ni(OH)}_2$ and suggests the presence of a Ni-hydroxide like phase in the most concentrated sample. The sample with the lowest concentration suggests specific bounds of Ni to the montmorillonite surface and the absence of a Ni-nucleation. To date, however the structural origin of the second peak of the lowest concentration is still under investigation using theoretical approaches.

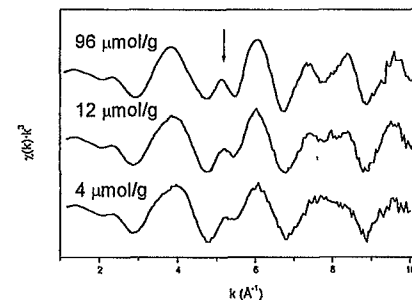


Figure 1: k^3 -weighted Ni K-edge EXAFS spectra for different Ni-concentrations sorbed onto montmorillonite

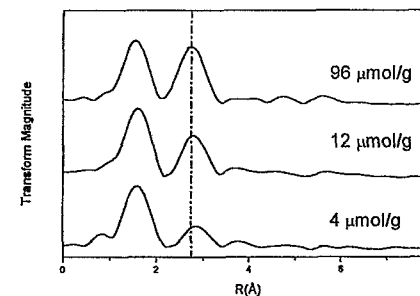


Figure 2: Concentration dependence of the Ni K-edge RDF of Ni sorbed onto montmorillonite

References

- [1] Baeyens B, and Bradbury M. H. 1997. *J. Contam. Hydrol.* 27, 199-222.

Experiment title: EXAFS Investigations of Uranyl Sulfate Complexes		Experiment number: 20_01_05
Beamline: BM 20	Date of experiment: from: 17/4/99 to: 19/4/99	Date of report: 24/8/99
Shifts: 6	Local contact(s): T. Reich, C. Hennig, A. Roßberg	<i>Received at ROBL:</i> 30.8.99
Names and affiliations of applicants (* indicates experimentalists): H. Moll ^{1,*} , T. Reich ^{2,*} , C. Hennig ^{2,*} , A. Rossberg ^{2,*} , I. Grenthe ¹		
1) The Royal Institute of Technology (KTH) Dept. of Chemistry, Inorganic Chemistry, Stockholm, Sweden 2) Forschungszentrum Rossendorf e.V., Institute of Radiochemistry, Dresden, Germany		

Report:
Experimental

Samples were prepared by taking aliquots of an acidic $\text{UO}_2(\text{ClO}_4)_2$ stock solution to get a final uranyl concentration of 0.05M. The sulfate concentration in the acidic test solutions were adjusted using H_2SO_4 or Na_2SO_4 . The solid, $\text{UO}_2\text{SO}_4 \cdot 2.5\text{H}_2\text{O}$, was prepared as described in /1/. The EXAFS spectra were recorded at the new Rossendorf Beamline (ROBL) at the ESRF in Grenoble. The transmission spectra were measured at room temperature using a cooled Si(111) double crystal monochromator of fixed-exit type ($E = 5\text{--}35$ keV). The higher harmonics were rejected by two Si and Pt coated mirrors. For energy calibration of the sample spectra, the spectrum from a Zr foil was recorded simultaneously. The ionization energy of the U L_{III} electron, E_0 , was arbitrarily defined as 17 185 eV. The data were treated using the WinXAS software /2/. Theoretical backscattering phase and amplitude functions, $\delta(k)$ and $F(k)$, used in data analysis were calculated using the FEFF7 /3/ program.

Results

The isolated EXAFS oscillations and the corresponding Fourier transforms for samples A to D are shown in Fig. 1. The FT peaks below 1.5 Å (without phase-shift) are artifacts of the spline removal and are not associated with any coordination distance. The obtained structural parameters are given in Tab. 1.

There are no EXAFS results about uranyl sulfate complexes published yet. In all samples uranium is surrounded by two O_{ax} atoms at 1.77 ± 0.01 Å. Approximately five O_{eq} atoms are coordinated to the linear uranyl group at 2.39–2.41 Å in the equatorial plane. The large Debye-Waller (DW) factor observed for the third shell in samples A–B indicates the difficulties to localize the S backscatterer, may be due to a broad distribution of U–S distances. In sample C, where $\text{UO}_2(\text{SO}_4)_2^{2-}$ is the dominant species, approximately two

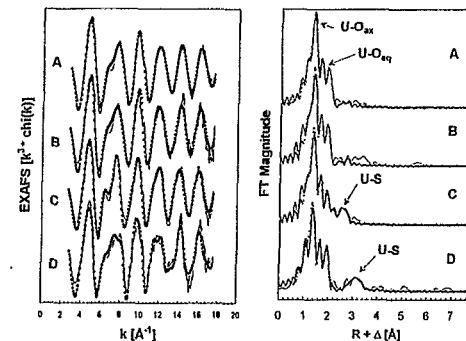
sulfur atoms were measured at 3.11 Å. Blatov et al. reported an U–S distance of 3.07 Å in the solid $\text{UO}_2\text{SO}_4 \cdot 2\text{CH}_3\text{CON}(\text{CH}_3)_2$, where SO_4^{2-} is bidentate coordinated to UO_2^{2+} /4/. If sulfate is bridging and monodentate bonded to uranyl, like in $\text{UO}_2\text{SO}_4 \cdot 2.5\text{H}_2\text{O}$, one expects a longer U–S distance. The EXAFS results confirm this assumption. And a U–S distance of 3.63 Å was measured. The structural parameter determined for $\text{UO}_2\text{SO}_4 \cdot 2.5\text{H}_2\text{O}$ are consistent with XRD measurements /5/.

By considering both previous structure information and the EXAFS data, we conclude that SO_4^{2-} is bonded in a bidentate mode to the uranyl unit in solution. The results of these study provide necessary structural information to interpret ongoing reaction dynamic investigations in the binary uranyl sulfate system.

 Tab. 1: EXAFS structural parameters for uranyl sulfate complexes in solution and in $\text{UO}_2\text{SO}_4 \cdot 2.5\text{H}_2\text{O}$.

Sample	Shell	R [Å]	N	σ^2 [Å ²]
A 82% UO_2SO_4 (aq) 12% UO_2^{2+}	U- O_{ax}	1.77	2f	0.0014
	U- O_{eq}	2.41	4.0	0.0071
	U-S	3.12f	1f	0.0105
B 50% UO_2SO_4 (aq) 50% $\text{UO}_2(\text{SO}_4)_2^{2-}$	U- O_{ax}	1.77	2f	0.0013
	U- O_{eq}	2.40	4.3	0.0068
	U-S	3.15	1f	0.0083
C 12% UO_2SO_4 (aq) 88% $\text{UO}_2(\text{SO}_4)_2^{2-}$	U- O_{ax}	1.78	2f	0.0013
	U- O_{eq}	2.44	5.1	0.0110
	U-S	3.11	2.4	0.0075
D $\text{UO}_2\text{SO}_4 \cdot 2.5\text{H}_2\text{O}$	U- O_{ax}	1.77	2f	0.0016
	U- O_{eq}	2.39	4.0	0.0048
	U-S	3.63	1.2	0.0021

f) parameter was held constant during the fit.


 Fig. 1: Raw U L_{III} edge k^3 -weighted EXAFS data for samples A–D and corresponding FT's.

References

- /1/ Cordfunke, E.H.P., *J. Inorg. Nucl. Chem.* **31**, 1327–1335 (1969).
- /2/ Ressler, T. *J. Synchrotron Rad.* **5**, 118–122 (1998).
- /3/ Zabinsky, S. I.; Rehr, J. J.; Ankudinov, A.; Albers, R. C.; Eller, M. *J. Phys. Rev. B* **52**(4), 52(4), 2995–3008 (1995).
- /4/ Blatov, V.A.; Serezhkina, L.B.; Serezhkin, V.N., *Zh. Struct. Khimii* **31**, 131 (1990).
- /5/ Brandenburg, N.P.; Loopstra, B.O., *Cryst. Struct. Comm.* **2**, 243 (1973).

Experiment title: EXAFS Study of the Interaction of Uranium(VI) with Humic Substances		Experiment number: 20_01_06
Beamline: BM 20	Date of experiment: from: 19.04.1999 to: 03.05.1999	Date of report: 20.08.1999
Shifts: 37	Local contact(s): Tobias Reich	<i>Received at ROBL:</i> 26.8.99
Names and affiliations of applicants (* indicates experimentalists): K. Schmeide*, S. Pompe*, M. Bubner, T. Reich*, A. Roßberg*, C. Hennig*, H. Funke*, K.H. Heise, G. Bernhard Forschungszentrum Rossendorf e. V., Institute of Radiochemistry, P.O. Box 51 01 19, D-01314 Dresden, Germany		

Report:

Introduction: The objective of this study was to obtain information about the binding of uranium(VI) onto functional groups of humic substances. Uranyl complexes of Kranichsee humic and fulvic acid (KHA and KFA: isolated from surface water of the mountain bog 'Kleiner Kranichsee' /1/), Aldrich humic acid (A2/97) as well as a synthetic HA type M42 /2/ were therefore investigated.

Experimental: The samples were prepared according to /3/. The uranyl loading was between 18 and 19 % of the carboxylic group capacity of the humic substances. Complex formation was confirmed by IR spectroscopy. The samples were dispersed in Teflon and pressed as 1.3 cm diameter pellets. The U content of the resulting pellets was 11 to 22 mg U. The EXAFS measurements were carried out at the Rossendorf Beamline at the European Synchrotron Radiation Facility in Grenoble. Uranium L_{III} -edge X-ray absorption spectra were collected in transmission mode. The Si(111) double-crystal monochromator was used in the channel-cut mode.

Results: The k^3 -weighted EXAFS spectra and the corresponding Fourier transforms are shown in Figs. 1 and 2. In both figures the solid lines represent the experimental data and the dotted lines the theoretical fit of the data. A two-shell fit to the experimental EXAFS data was used with oxygen atoms as backscatterers. The multiple scattering along the uranyl unit at 3.6 Å was also included in the fit. The coordination number (N) for the axial oxygen atoms and ΔE_0 were kept constant at 2 and -13.6 eV.

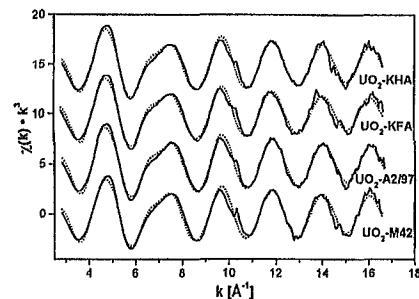


Fig. 1: k^3 -weighted U L_{III} -edge EXAFS spectra of uranyl complexes with KHA, KFA, A2/97 and M42

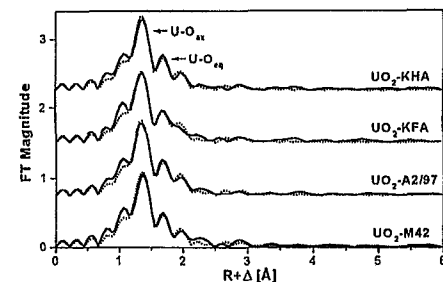


Fig. 2: Fourier transforms of the EXAFS spectra of uranyl complexes with KHA, KFA, A2/97 and M42

The EXAFS structural parameters of the uranyl humates are compiled in Tab. 1.

Tab. 1: Structural parameters of the uranyl humates

Sample	U - O _{ax}		U - O _{eq}		
	R [Å]	σ^2 [Å ²]	N	R [Å]	σ^2 [Å ²]
UO ₂ -KHA	1.78	0.001	5.2	2.39	0.012
UO ₂ -KFA	1.78	0.002	5.3	2.39	0.012
UO ₂ -A2/97	1.78	0.001	5.3	2.40	0.012
UO ₂ -M42	1.78	0.001	5.4	2.40	0.014

Error: N \pm 10 %, R \pm 0.02 Å

Axial U-O bond lengths (R) of 1.78 Å were determined for all uranyl humates. In the equatorial plane approximately five oxygen atoms were found at a mean distance of 2.40 Å. Since carboxylic groups are generally considered the main functional groups of the humic substances involved in the complexation of metal ions at pH \leq 4, the results of this EXAFS study were compared with the mean values of the bond distances found for crystalline uranyl carboxylate complexes of known structures given in /4/. It turned out that the mean bond distance of 2.40 Å in the equatorial plane determined for the humates is the same as that found for the carboxylates where the uranyl ions are bound monodentately.

Conclusion: Both for natural humic substances (KHA, KFA, A2/97) and for the synthetic HA type M42 comparable structures of uranyl complexes were found with predominantly monodentate coordination of the humic acid carboxylic groups onto uranium(VI) ions.

Acknowledgment: This work was supported by the EC Commission under contract no. F14W-CT96-0027.

References: /1/ Schmeide, K., et al., Report FZKA 6124, Forschungszentrum Karlsruhe, 161 (1998); /2/ Pompe, S., et al., Radiochim. Acta 82, 89 (1998); /3/ Bubner, M., et al., Report FZR-272, (1999); /4/ Dencke, M., et al., Radiochim. Acta 79, 151 (1997).

Experiment title: The Influence of Phenolic Hydroxyl Groups on the Complexation Behavior of Humic Substances with Uranyl(VI) Ions: EXAFS Investigations of solid UO_2^{2+} Complexes with Modified and Unmodified Humic Acids		Experiment number: 20_01_06
Beamline: BM 20	Date of experiment: from: 19.04.1999 to: 03.05.1999	Date of report: 20.08.1999
Shifts: 37	Local contact(s): Tobias Reich	<i>Received at ROBL:</i> 26.8.99
Names and affiliations of applicants (* indicates experimentalists): S. Pompe*, K. Schneide*, M. Bubner, T. Reich*, A. Roßberg*, C. Hennig*, H. Funke*, K.H. Heise, G. Bernhard Forschungszentrum Rossendorf e.V., Institute of Radiochemistry, P.O. Box 510 119, D-01314 Dresden, Germany		

Report:

To study the influence of phenolic OH groups on the short-range order surrounding of uranium(VI) in uranyl humate complexes we investigated solid uranyl humates of the modified synthetic humic acid (HA) type M1PB and of the modified natural HA Aldrich (A2/97PB) and Kranichsee (KHAPB) with blocked phenolic OH groups /1/. These samples were compared to uranyl humates of the original HA type M1, A2/97 and KHA.

Experimental: The preparation of the solid uranyl humates as well as their uranyl loadings are described in /2/. The samples dispersed in Teflon were pressed as 1.3 cm diameter pellets. U L_{III} -edge EXAFS transmission spectra were measured at room temperature at the Rossendorf Beamline at the ESRF. The monochromator, equipped with a Si(111) water cooled double-crystal system was used in the channel-cut mode.

Results: As examples, the k^3 -weighted U L_{III} -edge EXAFS and the corresponding Fourier transforms for the investigated uranyl humates of HA type M1 and M1PB as well as HA A2/97 and A2/97PB are depicted in Fig. 1 and Fig. 2. The EXAFS oscillations of all samples as well as the Fourier transforms are similar. The EXAFS oscillations were fitted to the EXAFS equation using a structural model with two coordination shells containing oxygen atoms as backscatterer and including multiple scattering effects along the uranyl unit (Tab. 1).

1).

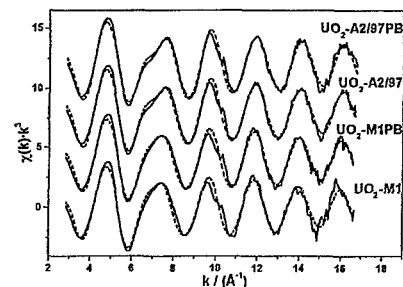


Fig. 1: k^3 -weighted U L_{III} -edge EXAFS spectra of solid uranyl humates of modified and unmodified HA. Solid lines: experimental data, dashed lines: fit results.

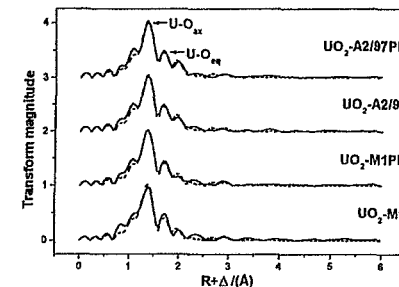


Fig. 2: Fourier transforms of the EXAFS shown in Fig. 1.

Tab. 1: EXAFS structural parameters. $\Delta E_0 = -13.6$ eV, $N_{ex} = 2$, errors in bond length (R) and coordination numbers (N) are ± 0.02 Å and $\sim 10\%$, respectively.

Sample	U-O _{ax}			U-O _{eq}		
	R (Å)	σ^2 (Å ²)	N	R (Å)	σ^2 (Å ²)	
UO ₂ -M1	1.78	0.002	5.2	2.38	0.014	
UO ₂ -M1PB	1.78	0.001	5.0	2.38	0.014	
UO ₂ -A2/97	1.78	0.001	5.3	2.40	0.012	
UO ₂ -A2/97PB	1.77	0.001	5.1	2.40	0.011	
UO ₂ -KHA	1.78	0.001	5.2	2.39	0.012	
UO ₂ -KHAPB	1.78	0.002	5.4	2.40	0.013	

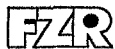
The modified HA show a smaller amount of phenolic OH groups than the unmodified HA /1/. Therefore, the spectra of the modified HA are more dominated by the interaction of UO_2^{2+} with carboxylic groups. The determined U-O_{eq} bond distances correspond to monodentate coordination of the carboxylic groups /3/. The structural parameters obtained for the solid uranyl humates of the unmodified HA do not differ from that of the modified HA. This indicates a comparable short-range order surrounding of the UO_2^{2+} ion. One can conclude that in the solid complexes the phenolic OH groups have only a small or no influence on the complexation of the UO_2^{2+} ions.

However, a contribution of phenolic OH groups to the complexation of UO_2^{2+} can not fully be excluded by the EXAFS results, because the obtained structural parameters represent an average over all interactions between HA and UO_2^{2+} . From EXAFS investigations concerning the complexation of pyrogallol with UO_2^{2+} at pH 4.8 /4/ it is known that phenolic OH groups can complex to the UO_2^{2+} ion with distances of 2.40 Å, which can not be distinguished from $R_{U-O_{eq}}$ of the humates.

References:

- /1/ Pompe, S., et al., Report FZR-272 (1999); /2/ Bubner, M., et al., Report FZR-272 (1999); /3/ Denecke, M., et al., Radiochim. Acta 79, 151, 1997; /4/ Roßberg, A., et al., Report FZR-247 (1999) p. 53

Acknowledgment: This work was supported by the BMBF under contract No. 02 E88150 and by the EC under contract No. F14W-CT96-0027.



ROBL-CRG

Experiment title: PRELIMINARY INVESTIGATION TO DETERMINE THE MAIN COMPLEX SPECIES IN THE AQUEOUS SYSTEM OF UO_2^{2+} WITH PROTOCATECHUIC ACID BY EXAFS SPECTROSCOPY		Experiment number: 20_01_06
Beamline: BM 20	Date of experiment: from: 19/4/99 to: 03/5/99	Date of report: 25/8/99
Shifts: 37	Local contact(s): C. Hennig, T. Reich, A. Roßberg	<i>Received at ROBL:</i> 30.8.99
Names and affiliations of applicants (* indicates experimentalists): A. Rossberg ¹ , T. Reich ¹ , C. Hennig ¹ , H. Funke ² , L. Baraniak ² , G. Bernhard ² , H. Nitsche ³ ¹ ESRF - ROBL / CRG, Avenue des Martyrs, B.P. 220, 38043 Grenoble Cedex, France ² Forschungszentrum Rossendorf e.V., Institut für Radiochemie, P.O. Box 510119, D-01314 Dresden, Germany ³ Lawrence Berkeley National Laboratory, The Glenn T. Seaborg Center, MS 70A-1150, Berkeley, CA 94720, U.S.A.		

Report:

Experimental

The speciation of the complexes on ionic strength of 0.1 M ($NaClO_4$) and 25 °C in the absence of CO_2 was calculated with the computer program RAMESES. The metal concentration was 1 mM $UO_2(ClO_4)_2$ and the PCS concentration was 50 mM. Uranium(VI) hydrolysis was considered in the calculations.

The $U L_{III}$ -edge spectra of the uranium(VI) complexes were measured at the Rossendorf Beamline using a Si(111) double-crystal monochromator in channel-cut mode. The fluorescence signal was measured with a 4-pixel germanium detector. The ionization potential of the $U L_{III}$ -edge was defined as 17,185 eV. The weights of the four detector channels were calculated according to their statistical signal-to-noise ratios. The dead-time corrected EXAFS spectra were analysed by the standard procedure, using the EXAFSPAK suite of programs and the theoretical scattering phases and amplitudes calculated with the scattering code FEFF6 [1].

Results and Discussion

The raw k^3 -weighted $U L_{III}$ -edge EXAFS of the complex systems and their corresponding Fourier transforms (FT) are shown in Fig. 1 and the fit results in Tab. 1. During the fitting procedure the coordination number (N) of the axial oxygen of the uranyl unit was kept constant at $N = 2$. The average of the radial $U-O_{ax}$ distance between uranium and axial oxygen is 1.79 ± 0.02 Å. The average Debye-Waller factor is 0.002 Å². The features in the k range from 6 Å⁻¹ to 8 Å⁻¹ and the radial distance of the equatorial oxygen change with the pH values (Fig. 1). The great distance of the equatorial oxygen of the 1:1 PCS complex at pH 4.3 indicates that the carboxylic group coordinates with the uranyl cation in a bidentate fashion (Tab. 1). The coordination number of carbon in the PCS complex is 2.4 atoms at pH 4.3. It is possible that at pH 4.3 two PCS ligands bind with the uranyl ion in a bidentate fashion. With increasing pH value, the bond distance of the equatorial oxygen decreases.

$UO_2^{2+}:L, UO_2^{2+}:L$		U-X equatorial			
PCS(L)	pH	Atom	R	$\sigma^2 \cdot 10^{-3}$	N
1:1, 53%	4.30	O	2.45	8	5.7
		C	2.88	3	2.4
1:1, 46%	4.45	O	2.40	12	7.0
1:1, 23%	4.83	O	2.37	13	7.3
1:2, 30%					
1:1, 10%	5.04	O	2.38	10	6.0
1:2, 65%					
1:2, 100%	5.54	O	2.37	8	6.0
1:2, 100%	6.03	O	2.36	9	6.4
1:2, 90%	6.75	O	2.36	10	6.6

Tab. 1: Fit results for the second coordination shell (N - coordination number, R - radial distance in Å, σ^2 - Debye-Waller factor in Å²).

At higher pH values, the PCS ligands coordinate with the uranyl cation in an o-diphenolic bonding fashion and the carboxylic group is not involved in the complexation. The calculated speciation of the PCS system shows at pH 4.8 the change from the carboxylic to the o-diphenolic coordination. The Debye-Waller factor for the equatorial oxygen has a maximum at this pH (Tab. 1). The similarity of the EXAFS spectra and coordination parameters of the uranium(VI) PCS and the BCT complexes increases with the pH [2]. The possible main complex species of PCA with the uranyl cation should be confirmed by principal component analysis of the EXAFS measurements. This can be used to validate the complexation constants for calculation of the speciation [3].

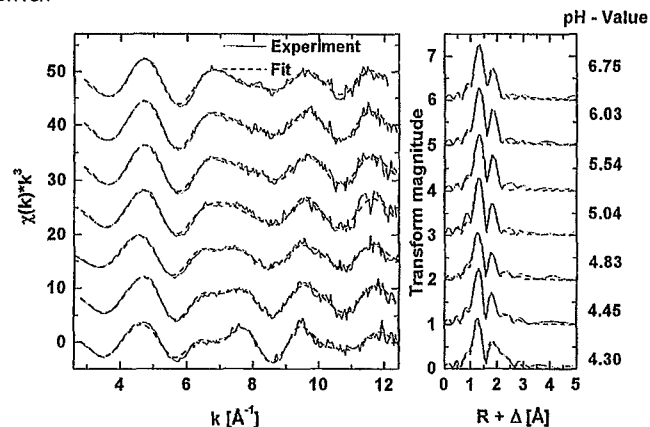


Fig. 1: Left: Raw k^3 -weighted EXAFS spectra of PCS complexes sorted by pH values. Right: Corresponding Fourier-transforms without phase corrections.

References

- [1] Zabinsky S. I., Rehr J. J., Ankudinov A., Albers R. C., Eller M. J., Phys. Rev. B 52 2995 (1995)
- [2] Rossberg A., et al., Annual Report FZR-247 (January 1999), p. 53
- [3] Baraniak L., et al., Annual Report FZR-247 (January 1999), p. 31

	Experiment title: Thorium L _{III} -edge EXAFS measurements of solutions containing polyhydroxy ligands	Experiment number: 20_01_007
Beamline: BM 20	Date of experiment: from: 4.2.1999 to: 11.2.1999 from: 3.6.1999 to: 8.6.1999	Date of report: 29.7.1999
Shifts: 12	Local contact(s): T.Reich	<i>Received at ROBL:</i> 3.8.99
Names and affiliations of applicants (* indicates experimentalists): *A. Scheidegger, Paul Scherrer Institut, CH-5232 Villigen PSI K. Vercammen, Paul Scherrer Institut, CH-5232 Villigen PSI M. Glaus, Paul Scherrer Institut, CH-5232 Villigen PSI *R. Dähn, Paul Scherrer Institut, CH-5232 Villigen PSI *P. Spieler, Paul Scherrer Institut, CH-5232 Villigen PSI		

Report:**Aims of the experiment and scientific background**

Organic ligands are inherent components of low- and intermediate level waste. They originate from decontaminating processes in nuclear power stations (e.g. citric acid, oxalic acids, EDTA), from organic compounds added to cement to change its properties (e.g. gluconic acid (Gluc)) and from the degradation of polymeric materials present in the waste (ion exchange resins, cellulose, bitumen). The degradation of cellulosic materials under alkaline conditions results in the formation of polyhydroxy type ligands (PHL) such as α -isosaccharinic acid (ISA) [1]. Due to their strong complexing properties, PHL may reduce the sorption of radionuclides on the repository matrix by several orders of magnitude or enhance the solubility of the radionuclides (hydr)oxides precipitations. This might result in an enhanced release of radionuclides from the waste repository into the biosphere.

In a first step the EXAFS studies at ROBL included two goals: To investigate the complexation of Th(IV) with ISA and Gluc under highly alkaline condition and to gain experience with how active samples can be transported to ROBL (transport and import permission).

Experiments + Results

Th samples were prepared in a glove box by reacting Th with ISA and gluconic acid at pH 13.3 in 0.3 M NaOH. The Th concentrations for the solutions were 0.1 -6.6 mM for ISA and 1-10 mM for Gluc. The samples were then packed into 4 ml PE cuvettes and tightly sealed. The EXAFS measurements were conducted in fluorescence mode (dilute samples) and transmittance mode (references).

Figure 1 shows the radial distribution functions of Th-ISA and Th-gluconic acid in comparison with a Th nitrate reference solution. The figure reveals that although structurally related, the spectra of Th/ISA and Th/gluconic acid are distinctly different beyond the first coordination shell. Data analysis suggests that the first coordination shell consists of 10 O atoms at distance of ~ 2.4 Å. The second shell of Th/ISA and Th/gluconic acid consists of C neighbouring atoms at ~ 3.1 Å and ~ 3.3 Å. Based on energy minimisation calculations, these distances are consistent with the polydentate binding of ISA and gluconic acid to the Th central atom. The structural origin of further Th shells is currently analysed using theoretical approaches.

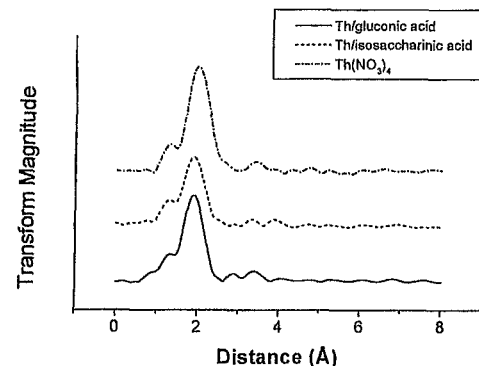
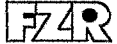


Fig. 1: Radial structure functions of Th-ISA, Th-gluconic acid and a Th nitrate solution

References

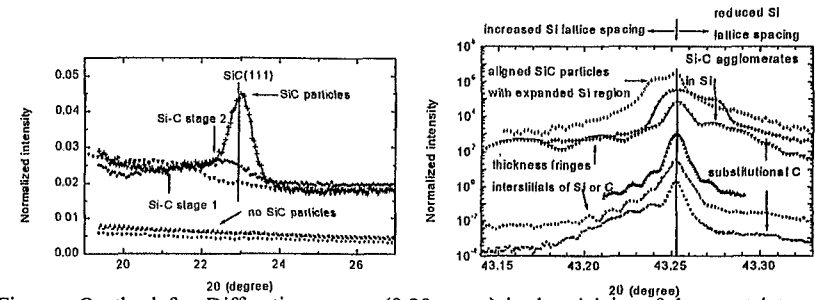
- [1] Van Loon L.R. and Glaus M.A. *PSI-Bericht 98-07* Paul Scherrer Institut Switzerland 1998. Also published as *Nagra Technical Report NTB 97-04*, Wettingen, Switzerland 1998.

 ROBL-CRG	Experiment title: Study of strain and SiC particle formation in Si implanted with C ions of medium fluence	Experiment number: 20_02_001
	Beamline: BM 20	Date of experiment: from: 10.2.98 to: 15.2.98
Shifts: 10	Local contact(s): Dr. N. Schell	<i>Received at ROBL:</i> 12.8.99
Names and affiliations of applicants (* indicates experimentalists): F. Eichhorn *, N. Schell * (a), W. Matz, R. Kögler Forschungszentrum Rossendorf Institute of Ion Beam Physics and Materials Research P.O.B. 510119, D-01314 Dresden, Germany (a) present address: ROBL-CRG at ESRF Grenoble		

Report:

Carbon is an important impurity in semiconductor silicon. It can deteriorate microelectronic device characteristics as leakage current and minority carrier lifetime or improve them due to the suppression of extended defects after implantation [1]. Moreover, implantation of C is applied for the formation of gettering layers [2] or preparing SiC crystallites. In dependence on the conditions of mixing C into Si the carbon is in different atomic surroundings. By implantation of C into Si the implanted region is in a non-equilibrium state and most of the C atoms are assumed to occupy interstitial positions. In thermodynamic equilibrium the solubility for C in Si is only 10^{-3} to 10^{-4} at.% C at 1200 to 1400 °C and the excess C is dissolved substitutionally or the new phase SiC is formed. It is known from previous investigations that SiC formation is not a single-step process [3]. The question how the implantation and annealing conditions influence the quality of the SiC layer can be only cleared up by studying the formation process in detail. Here we studied by synchrotron x-ray diffraction the strain in the crystalline material (Si substrate and SiC particles) due to implantation and the first stages of forming the SiC phase in the Si lattice (details in [4]).

Implantation of C ions with an energy of 195 keV into Si wafers heated up to 800 °C results in an elastic distortion of the Si host lattice and in the formation of crystalline SiC particles or their prestages depending on implantation dose and temperature. Only a Si lattice deformation without growth of SiC was observed if the fluence does not exceed 5×10^{15} C ions/cm². After implantation of C ions up to 4×10^{17} cm⁻² at a temperature of 500 °C, agglomerations of Si-C and an altered state of Si lattice deformation are found. By implantation of 4×10^{17} ions/cm² at 800 °C, particles of the 3C-SiC (β -SiC) phase grow, which are aligned to the Si matrix [4].



Figures: On the left - Diffraction curves ($\theta:2\theta$ scans) in the vicinity of the most intense 3C-SiC(111) reflection indicating the formation of Si-C prestages and crystalline SiC particles. Curves correspond to different implantation conditions (fluence in ions/cm² and temperature): ■ 5×10^{15} at room temperature, ● 5×10^{15} at 500 °C, ▲ 5×10^{15} at 800 °C, ▼ 5×10^{16} at 500 °C, ◆ 4×10^{17} at 500 °C, + 4×10^{17} at 800 °C.


On the right - Diffraction curves of the Si(400) reflection revealing the lattice strain component perpendicular to the sample surface. Characteristic features and their reason are marked.

[1] R. Liefing et al., IEEE Transactions on Electron. Devices Vol. 41 No.1 , 50 (1994).

[2] H. Wong et al., Appl. Phys. Lett. 52, 1023 (1988).

[3] M. Deguchi, M. Kitabatake, T. Hirao, N. Arai, T. Izumi, Jap. J. Appl. Phys. 31, 343 (1992).

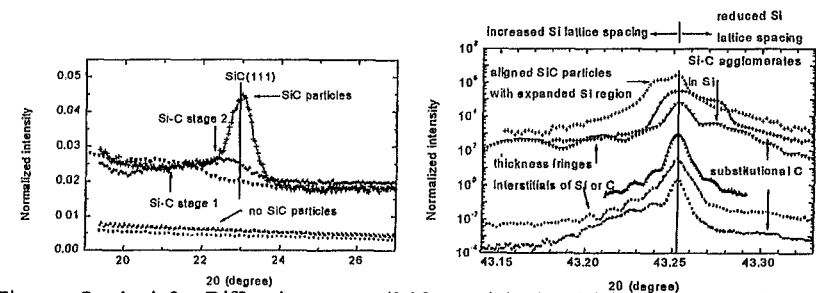
[4] F. Eichhorn, N. Schell, W. Matz, R. Kögler, J.Appl.Phys. 1999 (accepted for publication)

	Experiment title: Study of strain and SiC particle formation in Si implanted with C ions of medium fluence	Experiment number: 20_02_001
	Beamline: BM 20	Date of experiment: from: 10.2.98 to: 15.2.98
Shifts: 10	Local contact(s): Dr. N. Schell	<i>Received at ROBL:</i> 12.8.99
Names and affiliations of applicants (* indicates experimentalists): F. Eichhorn *, N. Schell * (a), W. Matz, R. Kögler Forschungszentrum Rossendorf Institute of Ion Beam Physics and Materials Research P.O.B. 510119, D-01314 Dresden, Germany (a) present address: ROBL-CRG at ESRF Grenoble		

Report:

Carbon is an important impurity in semiconductor silicon. It can deteriorate microelectronic device characteristics as leakage current and minority carrier lifetime or improve them due to the suppression of extended defects after implantation [1]. Moreover, implantation of C is applied for the formation of gettering layers [2] or preparing SiC crystallites. In dependence on the conditions of mixing C into Si the carbon is in different atomic surroundings. By implantation of C into Si the implanted region is in a non-equilibrium state and most of the C atoms are assumed to occupy interstitial positions. In thermodynamic equilibrium the solubility for C in Si is only 10^{-3} to 10^{-4} at.% C at 1200 to 1400 °C and the excess C is dissolved substitutionally or the new phase SiC is formed. It is known from previous investigations that SiC formation is not a single-step process [3]. The question how the implantation and annealing conditions influence the quality of the SiC layer can be only cleared up by studying the formation process in detail. Here we studied by synchrotron x-ray diffraction the strain in the crystalline material (Si substrate and SiC particles) due to implantation and the first stages of forming the SiC phase in the Si lattice (details in [4]).

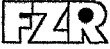
Implantation of C ions with an energy of 195 keV into Si wafers heated up to 800 °C results in an elastic distortion of the Si host lattice and in the formation of crystalline SiC particles or their prestages depending on implantation dose and temperature. Only a Si lattice deformation without growth of SiC was observed if the fluence does not exceed 5×10^{15} C ions/cm². After implantation of C ions up to 4×10^{17} cm² at a temperature of 500 °C, agglomerations of Si-C and an altered state of Si lattice deformation are found. By implantation of 4×10^{17} ions/cm² at 800 °C, particles of the 3C-SiC (β -SiC) phase grow, which are aligned to the Si matrix [4].



Figures: On the left - Diffraction curves ($\theta:2\theta$ scans) in the vicinity of the most intense 3C-SiC(111) reflection indicating the formation of Si-C prestages and crystalline SiC particles. Curves correspond to different implantation conditions (fluence in ions/cm² and temperature): ■ 5×10^{15} at room temperature, ● 5×10^{15} at 500 °C, ▲ 5×10^{15} at 800 °C, ▼ 5×10^{16} at 500 °C, ◆ 4×10^{17} at 500 °C, + 4×10^{17} at 800 °C.

On the right - Diffraction curves of the Si(400) reflection revealing the lattice strain component perpendicular to the sample surface. Characteristic features and their reason are marked.

- [1] R. Liefing et al., IEEE Transactions on Electron. Devices Vol. 41 No.1 , 50 (1994).
- [2] H. Wong et al., Appl. Phys. Lett. 52, 1023 (1988).
- [3] M. Deguchi, M. Kitabatake, T. Hirao, N. Arai, T. Izumi, Jap. J. Appl. Phys. 31, 343 (1992).
- [4] F. Eichhorn, N. Schell, W. Matz, R. Kögler, J.Appl.Phys. 1999 (accepted for publication)

 ROBL-CRG	Experiment title: Specular reflectivity on Co/Cu multilayers near absorption edges	Experiment number: 20_02_002
	Beamline: BM 20	Date of experiment: Feb. 6 th , 1998 from: May. 10 th , 1998 to: May. 12 th , 1998
Shifts: 8	Local contact(s): N. Schell	Received at ROBL: 10.08.99
Names and affiliations of applicants (* indicates experimentalists): * Dr. F. Prokert, FZ-Rosendorf, FWIS * Dr. W. Matz, FZ-Rosendorf, FWIS * Dr. N. Schell, CRG ROBL at ESRF, Grenoble and FZ- Rosendorf		
Report: For multilayer (ML) systems showing giant magnetoresistance it is of interest to study layer and interfacial properties [1],[2]. Two types of samples with different layer thicknesses of Co- and Cu-layers: Si/SiO ₂ /8x[Co(4nm)/Cu(4nm)] (Co/Cu-ML 8x[4/4]) and Si/SiO ₂ /4x[Co(8nm)/Cu(8nm)] (Co/Cu-ML 4x[8/8]) were investigated in the 'as-deposited' state. The MLs were prepared by crossed beam pulsed laser deposition (CB PLD) technique. The layer properties like thickness, mass density and interface roughness of the different samples were studied using specular X-ray reflection (XRR). The high brilliance and tunable wavelength of the synchrotron radiation at ROBL allowed to improve the low contrast for this material combination by setting the X-ray wavelength to the absorption edge of one of the layer materials. Due to the small divergence and the high intensity of the incident beam the angular resolution of the detected beam could be matched to resolve adequately the ML Bragg peaks and the Kiessig fringes. The decrease of intensity could be followed over seven orders. The specular XRR were measured on both types of samples at the K-edge energy of Co (7.708 keV) and Cu (8.974 keV), respectively. With two independent data sets of each sample, the accuracy of the results, obtained from the simulation codes REFSIM (Siemens) and/or REFS (Bede Scientific), could be improved by a cross-check of the fitted values.		

Besides mass density (ρ) and thickness (d) of the layers, we get the rms-roughness values (σ_{RMS}) of the surface and the ML interfaces. The quality of the fits (see Fig. 1) could be improved by introducing a copper oxide capping layer. Further was found that the first Co-layer on the substrate and the last Cu-layer on the top differ in their parameters from the other layers which could be simulated as Co/Cu-stack by a common parameter set. Table 1 shows the results obtained from MLs of two different charges both prepared by CB PLD.

Table 1 Simulation results of two charges of Co/Cu-MLs

ML type	single layers	CB PLD samples charge 1			CB PLD samples of charge 2		
		d (nm)	ρ (g/cm ³)	σ_{RMS} (nm)	d (nm)	ρ (g/cm ³)	σ_{RMS} (nm)
4x[8/8]	Co	13.68	8.4	2.8	17.05	8.7	1.6
	Cu	1.58	8.8	0.8	1.07	8.7	1.6
8x[4/4]	Co	6.67	8.5	1.33	8.2	8.4	1.3
	Cu	1.39	8.8	0.55	1.10	8.4	1.3

(layer thickness $d = d_{\text{Co}} + d_{\text{Cu}}$, ρ - mass density, σ_{RMS} - rms-roughness)

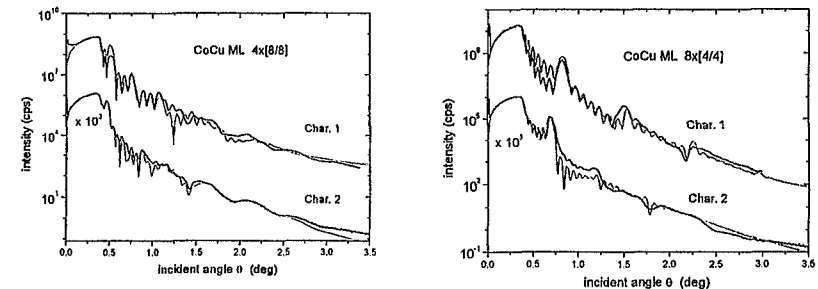


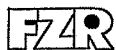
Fig. 1 Measured (thick lines) and simulated (thin lines) angular dependence of specular reflectivity of Co/Cu-MLs. (Co/Cu-ML 4x[8/8] on the left, Co/Cu-ML 8x[4/4] on the right)

Results

In the 'as-deposited' state the MLs, obtained by CB PLD technique, have an extended Co/Cu interface. However, the σ_{RMS} -roughness, especially for the Cu-layers, varies strongly with the deposition conditions. The thickness excess and the higher σ_{RMS} -roughness of the Co-layers are also dependent on preparation.

References

- [1] D. E. Joyce, C.A. Faunce, P. J. Grundy, B. D. Fulthorpe, T.P.A. Hase, I. Pape, B. K. Tanner, *Phys. Rev.* **B58**, 5594 (1998)
- [2] M.A. Parker, T.L. Hylton, K.R. Coffey, J.K. Howard, *J. Appl. Phys* **75**, 6382 (1994)



ROBL-CRG

Experiment title: Exploring investigations of ultrafine-grained nickel after plastic shear loading and cyclic plastic deformation		Experiment number: 20_02_003
Beamline: BM 20	Date of experiment: from: 02. 04. 98 to: 05. 04. 1998	Date of report: 28. 08. 1998 <i>Received at ROBL:</i> 10.9.98
Shifts: 9	Local contact(s): Dr. Norbert Schell	
Names and affiliations of applicants (* indicates experimentalists): Dr. Ellen Thiele*, Dr. Michael Hecker* Institute of Physical Metallurgy, Technical University Dresden D-01062 Dresden Germany		

Report:

CHANGE OF INTERNAL STRAINS AND STRESSES IN ULTRAFINE-GRAINED NICKEL DUE TO CYCLIC PLASTIC DEFORMATION

E. Thiele¹, M. Hecker¹ and N. Schell²

¹ Institut für Physikalische Metallkunde, Technische Universität Dresden

² Institut für Ionenstrahlphysik und Materialforschung, FZ Rossendorf

Ultrafine-grained (UFG) materials with a mean grain size of some 100nm, prepared by equal channel angular extrusion (ECAE) from compact material are of a great interest for theoretical and experimental investigations due to their outstanding physical properties. They show a very high yield stress and microhardness in comparison with conventional polycrystalline samples. However, the structure and the defects, responsible for the mechanical behaviour, are non-stable against thermal treatment. Corresponding to the application fields of the materials, also the stability against cyclic deformation at different temperatures should be investigated.

To carry out fatigue experiments, samples with a rectangular cross section were cut from UFG nickel billets of 99.99% purity. The loading axis of the samples was parallel to ECAE die axis.

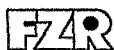
The cyclic plastic deformation of the samples was performed at room temperature and at 200°C in a servohydraulic materials testing machine at a constant plastic strain amplitude $\epsilon_{pm} = 5 \cdot 10^{-4}$. A cyclic softening was observed till the stress amplitude σ_n remained nearly constant. As expected, σ_n decreased with increasing deformation temperature. To achieve a symmetric plastic strain amplitude, in the tension half cycle a higher amount of maximum stress was required than in the compression half cycle.

The grain structure was observed using the orientation contrast in a scanning electron microscope. No significant changes of the grain size distribution were detected after the cyclic deformation.

Measurements of X-ray diffraction profiles were performed at the synchrotron radiation beamline ROBL of the Forschungszentrum Rossendorf at the European Synchrotron Facility in Grenoble. The basic instrument was a 6-circle goniometer. Applying monochromatic synchrotron radiation with an energy of 8.05 keV, the instrumental broadening was negligible in comparison with the strain induced broadening of the profiles measured at the UFG samples.

To estimate the spectrum of internal strains, diffraction profiles were measured for different {hkl}-types of lattices planes parallel to the sample surface. From the shape changes of the profiles one can conclude that the width of the strain spectrum is reduced by the cyclic plastic deformation especially for higher temperatures though no recrystallisation occurs. Taking into account the variation of the profile shape with the {hkl}-type of the reflection as well as the dependence of the profile position on the measuring direction, long-range granular stresses should be present. The mean dislocation density, calculated on the basis of the Krivoglaz-Wilkens theory, was found to be correlated with the deformation state of the samples.

Proc. EPDIC-6, August 22 – 25, 1998, Budapest – Hungary, p. 61 (a full length paper will be published in *Mat. Sci. Forum*)



ROBL-CRG

Experiment title: <i>Anisotropic Deformation of Nb Films during H Load</i>		Experiment number: 20_02_004
Beamline: BM 20	Date of experiment: from: 15.04.1998 to: 22.04.1998	Date of report: Mai 1998
Shifts: 16	Local contact(s): Dr. Norbert Schell	<i>Received at ROBL:</i> 01.06.1998

Names and affiliations of applicants (* indicates experimentalists):

Prof. Dr. J. Peisl, Dipl. Phys. T. Edelmann*, Dipl. Phys. S. Schmid*, F. Berberich*
Sektion Physik der LMU München
Geschwister-Scholl-Platz 1
80539 München
Germany

Report:

Some metals like niobium can dissolve large amounts of hydrogen, up to concentrations of one H atom per Nb atom. Hydrogen is thereby located in the Nb host lattice on tetrahedral interstitial sites and expands the lattice isotropically. The resulting long range displacement field causes an indirect elastic interaction between the H atoms. In thin Nb layers on sapphire, elastic displacements are influenced by the film surface as well as by the interface between film and substrate. It is well known that for low H concentrations thin epitactically grown Nb films will expand only perpendicular to the surface. With higher loading pressures a lateral anisotropic lattice expansion will also result.

The aim of our measurements at ROBL was to observe the cross over from one dimensional to three dimensional lattice expansion by measuring the lattice parameters under in-situ conditions and to determine the degree of anisotropy of the lattice expansion in dependence of the H content.

The lattice parameter in the growth direction is measured by conventional Bragg diffraction; the lateral lattice parameters are accessible under grazing incidence and exit angles (GID). Specular reflectivity under small angles shows the change in film thickness as well as interface roughness at the cross over from one to three dimensional expansion.

Previous measurements showed that loading the sample with hydrogen causes an irreversible change in its morphology. Thus, it is absolutely necessary to keep the sample in a constant environment and to allow all three measuring modes (Bragg, GID, reflectivity) at the same time. In order to achieve those demanding conditions a specially adapted UHV chamber for the ROBL six-circle-diffractometer was constructed. It allows in-situ H loading without restricting the necessary diffractometer's degrees of freedom.

Two sample systems with different Nb film thicknesses were available. Both were covered with a protecting layer of palladium appr. 100 Å thick. The samples were exposed to H pressures from 0.1 to 50.0 mbar at temperatures between 200 °C and 300 °C. The Nb films were (110) oriented. With a scintillation counter angular and radial scans were measured around the Bragg reflexes (110), (1 $\bar{1}$ 0), (1 $\bar{1}$ 2) and (002).

The data evaluation is not yet complete. However, the following figures for the appr. 750 Å thick Nb film show as typical examples the changes of the data curves without H atmosphere and with 50 mbar H atmosphere.

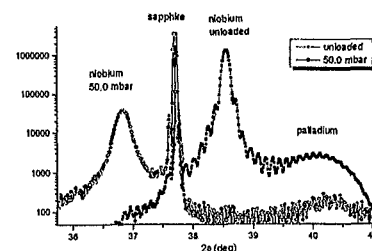


Figure 1.

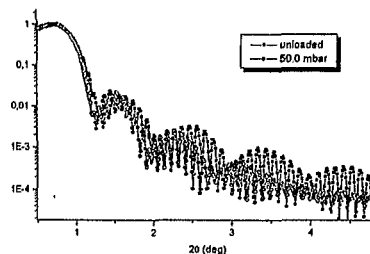


Figure 2.

Figure 1 to the left shows the Bragg measurement in radial direction around Nb (110). The H induced shift of the Bragg reflex corresponds to a relative lattice expansion of 4 %. While the unloaded sample shows so called Laue fringes (which serve as a measure for the crystalline quality of the film), they are no longer recognizable in the loaded sample. Figure 2 to the right shows the change in specular reflectivity after H loading and thereby reveals the change in film thickness.

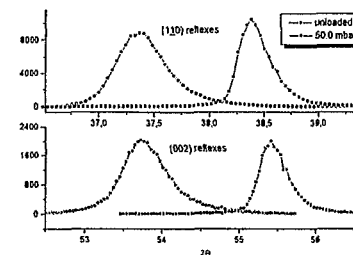
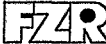


Figure 3.

Figure 3 above shows the lattice expansion in two lateral crystallographic directions, vertically oriented to each other (GID data). The relative lattice expansion in (1 $\bar{1}$ 0) is 2.4 %, in (002) direction 2.8 %.

 ROBL-CRG	Experiment title: Ion beam induced recrystallization of amorphous SiC	Experiment number: 20_02_005
	Beamline: BM 20	Date of experiment: 9./10.5.98, 10.-12.9.98, 27-30.10.98, 25.6.99
Shifts: 21	Local contact(s): Dr. N. Schell	<i>Received at ROBL:</i> 12.8.99
Names and affiliations of applicants (* indicates experimentalists): A. Höfgen *, F. Eichhorn *, N. Schell * (a), F. Prokert *, M. Betzl * Forschungszentrum Rossendorf Institute of Ion Beam Physics and Materials Research P.O.B. 510119, D-01314 Dresden, Germany (a) present address: ROBL-CRG at ESRF Grenoble		

Report:

Nanocrystalline materials have attracted considerable interest, then the reduced size of the crystallites causes changes in their optical, mechanical and thermodynamic properties with respect to the bulk material. In the case of silicon carbide, which is one of the most promising semiconductor materials for high temperature, high-frequency, and high-power electronic devices, it has been shown recently that ion implantation can stimulate the processes of nucleation and grain growth [1]. Therefore, in this investigation the crystallization process in dependence on the implantation parameters was studied in detail.

Single-crystalline (c) 6H-SiC wafers with 3.5° off-axis (0001) orientation were used as substrate material. An 1.8 µm thick amorphous surface layer was generated by a 5 MeV Si⁺ implantation at room temperature. By 300 keV Al-implantation the recrystallization was stimulated in a 400 nm thick surface layer. The implantation parameters were varied in a dose range from 3×10¹⁵ to 3×10¹⁷ Al/cm² at temperatures from 300 to 700 °C. Synchrotron x-ray diffraction was used to ascertain the morphology and grain size of the recrystallized surface layers. Due to the low divergence of the synchrotron beam it was possible to restrict the

penetration depth of the x-rays to less than 0.5 µm by grazing incidence. In this case, only reflections from the polycrystalline surface layer contribute to the diffraction signal.

In Fig. 1 the diffraction patterns (dotted curve) of samples as-amorphized and implanted with 3 × 10¹⁷ Al/cm² at 300 °C are shown. After Al-implantation the shape of the diffraction curve changes and diffraction peaks typical for polycrystalline material appear. Obviously, recrystallization occurs already at an implantation temperature of 300 °C, well below the SiC thermal recrystallization temperature of about 800 °C [2]. This clearly demonstrates that ion beam irradiation strongly enhances the kinetics of the amorphous to polycrystalline phase transition in SiC. The measured diffraction curve shows a very good correspondence with the 3C-powder diffraction data. In particular, nearly identical intensity ratios of the diffraction peaks are observed. Therefore, it can be assumed that randomly oriented grains of 3C-SiC polytype are formed during Al-implantation. From width of the diffraction peaks an average grain size of 9 nm was determined. Furthermore, 3C-SiC crystals with an expanded lattice ($\Delta a/a=0.014$) were observed (see shoulders at smaller diffraction angles). This may be caused by lattice defects due to the recrystallizing implantation process.

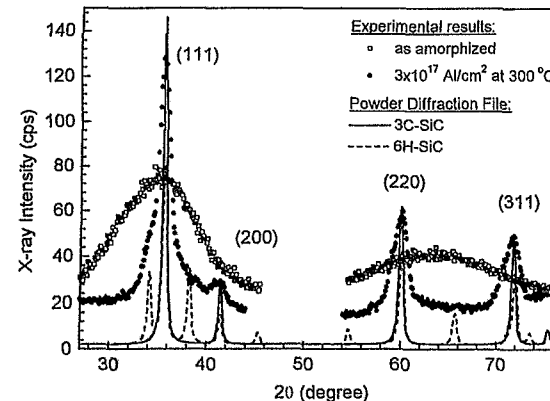
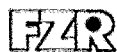


Fig. 1
x-ray ($\lambda=0.154$ nm) diffraction patterns for grazing incidence (0.35°) of samples as-amorphized and implanted with 3 × 10¹⁷ Al/cm² at 300°C. The theoretical powder diffraction patterns of 3C-SiC and 6H-SiC are plotted for comparison.

References

- [1] V. Heera, J. Stoemenos, R. Kögler, and W. Skorupa, *J. Appl. Phys.* 77, 2999 (1994).
- [2] A. Höfgen, V. Heera, F. Eichhorn, and W. Skorupa, *J. Appl. Phys.* 84, 4769 (1998).



Experiment title:
Stress in Ni/Cu Multilayers

Experiment number:
20_02_006

ROBL-CRG

Beamline: BM 20	Date of experiment: from: 03.07.1998 to: 04.07.1998	Date of report: 27.10.98
Shifts: 4	Local contact(s): Dr. Norbert Schell	Received at ROBL: 27.10.98

Names and affiliations of applicants (* indicates experimentalists):

Prof. Dr. J. Böttiger*, K.O. Schweitz*
Dept. Physics and Astronomy
University of Aarhus
Ny Munkegade
DK - 8000 Aarhus

Report:

The experiments at ROBL led to an article submitted to J. Appl. Phys. under the title

Tensile and compressive interface stress in Cu/Ni and Au/Ni multilayers

K.O. Schweitz^{a)}, J. Böttiger^{a)}, J. Chevallier^{a)}, R. Feidenhans^{1 b)}, M.M. Nielsen^{b)},
F.B. Rasmussen^{b)}, W. Matz^{c)} and N. Schell^{c)}

^{a)} Institute of Physics and Astronomy, University of Aarhus, DK-8000 Aarhus C, Denmark

^{b)} Condensed Matter Physics and Chemistry Department, Risø National Laboratory, DK-4000, Roskilde, Denmark

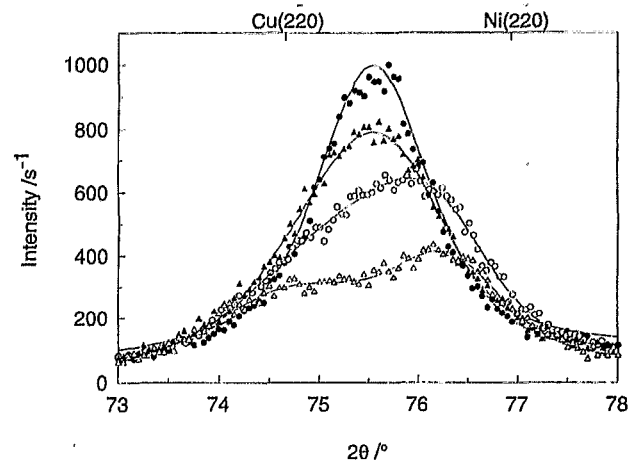
^{c)} Forschungszentrum Rossendorf, D-01314 Dresden, Germany

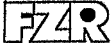
In this paper, we present studies of the interface stress in a multilayer with coherent interfaces, Cu/Ni, and in Au/Ni multilayers with incoherent interfaces. The <111>-textured multilayers were deposited by use of DC-magnetron sputtering and bulk and interface stresses were obtained from X-ray diffraction and measurements of substrate curvatures. The interface stress in Cu/Ni multilayers was found to be $0.77 \pm 0.19 \text{ J/m}^2$, i.e. a *tensile* interface stress in a metallic multilayer. The coherent/incoherent transition in Cu/Ni multilayers is observed at a critical bilayer repeat length of about 10.5 nm, in agreement with theory.

The interface stress in Au/Ni multilayers is found to be compressive, in agreement with theory, but the value of $-8.46 \pm 0.99 \text{ J/m}^2$ is much larger than both the prediction by theory and more than twice as large as values reported for other systems. For the sample having the smallest repeat length, interface roughness and lattice parameters show, that this sample has weakly cumulative interfaces and a strong coherency effect, in contrast to samples with larger repeat lengths. This may explain the observed deviation of the interface stress.

In both systems, the high level of strain makes it necessary to include third-order stiffness coefficients in calculating the stress in the strong <111>-textured Cu/Ni and Au/Ni-multilayers.

The following figure shows as an example GIXRD diffractograms (grazing incidence X-ray diffraction) at the six-circle diffractometer of ROBL for Cu/Ni multilayers of four different bilayer repeat lengths. (The filled spheres, filled triangles, opened spheres and opened triangles represent bilayer repeat lengths of 5.6 nm, 10.5 nm, 14.8 nm and 23.1 nm, resp. The lines are fittings by use of Voigt peaks.)



 ROBL-CRG	Experiment title: Diffuse scattering on Co/Cu multilayers near absorption edges	Experiment number: 20_02_007
	Beamline: BM 20	Date of experiment: May, 13 th , 1998 from: May 5 th , 1998 to: May 7 th , 1998 from: Sept. 6 th , 1998 to: Sept. 7 th , 1998
Shifts: 10	Local contact(s): N. Schell	<i>Received at ROBL:</i> 10.8.99
Names and affiliations of applicants (* indicates experimentalists): * Dr. F. Prokert, FZ-Rosendorf, FIWS * Dr. W. Matz, FZ-Rosendorf, FIWS * Dr. M. Betzl, FZ-Rosendorf, FIWS DP. J. Noetzel, FZ-Rosendorf, FIWS Dr. E. Wieser, FZ-Rosendorf, FIWS * Dr. N. Schell, CRG ROBL at ESRF, Grenoble and FZR		
Report For multilayer (ML) systems showing giant magnetoresistance it is of interest to study layer and interfacial properties [1], [2]. Two types of samples with different layer thicknesses of Co- and Cu-layers $\text{Si/SiO}_2/8x[\text{Co}(4\text{nm})/\text{Cu}(4\text{nm})]$ and $\text{Si/SiO}_2/4x[\text{Co}(8\text{nm})/\text{Cu}(8\text{nm})]$ were investigated in the 'as-deposited' state and after tempering at 500°C for 2h. The ML were prepared by crossed beam pulsed laser deposition (CB PLD) technique. The layer properties like thickness and interface roughness of the different samples were studied using specular and non-specular X-ray reflection (XRR). The high brilliance and tunable wavelength of the synchrotron radiation at ROBL allowed to improve the low contrast for this material combination by setting the X-ray wavelength to the absorption edge of one of the layer materials. Due to the small divergence of the incident beam and by use of a sufficiently small receiving aperture the angular resolution of the detected beam could be matched to resolve adequately the specular peak from the diffuse scattering. The high intensity of the beam allows to measure the distribution of the diffuse scattered intensity over wide regions of the reciprocal space. Assuming that the roughness structure of surface and interfaces in the Co/Cu-MLs is sufficiently self-affine, it can be described besides the rms-roughness σ_{RMS} by two additional parameters [3]. In Sinha's representation of the height-height autocorrelation function the correlation length ξ and the Hurst parameter h characterize		

the lateral cut-off length and the surface jaggyiness, respectively. From coherence effects in the diffuse scattering, occurring in MLs, the roughness correlation between the layers can be estimated and by this the part of the correlated roughness (σ_{COR}) included in σ_{RMS} -roughness ($\sigma_{\text{RMS}}^2 = \sigma_{\text{COR}}^2 + \sigma_{\text{UNCOR}}^2$) is quantified.

Table 1 shows the results obtained (using Bede REFS Code) from the two types of the CB PLD-prepared MLs in the 'as-deposited' state and after tempering.

Table 1 Simulation results for the Co/Cu MLs in the 'as-deposited' state and after tempering

ML type	'as-deposited'				after tempering at 500°C 2h			
	σ_{RMS} (nm)	ξ (nm)	h	$\sigma_{\text{COR}}/\sigma_{\text{RMS}}$	σ_{RMS} (nm)	ξ (nm)	h	$\sigma_{\text{COR}}/\sigma_{\text{RMS}}$
4x[8/8]	Co 1.4	4000	0.25	0.4	Co 1.20	20	0.6	0.10
	Cu 1.2				Cu 0.80			
8x[4/4]	Co 2.3	4200	0.25	0.5	Co 1.60	15	0.7	0.05
	Cu 0.8				Cu 0.85			

Additionally, from the position of the Yoneda peaks (see Fig.1) the critical angle θ_c of the surface layer is well defined. It can be used for determination of the mass density ρ using the relation $\theta_c \propto \sqrt{\rho\lambda}$.

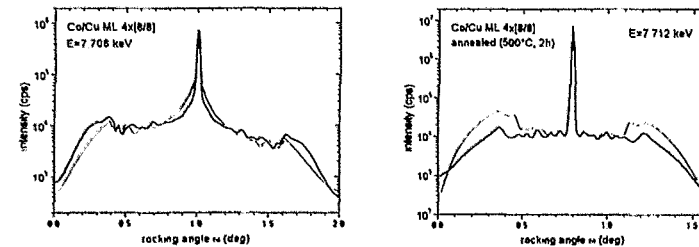



Fig 1 Diffuse scattering (transversale scans) of Co/Cu 4x[8/8]-MLs in the 'as-deposited' state (on the left) and after tempering at 500°C for 1h (on the right). (measured curves - thick lines; simulations - thin lines)

Results

Whereas in the 'as-deposited' state the structure of the interface is characterized by a high jaggyiness, which means that the fractal dimension ($D = 3 - h$) reaches values of about 2.75, after tempering the interface is smoothed and the lateral correlation length is drastically shortened. This is accompanied by a reducing of the roughness conformity.

References

- [1] B.D. Fulthorpe, D.E. Joyce, T.P.A. Hase, B.K. Tanner, P.J. Grundy, *XTOP* 98, 9.-11. 9. 1998 Durham UK (Abstracts) P3.31 and *Phys. Rev. B* 58, 5594 (1998)
- [2] Ping Wu, E.Y. Jiang, H.L. Bai, and H.Y. Wang, *phys.stat.sol (a)* 161, 389 (1997)
- [3] S.K. Sinha, *J. Phys. III France* 4, 1543- 1557 (1994)

 ROBL-CRG	Experiment title: Oxidation kinetics of polycrystalline metal surfaces	Experiment number: 20_02_008
	Beamline: BM 20	Date of experiment: from: Sept. 3 th , 1998 to: Sept. 5 th , 1998
Shifts: 8	Local contact(s): N. Schell	<i>Received at ROBL:</i> 06.09.1999
Names and affiliations of applicants (* indicates experimentalists): * A. Knoll ENSAIS – LMCM 24, boulevard de la Victoire, F-67000 Strasbourg A.Cornet ENSAIS – LMCM 24, boulevard de la Victoire, F-67000 Strasbourg E. Smigiel ENSAIS – LMCM 24, boulevard de la Victoire, F-67000 Strasbourg * Dr. F. Prokert, FZ-Rossendorf, FWIS * Dr. N. Schell, CRG ROBL at ESRF, Grenoble and FZ- Rossendorf		
Report The oxidation behaviour of metals at elevated temperatures became of paramount importance, since it is of interest in many domains of material science and industrial engineering. It is now essential to control high temperature oxidation and therefore to investigate the kinetics of the growth of oxide films of the different material systems. Grazing X-Ray Reflectometry for exemple allows to determine the thicknesses of thin layers on a substrate by interference of the reflected X-Ray beam from several Ångstrom up to several hundred nanometers. In our experiments we investigated the oxidation behaviour of an polished XC15-steel samples to show the interest of this method. After isothermal heating of the samples the thicknesses of the oxide layers were determined in function of the heating time. This allowed to kinetics of oxide growth in function of heating temperature.		

The oxidized samples were oxidized at 300°C in the laboratory LMCM at ENSAIS in Strasbourg. At ROBL, the samples were mounted on the goniometer and specular and diffuse reflectivity was measured under atmospheric pressure and room temperature. Figure 1 shows the specular reflectivity curve of the the XC15 steel samples in function of heating time. By simulation, we determined the oxide layer thickness in function of heating time and so the oxidation kinetics of the steel sample.(figure 2)

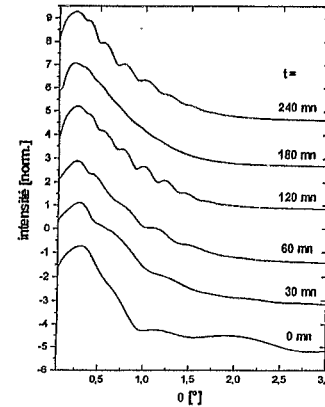


Fig 1. Reflectivity curves

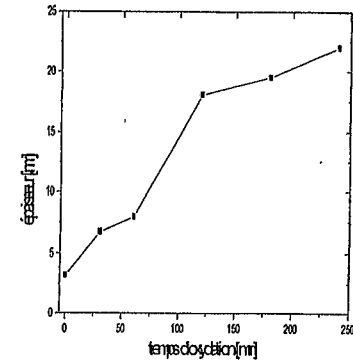



Fig 2. Oxidation kinetic

We observe in Figure 2 two different regions of oxidation behaviour. In the first zone a logarithmic growth can be observed. After a breakaway at about 70mn oxidation time, a parabolic growth behaviour can be observed. This two different zones correspond to two different oxidation behaviour. The breakaway is due to the change of the oxidation mechanism. This results could be reproduced on a laboratory X-ray source and confirmed the existing theories of high temperature oxidation of metals.

Diffuse reflectivity measurements results were compared to AFM measurements on the same samples and confirmed the experimental results obtained by diffuse XRR.

	Experiment title: Reciprocal space mapping (RSM) of Si after C implantation / formation of SiC	Experiment number: 20_02_009
	Beamline: BM 20	Date of experiment: 13.-18.9.98, 30.10.-1.11.98
Shifts: 15	Local contact(s): Dr. N. Schell	<i>Received at ROBL:</i> 12.8.99
Names and affiliations of applicants (* indicates experimentalists): F. Eichhorn *, N. Schell * (a), W. Matz, P. Reichel *, M. Betzl * Forschungszentrum Rossendorf Institute of Ion Beam Physics and Materials Research P.O.B. 510119, D-01314 Dresden, Germany (a) present address: ROBL-CRG at ESRF Grenoble		

Report:

Silicon carbide is well known as a wide band gap semiconductor with a high thermal and chemical stability for realizing electronic devices for high frequency, high power and high temperature applications. Ion implantation of C into Si is a suitable method for synthesizing SiC. In this experiment the formation of SiC crystallites is studied if the volume concentration of C is near 0.45 of the stoichiometric value after implantation of $4 \times 10^{17} \text{ cm}^{-2}$ C ions with an energy of 195 keV at 500 °C or 800 °C. The grown particles were identified as cubic 3C polytype crystallites by x-ray diffraction, and the strain in the Si matrix and its changes were followed (see report to the ROBL experiment 20_02_001). Furthermore the orientation relation between the lattice of the SiC particles and the Si matrix is determined by the measurement of reciprocal space maps (RSM) of symmetric SiC(002) - Si(004) and asymmetric SiC(113) - Si(113) reflection pairs. An orientation alignment of the cubic axes of the SiC crystallites to the Si matrix is confirmed.

Fig. 1 shows the RSM near the SiC(002) reflection for Si(001) wafers implanted with $4 \times 10^{17} \text{ cm}^{-2}$ C ions with an energy of 195 keV. The centre of the Si(004) reflection lies at $q_{\parallel}=0$ and $q_{\perp}=46.3 \text{ nm}^{-1}$. For implantation at the lower temperature of 500 °C the cubic axes of the SiC crystallites are orientated with a nearly isotropic spread (FWHM $\approx 4.5^\circ$) parallel to Si [001] direction.

A higher volume part of SiC grows during carbon implantation at 800 °C – the maximum intensity of the SiC(002) intensity is 3.5 times higher than in the former case. Furthermore, a more complex distribution is found (right hand side of Fig. 1): The majority of crystallites is highly aligned with a spread of 2.5° isotropically distributed around [001] shown by the symmetric top of the SiC peak, whereas the minority is anisotropically distributed around this axis with preferences into the $\langle 111 \rangle$ directions (streaks at the bottom of the SiC peak).

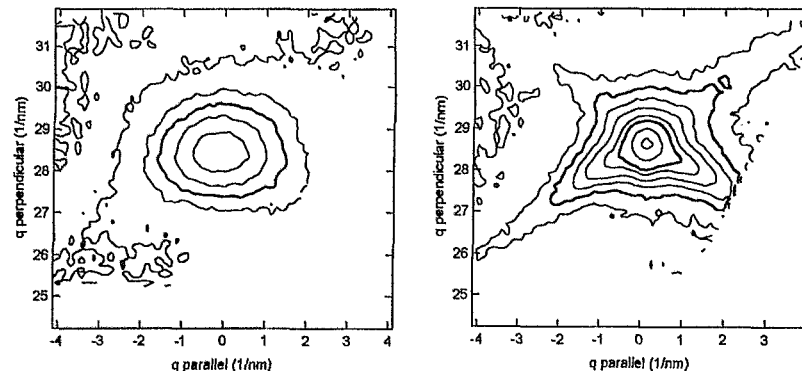
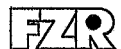


Fig. 1
 Reciprocal space maps near the SiC(002) reflection for Si wafers implanted with $4 \times 10^{17} \text{ cm}^{-2}$ C⁺ with an energy of 195 keV at 500 °C (on the left) or 800 °C (on the right), respectively. The isointensity lines are chosen in a logarithmic scale, the bulk ones corresponds to 512 counts and 2048 counts per 3 sec.



ROBL-CRG

Experiment title: Depth distribution of nitrides in Ti64 after N implantation		Experiment number: 20_02_010
Beamline: BM 20	Date of experiment: from: 6.11.98 to: 11.11.99	Date of report: 24.8.99
Shifts: 10	Local contact(s): N. Schell	<i>Received at ROBL:</i> 31.8.99
Names and affiliations of applicants (* indicates experimentalists): *F.Berberich, *W. Matz, *N.Schell#, E. Richter Forschungszentrum Rossendorf, Institute of Ion Beam Physics and Materials Research, P.O. Box 510119, D-01314 Dresden, Germany #also ROBL-CRG at ESRF		

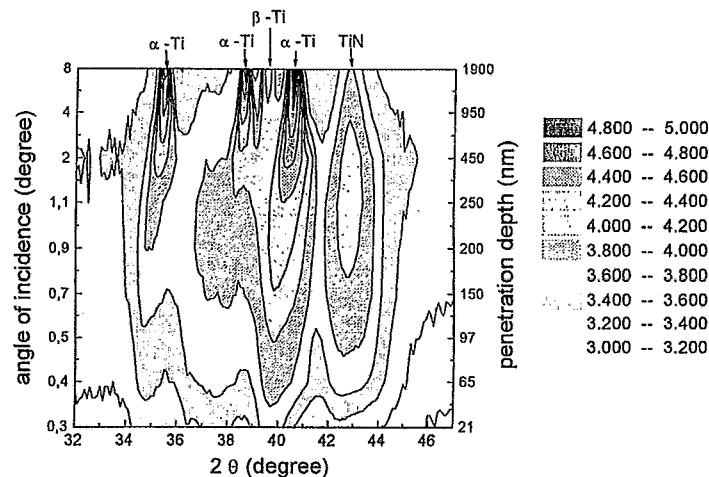
Report:

The technical alloy Ti-6Al-4V (wt.-%) was implanted with nitrogen in order to enhance surface hardness. The as-received alloy has a duplex structure, where the main component is the hexagonal α -phase. The cubic β -phase as the minor component is stabilised by V. The beam line implantation of N at 80 keV produces a Gaussian depth distribution with the centre at 130 nm and a FWHM of about 120 nm. From laboratory X-ray diffraction it was found that for doses $>3 \times 10^{17}$ N⁺/cm² the TiN phase is formed. The aim of the experiment was to check the correlation between nitrogen depth distribution and formation range of TiN. Because of the shallow profile one needs low incidence angles and low divergence of the beam. A sample implanted with a dose of 6×10^{17} N⁺/cm² was investigated in grazing incidence technique with incidence angles from 0.3° to 8°. At $\lambda = 0.154$ nm the intensity in the angular range $2\theta = 32^\circ$ - 47° was recorded. Bragg reflections from all 3 interesting phases are located in this range. The figure shows the 2D intensity plot of the measurements. Note, that the angle / depth -scales are not linear. We were not successful in correcting the data for the penetration depth. The intensity is always the accumulated scattering for the given angle of incidence. For this reason the calculated penetration depth of the X-rays using the density of Ti6Al4V of 4.43 g/cm³ is given as the right scale of the figure. Existing correction

procedures [1,2] assume a multilayer structure with flat, sharp interfaces. In the case of the implantation profile one has a smooth change in the concentration and obviously also in the phase content.

The following conclusions can be drawn from the obtained data.

- The ion implantation destroys most of the crystallinity of the alloy near the surface.
- The lattice of the α -Ti-phase is expanded in the implantation region. At greater depth (bulk region) the peak positions are shifted to higher Bragg angles.
- The TiN phase is formed in the region of partially amorphous material. The maximum of the Bragg reflections of the base alloy were observed in a depth three times higher than the maximum of TiN. The destroyed lattice of the alloy is one prerequisite for forming crystalline TiN directly during implantation without further annealing.
- The strong line broadening for TiN peaks indicates small crystallites in all depths. The estimated crystallite size is about 5-6 nm.
- The apparent maximum of TiN phase is about two times deeper than the maximum of N implantation. This is an effect of the accumulation of intensity. It is necessary to adapt depth correction procedures to smooth distribution functions rather than step like functions.



[1] P. Predecki, Powder Diffraction, 8 (1993) 122

[2] Jian Luo, Kun Tao, Thin Solid Films, 279 (1996) 53

	Experiment title: Short range structure of bulk amorphous metallic alloys	Experiment number: 20_02_011
Beamline: BM 20	Date of experiment: from: Dec. 2 th , 1998 to: Dec. 5 th , 1998	Date of report: May 10 th , 1999
Shifts: 9	Local contact(s): N. Schell	<i>Received at ROBL:</i> 02.08.1999
Names and affiliations of applicants (* indicates experimentalists): * Dr. N. Mattern, IFW Dresden, Helmholtzstr. 20, 01069 Dresden * Dr. L.Q. Xing, IFW Dresden, Helmholtzstr. 20, 01069 Dresden Dr.J.Eckert, IFW Dresden, Helmholtzstr. 20, 01069 Dresden * Dr. N. Schell , FZ Rossendorf		
Report: Zr-Ti-Al-Cu-Ni alloys belong to the family of new multicomponent metallic glasses with extended supercooled liquid region which can be obtained not only by rapid quenching but also by slow cooling from the melt. This allows preparation of thin ribbons as well as of bulk glassy samples. The question whether or not structural differences exist in the amorphous state due to different cooling rate could be answered by the diffraction measurements. Fig. 1 compares the X-ray diffraction patterns of amorphous $Zr_{57}Ti_5Cu_{20}Al_{10}Ni_8$ alloy obtained by rapid quenching and by copper mold casting. Small differences in the scattering curve indicate a somewhat higher degree of order in the slowly cooled sample. These differences are similar to that during annealing of the rapidly quenched material. The sample prepared by copper mold casting corresponds to a relaxed amorphous state. Annealing at elevated temperatures allows structural investigations of the progress of crystallization and the development of stable or metastable nanoscale phases from the supercooled liquid. This offers the possibility to produce bulk nanoscale materials or amorphous/nano(quasi)crystalline phase mixtures by crystallization. Amorphous $Zr_{62-x}Ti_xCu_{20}Al_{10}Ni_8$ with 3 at% Ti forms quasicrystals as the first stage of crystallization [1]. With increasing Ti content the formation of nano-quasicrystals was concluded from		

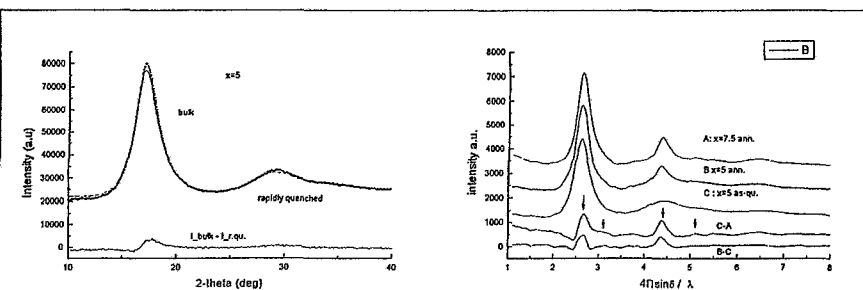


Fig. 1: Comparison of diffraction patterns of amorphous $Zr_{57}Ti_5Cu_{20}Al_{10}Ni_8$

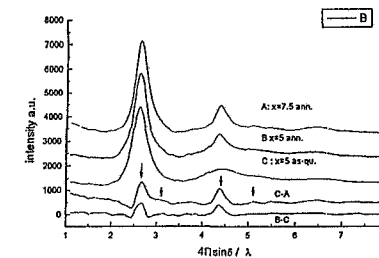
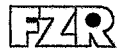


Fig. 2: Diffraction patterns of as-quenched and annealed states $Zr_{62-x}Ti_xCu_{20}Al_{10}Ni_8$

conventional X-ray diffraction measurements [1]. Fig. 2 shows the obtained diffraction patterns for the alloys with 5at% and 7.5at% Ti in the as-quenched state as well as after annealing above the first crystallization peak in DSC. The XRD of the annealed states are characterized by an increase of the intensities of the first and the second maximum but strongly broadened. The formation of an ultrafine nanostructured state 2-3 nm in size can be concluded from the diffraction curves for Ti content ≥ 5 at.%. There are only small differences between 5at% Ti and 7.5at%Ti content. The calculated difference curves between the annealed state and the as-quenched state, also shown in Fig. 2, indicate clearly that the structure of the nanophase is different from the quasicrystalline state obtained for 3at% Ti. The position of maxima in the difference curve are in agreement with a fcc structure. The diffraction curves point to still existing amorphous phase. Further experiments including Transmission Electron Microscopy and Neutron Small Angle Scattering work and are in preparation to get additional informations on the microstructure of the annealed samples.

[1] L.Q.Xing, J.Eckert, W. Löser, L.Schultz: High-strength materials produced by precipitation of icosahedral quasicrystals in bulk Zr-Ti-Cu-Ni-Al amorphous alloys, Appl.Phys.Lett, Vol.74, No. 5,(1999) 664-666



ROBL-CRG

Experiment title: Diffraction of Synchrotron Radiation on Bi-2223 / Ag Superconductors	Experiment number: 20_02_012
--	--

Beamline: BM 20	Date of experiment: from: 3.12.98 to: 4.12.98	Date of report: 31.3.99
---------------------------	---	-----------------------------------

Shifts: 3	Local contact(s): Dr. N. Schell	Received at ROBL: 01.04.99
---------------------	---	--------------------------------------

Names and affiliations of applicants (* indicates experimentalists):

Dr. T. Fahr, IFW Dresden, Abt. 26, Helmholtzstr. 20, 01069 Dresden (*)
 Dr. N. Mattern, IFW Dresden, Abt. 32, Helmholtzstr. 20, 01069 Dresden

Report:

Preliminary diffraction measurements at fully processed multifilamentary Bi-2223/Ag superconductors were performed at ambient temperature without removing the silver surrounding the ceramic material. The experiments were carried out in transmission and reflection arrangements of the tape conductors (Fig. 1). In both geometries usefull diffraction patterns were recorded (Fig. 2, Fig. 3). The analysis of a (200) fibre texture of the superconducting phase of 3 types of superconducting tapes reveals a correlation of the texture degree with the superconducting critical current densities measured at these conductors:

tape	texture degree	critical current density (kA/cm ²)
1	0,793	15,4
2	0,846	20
3	0,909	25,8

The next step should be the adaption of a high temperature chamber to the diffractometer at ROBL to perform high temperature measurements on unprocessed specimens to study the formation and the texture evolution of the Bi-2223 phase during the annealing process in the tape fabrication starting from a multiphase precursor.

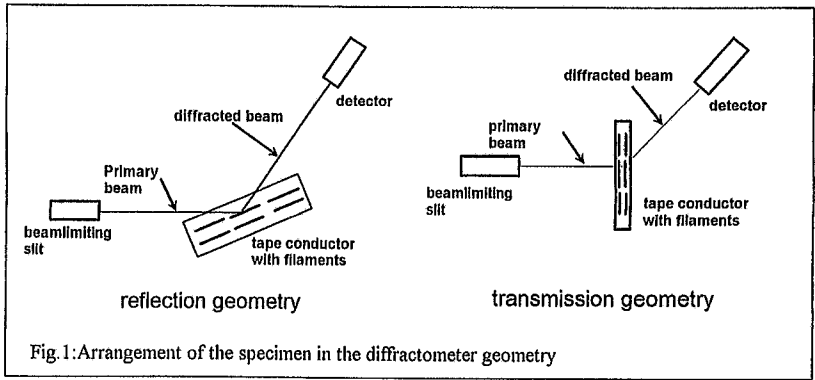


Fig. 1: Arrangement of the specimen in the diffractometer geometry

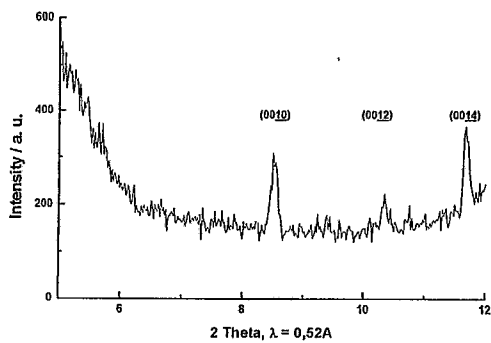


Fig. 2: diffraction pattern recorded in reflection geometry

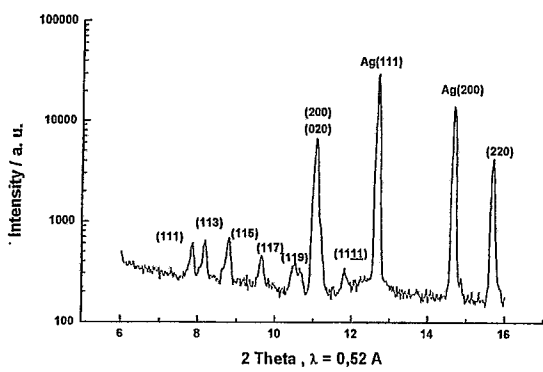
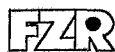


Fig. 3: diffraction pattern recorded in transmission geometry



ROBL-CRG

Experiment title: Interfacial roughness in GMR multilayers		Experiment number: 20_02_013
Beamline: BM 20	Date of experiment: from: Dec. 6 th , 1998 to: Dec. 9 th , 1998	Date of report: May 10 th , 1999
Shifts: 9	Local contact(s): N. Schell	<i>Received at ROBL:</i> 20.5.99
Names and affiliations of applicants (* indicates experimentalists): Dr. C.M. Schneider, IFW Dresden, Helmholtzstr. 20, 01069 Dresden Dr. N. Mattern, IFW Dresden, Helmholtzstr. 20, 01069 Dresden * Dr. M. Hecker, IFW Dresden, Helmholtzstr. 20, 01069 Dresden * D. Tietjen, IFW Dresden, Helmholtzstr. 20, 01069 Dresden		

Report:

To investigate multilayer systems showing giant magnetoresistance (GMR), it is of interest to correlate layer and interfacial properties of such systems both with parameters of the sample preparation and with the resulting GMR. In the present study samples with different combinations of Co-, Cu- and NiFe-layers of about 2 nm thickness corresponding to the second maximum of the GMR were prepared by DC magnetron sputtering. The layer properties like layer thickness and interface roughness and the lattice properties like strains and crystallographic texture of the different samples were compared using methods of X-ray reflection and wide angle diffraction, respectively. The high brilliance and tunable wavelength of the synchrotron radiation at the ROBL beamline allowed to improve the contrast for the different material combinations by setting the X-ray wavelength to the absorption edge of one of the layer materials (in most cases Cu) and to measure the diffuse scattering with intensity sufficient for evaluation.

An example of the specular scattering experiments is given in Fig. 1a. Both the values of the rms interface roughness and of the layer thickness were found to be correlated with the layer combination. For instance, the Co/Cu layer combination shows smaller roughness and larger layer thickness compared with the NiFe/Cu system.

Apparently, the larger adhesion between Co and Cu does not only increase the layer thickness but also reduces the interface roughness. A similar interpretation may be obtained from the measurement of samples containing additional thin layers of a third material between the main components of the multilayer. We found that thin additional Co layers of about 0.3 nm thickness reduce the roughness of the interfaces in NiFe/Cu multilayers, whereas additional NiFe layers in the Co/Cu system reduce the thickness of the Co and Cu layers; apparently due to the smaller adhesion between NiFe and the other two multilayer components.

Though the specular part of the scattering in the low angle region shows significant differences between the samples, the diffuse scattering looks rather similar for all samples. Lateral correlation lengths of about 10nm and values of the Hurst parameter of about 0.6 result from transverse and offset scans independent of the layer composition. The corresponding characteristics of the interface morphology seem to be influenced more by the sputtering technique than by the multilayer composition.

Wide angle diffraction measurements reveal a preferred {111}-orientation of the lattice planes parallel to the interfaces with a half width of the texture of $\text{FWHM} \approx 30^\circ$ and profile shapes influenced by size-strain-effects for all samples (Fig. 1b). A lower limit of the mean crystallite size was estimated to be about 10 nm, which is larger than the layer thickness and indicates the columnar structure of the grains. This structure can also be deduced from the multilayer peaks of the {111}-reflection. The satellites of already the first order are very weak due to internal strains and interface roughness. A comparison of the measured profiles with those calculated using a kinematical model including interface roughness indicates the presence of coherence strains diminishing the lattice mismatch at the interfaces.

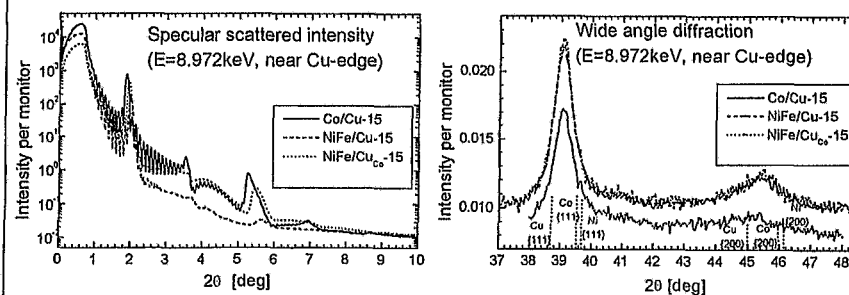


Fig. 1: Scans of a Co/Cu-multilayer (red), a NiFe/Cu-multilayer (blue) and a NiFe/Cu-multilayer with a thin additional Co-layer at the interfaces (cyan) in the low angle region (a, left) and in the wide angle region (b, right). The bilayer number of the multilayers is 15.

Experiment title: HIGH- PRECISION DETERMINATION OF ATOMIC POSITIONS IN 6H- AND 4H-SiC CRYSTALS		Experiment number: 20_02_014
Beamline: BM 20	Date of experiment: from: 12/10/98 to: 12/17/98	Date of report: 5/19/99
Shifts: 17	Local contact(s): Dr. Norbert Schell	<i>Received at ROBL:</i> 20.5.99

Names and affiliations of applicants (* indicates experimentalists):

Andreas Bauer*
 Dr. Jürgen Kräublich*
 Bettina Köcher*
 Prof. Dr. Konrad Goetz
 Friedrich Schiller University of Jena, Institute of Optics and Quantumelectronics
 Department of X-ray Physics
 Max-Wien-Platz 1, D-07743 Jena /Germany

Report:

The measurement of the "quasiforbidden" reflections is a very sensitive method in order to determine very small changes of atomic positions (e.g. relaxations), deformations of the charge density in dependence of the chemical bonding or differences of atomic vibrations. We used this method to determine the atomic positions of 4H- and 6H-SiC crystals with high precision. This was necessary to examine the polytype-depending displacements of the C- and the Si- atomic positions from the ideal tetrahedron and to compare these results with *ab initio* calculations [1][2]. Such atomic displacements of the carbon atoms ($\epsilon(j)$) and the silicon atoms ($\delta(j)$) are in order of magnitude of 10^{-4} times the *c*-lattice constant. These small displacements result in a non-vanishing integrated intensity of the "quasiforbidden" reflections. Since these integrated intensities are essentially smaller than the intensities of the occurring "Umweg" reflections, a correction of the influence of the "Umweg" reflections is necessary. To carry on former investigations we made measurements at BM 20 at the ESRF to:

- get more precise results by means of refined "Umweg" corrections.
- get unambiguous structure models by measurement of extreme weak reflections (especially asymmetric reflections).
- specify the "absolute" structure by determination of the phase invariant ϕ_{inv} at multiple beam cases, i.e. differentiation of structure models, which only differ from each other in the sign of the atomic displacements.

In order to achieve this goal high primary X-ray intensity ("quasiforbidden" reflections) and a six-circle-diffractometer (rotation about any desired lattice plane normal) was necessary.

Since the evaluation of point (i) and (ii) has not been finished up to now, only point (iii) will be discussed in the following.

Since the relaxed structure is characterized by the atomic displacements ($\delta(j)$, $\epsilon(j)$) from the ideal tetrahedron structure, both structures $S_+ = (\delta(j), \epsilon(j))$ and $S_- = (-\delta(j), -\epsilon(j))$ result in the same integrated intensities,

because of $|F_+(H)| = |F_-(H)|$, where H is the reciprocal lattice vector of the "quasiforbidden" reflection. Therefore the both structures cannot be distinguished by measurement of the integrated intensities only. Because of

$$\phi_+(H) = \phi_-(H) \pm 180^\circ$$

for small displacements $\delta(j)$ and $\epsilon(j)$ the "absolute" structure can be determined if the phases of the structure factor of the "quasiforbidden" reflections are known. The measurement of these phases becomes possible by superposition of the "quasiforbidden" reflection H with "Umweg" reflections [3]. When choosing a three beam geometry the two remaining reflections L and $H - L$ have to be strong reflections, because strong reflections are independent of the relaxations. If the phase invariant

$$\phi_{inv} = \phi_L + \phi_{H-L} - \phi_H$$

is close to 0° or 180° , the wings of the peaks in the azimuth scan (rotation about the lattice plane normal of the weak reflection H) of the "Umweg" reflections are strongly asymmetric. The model S_+ shows the inverse asymmetry compared with the model S_- (FIG. 1).

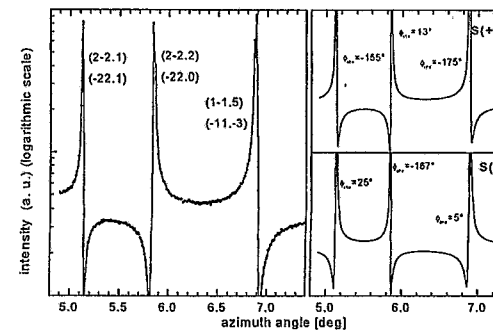
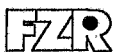


FIG. 1: Left: experimental azimuth scan of the 4H-SiC 00.2 reflection. In brackets the Miller indices of the strong reflections L and $H - L$. Top right: simulation of the 4H-SiC 00.2 reflection according to Ref. [4] model S_+ with the phase invariant. Bottom right: simulation of the 4H-SiC 00.2 reflection according to Ref. [4] model S_- with the phase invariant.

In order to distinguish the model S_+ from S_- , reflections with small Miller indices are particularly useful, since the influence of temperature vibrations can be neglected for silicon carbide in this case.

Comparing the measured data with the simulation of the "Umweg" peaks according to Ref. [4] we found a good agreement with the model S_+ in the case of 4H-SiC (FIG. 1) as well as for 6H-SiC (without figure). These results also match with the *ab initio* calculations in Ref. [2].

- Bauer A. et al.: High-precision determination of atomic positions in crystals: The case of 6H- and 4H-SiC, Physical Review B, Vol. 57, Number 5, 1 February 1998, 2647-2650.
- Käckell P.: Siliziumkarbid - Strukturelle und elektronische Eigenschaften verschiedener Polytypen, Dissertation, Friedrich-Schiller-Universität Jena, 1996.
- Weckert E., Hümmner K.: Multiple-Beam X-ray Diffraction for Physical Determination of Reflection Phases and its Applications, Acta Cryst. (1997), A 53, 108-143.
- Shen Q: A New Approach to Multibeam X-ray Diffraction Using Perturbation Theory of Scattering, Acta Cryst. (1986), A 42, 525-533.



ROBL-CRG

Experiment title:

Observation of Extrinsic Stacking Faults in B implanted Si by CTR Scattering

Experiment number:

20_02_015

Beamline:

BM 20

Date of experiment:

from: 14.2.99 to: 21.2.99

Date of report:

7.7.99

Shifts:

21

Local contact(s): N. Schell**Received at ROBL:**

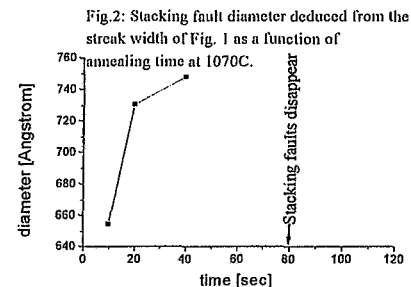
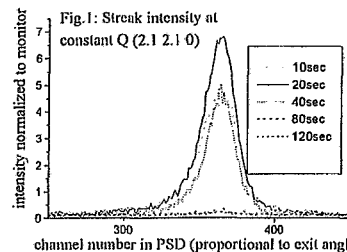
20.7.99

Names and affiliations of applicants (* indicates experimentalists):

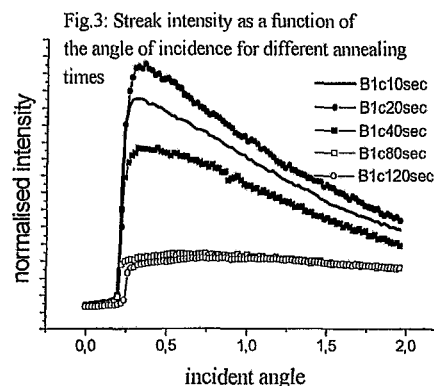
Dr. T.H. Metzger, Prof. Dr. J. Peisl, I. Kegel*
 Ludwig-Maximilians-Universität Muenchen
 Sektion Physik, Geschwister-Scholl-Platz 1,
 D-80539 Muenchen, Germany
 Jim Patel SSRL Stanford university, USA
 F. Berberich*, Forschungszentrum Rossendorf

Report: We have investigated the defect formation in Si after boron implantation at different annealing stages by grazing incidence diffuse x-ray scattering. The starting material was Si (001) implanted by 32 keV B to a dose of $6 \times 10^{15} \text{cm}^{-2}$ and annealed for 15 minutes at 750°C to recrystallise the damaged near surface layer. The aim of the experiment was to study the transition from B-I clusters at 750°C to mainly extrinsic stacking faults (SF) which were found previously at annealing conditions of 1070°C and 10 seconds. The grazing incidence diffuse scattering was first measured in-situ in a furnace which allowed for temperatures up to 1500°C in a vacuum of about 10^{-7} Torr. The in-situ studies failed because the heat transfer between the heater and the sample was not good enough. Instead a set of 5 samples which had been treated ex-situ by rapid thermal annealing (RTA) at 1070°C for different times (10s, 20s, 40s, 80s, 120s) have been investigated. An intensity "slice" along [001] has been measured by use of a position sensitive detector (PSD) placed while the scattering vector pointed at the position (2.1 2.1 0). Here the diffuse intensity rod in [111] direction, which indicates the presence of SF on (111) planes is most pronounced as can be seen in Fig. 1 for all samples. Most surprisingly the SF grow and disappear in a very short time window of only 80 sec. At 10 sec the streak intensity is smaller than at 20 sec, the SFs are growing. The width of the streak along the exit angle is directly linked to the lateral extension of the SF and is easily converted in a SF diameter of 66 nm at 10 sec

which continues to increase with time as shown in Fig.2. At 40 sec the streak intensity decreases, indicating the dissolution of the SFs and at 80 sec the SFs have completely vanished.



The integrated peak intensity in Fig. 1 is proportional to the number of SF which will be used, together with the SF diameter from Fig. 2, to study the growth kinetics of the SFs. Another important question is the depth distribution of the SFs. The intensity in the PSD was studied as a function of the incident angle, keeping the scattering vector constant at (2.1 2.1 0) as shown in Fig.3 for the different annealing times.



The information on the depth distribution of the SF will be deduced from the functional dependence of the curves in Fig. 3. In conclusion: we have discovered stacking fault formation in B implanted Si which depends sensitively on the annealing temperature and time. The SF grow and disappear again in a short time window of only 80 sec. The trapping of the Si interstitial atoms in SFs provides a mechanism to explain the low transient enhanced diffusion of Boron at 1070°C , because free Si interstitials are needed for the interstitialcy mechanism of the anomalous fast B diffusion in B implanted Si. We have also found that at 750°C only a few SF are already present with a diameter of about 10nm.



ROBL-CRG

Experiment title:
XR-study of ion beam induced mixing effects in Co/Cu-multilayers

Experiment number:
20_02_016

Beamline: BM 20

Date of experiment: from: May 12th, 1999 to: May. 15th, 1999

Date of report: July 20th, 1999

Shifts: 12

Local contact(s): N. Schell and F. Berberich

Received at ROBL: 16.8.99

Names and affiliations of applicants (* indicates experimentalists):

- * Dr. F. Prokert, FZ- Rossendorf, FIWS
- * DP. J. Noetzel, FZ- Rossendorf, FIWS
- Dr. E. Wieser, FZ- Rossendorf, FIWS
- * Dr. N. Schell, CRG ROBL at ESRF, Grenoble and FZR
- * DP. F. Berberich, CRG ROBL at ESRF, Grenoble and FZR

Report

The study of ion-beam modification of Co/Cu multilayers (Co/Cu ML) is part of investigation of the intermixing properties of Co-Cu systems [1], [2]. Two types of C/Cu MLs, Si/SiO₂/8x[Co(4nm)/Cu(4nm)] and Si/SiO₂/4x[Co(8nm)/Cu(8nm)], were investigated in the 'as-deposited' state and after ion-beam mixing. The MLs, prepared by crossed beam pulsed laser deposition (CB PLD), were implanted with low (2.5x10¹⁵ Cu⁺/cm²), medium (5x10¹⁵ Cu⁺/cm²) and high (2x10¹⁶ Cu⁺/cm²) doses of 150 keV-Cu⁺ ions. The high brilliance and tunable wavelength of the synchrotron radiation at ROBL allowed to improve the low contrast for this material combination by setting the X-ray wavelength to the absorption edge of one of the layer material.

Information about the changes in density, layer thickness and interface roughness due to mixing by ion bombardment come from the reflectivity (XXR) of the 'as-deposited' and the implanted specimens. Specular (Fig.1) and non-specular (diffuse) XXR were measured on both types of samples at the K-edge energy of Co (7.708 keV) and Cu (8.9737 keV), respectively. With these two independent data sets of the same samples, the accuracy of the simulations, obtained from the codes REFSIM (Siemens) and/or REFS (Bede Scientific), could be improved by the cross-check of the fitted parameters.

70

Table 1 Results from specular XRR of Co/Cu-MLs (Charge 2)

ML type	single layers	'as deposited'			low-dose Cu ⁺ implanted		
		d (nm) d _{Co} /d _{Cu}	ρ (g/cm ³)	σ _{RMS} (nm)	d (nm) d _{Co} /d _{Cu}	x Co _x Cu _{1-x}	σ _{RMS} (nm)
4x[8/8]	Co	16.95	8.6	1.5	16.55	0.8	2.4
	Cu	1.08	8.8	1.5	1.03	0.2	2.3
8x[4/4]	Co	8.0	8.4	1.2	8.0	0.50	1.45
	Cu	1.05	8.8	1.15	1.05	0.15	1.35

Table 2 Results obtained from diffuse scattering (transversal scans) of Co/Cu-MLs (Charge 1)

ML type	'as-deposited'				after high-dose Cu ⁺ -implantation			
	σ _{RMS} (nm)	ξ (nm)	h	σ _{COR} /σ _{RMS}	σ _{RMS} (nm)	ξ (nm)	h	σ _{COR} /σ _{RMS}
4x[8/8]	Co	4000	0.25	0.4	{CoCu}	100	0.6	0
	Cu				3.4			uncorr.
8x[4/4]	Co 1.25	4200	0.25	0.5	{CoCu}	100	0.6	0
	Cu 0.82				3.3			uncorr.

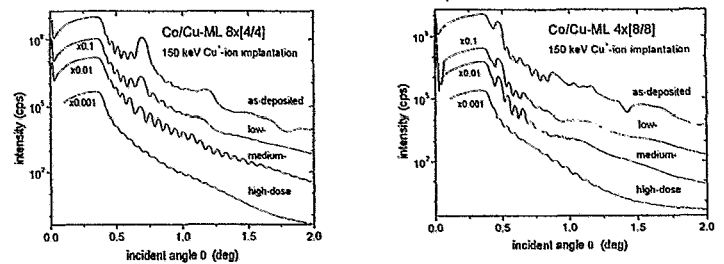



Fig.1 Specular XRR of Co/Cu-8x[4/4]MLs (on the left) and Co/Cu-4x[8/8] MLs (on the right) in the 'as-deposited' state and after low-, medium-, and high-dose 150 keV Cu⁺-ion implantation

Results

As expected, due to the ion-beam mixing the Co-Cu-interface regions increase and the ML-structure is successively dissolved. Certainly the used modelling, based on the Paratt formalism and the Névot-Croce roughness model, must be stressed to describe such an extended interface structure. Nevertheless, useful information about σ_{RMS}-roughness and interface topology follows also from these rough simulations. Besides the formation of graded interfaces (Co_xCu_{1-x}) the initially jagged layers will be smoothed by ion-impact processes as shown by the strong decrease of the h- and ξ-parameters. With increase of the graded interfaces the ML roughness conformity disappears.

References

- [1] D.E.Joyce, et al., Phys.Rev.B 58 (1998) 5594-5601
- [2] Ping Wu et al., phys.stat.sol.(a) 161 (1997) 389- 397

 ROBL-CRG	Experiment title: Study of self-organized dots on the surface of implanted and annealed silicon	Experiment number: 20_02_017
	Beamline: BM 20	Date of experiment: from: 21.2.99 to: 28.2.99
Shifts: 18	Local contact(s): Dr. N. Schell, F. Berberich	<i>Received at ROBL:</i> 12.8.99
Names and affiliations of applicants (* indicates experimentalists): F. Eichhorn *, J. Sass (a), K. Mazur (a), N. Schell * (b), F. Berberich * (b) Forschungszentrum Rossendorf, Institute of Ion Beam Physics and Materials Research P.O.B. 510119, D-01314 Dresden, Germany (a) Institute of Electronic Materials Technology, ul. Wólczyńska 133, PL 01-919 Warszawa, Poland (b) present address: ROBL-CRG at ESRF Grenoble		

Report:

To follow the stability of semiconductor material under non-standard conditions of treatment Si(001) wafers were implanted with $2.5 \times 10^{15} \text{ cm}^{-2} \text{ Ge}^+$ ($E = 1 \text{ MeV}$, or 4 MeV) and annealed at $650 \text{ }^\circ\text{C}$ for 1 h. The samples were characterized by high-resolution XRD, REM and AFM, respectively. As revealed by XRD a strain gradient perpendicular to the surface is formed by the implantation process. The strain reaches values of 0.00140 after 1 MeV and 0.00116 after 4 MeV implantation. Due to subsequent thermal treatment the strains are reduced to 0.00085 and 0.00106, respectively, and lattice defects grow as indicated by the diffuse scattering. Furthermore, transverse intensity oscillations were observed in the reciprocal space map. It was confirmed by AFM and SEM that the reason for them is a self-organized system of dots on the surface. The dots are nearly cones with a bottom diameter of 360 nm and a height of 40 nm. Their mean distance is about $1.5 \text{ } \mu\text{m}$ and they are preferentially arranged in rows along $\langle 110 \rangle$ directions. Storing the samples at normal laboratory conditions the dots disappear after about 8 and 16 months, respectively.

The aim of the experiment is to reproduce the conditions for the growth of the dots by in-situ thermal treatment and their detection by a quick x-ray scattering method. A formerly implanted ($2.5 \times 10^{15} \text{ cm}^{-2} \text{ Ge}^+$ of 4 MeV) and annealed (at $650 \text{ }^\circ\text{C}$ for 1 h) Si(001) wafer was heated in a furnace from $600 \text{ }^\circ\text{C}$ to $905 \text{ }^\circ\text{C}$ in steps of $50 \text{ }^\circ\text{C}$ for 20 min in each case. According to the findings above, it is expected that during this annealing procedure surface dots grow. The grazing incidence small-angle x-ray scattering (GISAXS) geometry [1], highly sensitive to mesoscopic dots at the surface, is the suitable tool to study surfaces independent on their crystalline or non-crystalline nature. At an annealing temperature of $850 \text{ }^\circ\text{C}$ some marks of an ordered surface structure (see Fig. 1, arrows mark fringe maxima) may be seen. From them a surface structure period of 320 nm can be calculated. At other temperatures such fringes were not be observed.

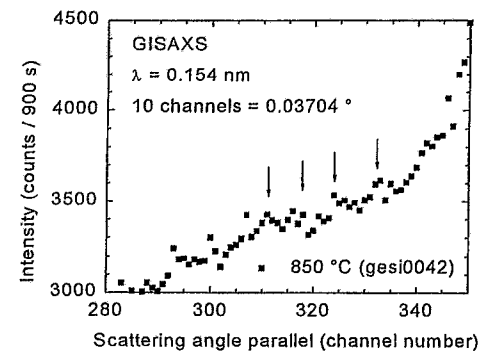


Fig. 1

GISAXS diagram of Si(001) implanted with $2.5 \times 10^{15} \text{ cm}^{-2} \text{ Ge}^+$ (4 MeV) and formerly annealed at $650 \text{ }^\circ\text{C}$ for 1 h as-measured for an annealing temperature of $850 \text{ }^\circ\text{C}$

The authors acknowledge the assistance of Dr. T. H. Metzger, Ludwig-Maximilians-Universität München, in the GISAXS measurements.

[1] T. H. Metzger, I. Kegel, R. Paniago, J. Peisl, J. Phys. D: Appl. Phys. 32 (1999) A202.

Experiment title: ROBL-CRG	Experiment number: 20_02_018
Beamline: BM 20	Date of report: 10.8.99
Shifts: 9	Date of experiment: from: 25.2.99 to: 28.2.99
Local contact(s): Dr. N. Schell	
Names and affiliations of applicants (* indicates experimentalists): F. Eichhorn*, R. Kögler, N. Schell* (a) Forschungszentrum Rossendorf Institute of Ion Beam Physics and Materials Research P.O.B. 510119, D-01314 Dresden, Germany (a) present address: ROBL-CRG at ESRF Grenoble	

Report:

The aim of the experiment is to measure the lattice expansion of MeV-ion-implanted Si. Especially the behaviour of n-doped (P) and p-doped (B) Si wafers with (001) and (111) surface planes should be compared. It can be assumed that the strain differs because of the crystallographic anisotropy of Young's modulus. According Hook's law $\epsilon = (1/E)\sigma$, for a given stress σ introduced by ion implantation different strain values ϵ (directed normally to the surface) results for different crystallographic orientation of the Si wafer due to different values of Young's modulus ($1/E_{\langle 001 \rangle} = 7.68 \cdot 10^{-12} \text{ m}^2/\text{N}$ and $1/E_{\langle 111 \rangle} = 5.32 \cdot 10^{-12} \text{ m}^2/\text{N}$, that is for the same stress $\epsilon_{\langle 001 \rangle} = 1.44 \cdot \epsilon_{\langle 111 \rangle}$). This difference should result in a different gettering capability of the implanted layer for metallic impurities and may explain the observed „anomalous“ metal gettering in the $R_{\text{p}}/2$ region [1].

The samples were implanted with $5 \times 10^{15} \text{ cm}^{-2} \text{ Si}^+$ of 3.5 MeV and studied in the as-implanted state and after an annealing at 800 °C or 900 °C for 30min. The maximum strain is in the range of $5 \cdot 10^{-4}$ and the depth distribution of the strain and implants reaches 3 μm .

To extract the necessary data, reflections with net planes parallel and inclined to the surface of the sample are studied. In the following table the diffraction parameters for the used reflections are given for the x-ray wavelength $\lambda=0.1608 \text{ nm}$, the maximum wavelength for realizing beam propagation through the goniometer for all the chosen reflections.

(h k l)	2 θ (°)	Incidence angle (°)	Inclination angle (°)
Surface (001)			
--- sym. Case (0 0 4)	72.633	36.317	0.000
--- asym. Case (1 1 3)	58.821	4.171 and 54.650	25.239
Surface (111)			
--- sym. Case (1 1 1)	29.719	14.860	0.000
--- asym. Case (1 3 3)	80.389	18.193 and 62.196	22.002

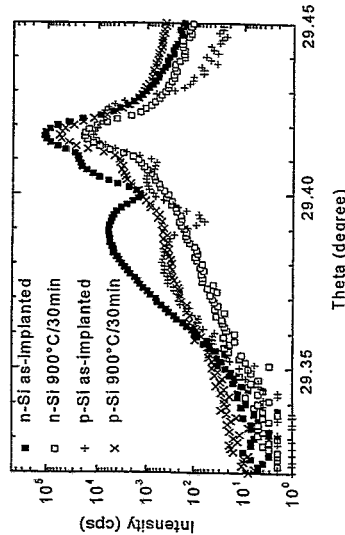


Fig. 1
Asymmetric Si(113) reflection for grazing incidence of the x-ray beam ($\lambda = 0.1608 \text{ nm}$) for Si(001) wafers implanted with $5 \times 10^{15} \text{ cm}^{-2} \text{ Si}^+$ of 3.5 MeV energy

In Fig. 1 diffracted intensities of the asymmetric Si(113) reflection are given. In this case, strain ϵ_{\perp} as well as strain ϵ_{\parallel} contribute to the measured signal. The strain measured in p-Si is approximately 20 % higher than that in n-Si and more stable against an annealing treatment. This is confirmed by other reflections, too. Wafers with (111) surface give a similar result. Significant different strain for (001) and (111) orientated wafers were not found because of the limited accuracy, but the first results in this long-term experiment will be used for optimization of forthcoming measurements.

[1] R. Kögler, R.A. Yankov, J.R. Kaschny, M. Posselt, A.B. Danilin and W. Skorupa, Nucl. Instrum. and Meth. B 142 (1998) 493.

Experiment title: <i>in-situ</i> temperature dependent measurements of phase transformations in N-implanted Ti6Al4V alloys		Experiment number: 20_02_019
Beamline: BM 20	Date of experiment: from: 9.5.99 to: 10.5.99 19.6.99 22.6.99	Date of report: 26.08.99
Shifts: 15	Local contact(s): N. Schell	Received at ROBL: 30.8.99
Names and affiliations of applicants (* indicates experimentalists): *F. Berberich ^{o)} , *W. Matz, E. Richter, *N. Schell ^{o)} Forschungszentrum Rossendorf, PF 510119, D-01314 Dresden Institute of Ion Beam Physics and Materials Research ^{o)} also ROBL-CRG at ESRF		

Report (first part):

The experiments are part of a general work to investigate the structural mechanisms of the enhanced hardness of the technical alloy Ti-6Al-4V due to N⁺ implantation and its degeneration. Samples were implanted with doses (1 - 6) x 10¹⁷ N⁺/cm² at 80 keV. The structural implications of the loss of hardness during annealing were studied by in-situ XRD-experiments with synchrotron radiation at a sample implanted with a dose of 6x10¹⁷ N⁺/cm². Additional sample characterisation was performed by SEM, ERDA and Vickers hardness.

The as-received sample shows only Bragg peaks of the hexagonal α -phase, which is the main phase, and peaks of the cubic β -phase. After the ion implantation we observe the TiN_{0.3} at first and then the TiN Bragg peaks. The intensity of these peaks show a direct correlation to the implanted doses. The Bragg peaks of both nitride phase are significantly broadened. From the line broadening a mean crystalline size of 5 nm was estimated. It was concluded that the observed hardening of the alloy is of precipitation type rather than the formation of a TiN layer.

The in-situ experiment with a Ti-6Al-4V sample implanted with a dose of 6 x 10¹⁷ N⁺/cm² was performed at ROBL with a high temperature diffraction chamber. The investigated temperature region was from 500°C to 750°C in steps of 50K. At each temperature two X-ray patterns were recorded; for an angle of incidence of 1° (approximate penetration depth of 200 nm) and another one for 4° (up to 1000 nm depth).

each diffraction pattern was 30 min. So the duration of the in-situ experiment corresponds to the typical annealing time used for these alloys.

At 500°C the pattern consists of the Bragg peaks from both Ti phases and from TiN formed by implantation. With increasing temperature the intensity of the TiN peaks decreases. The formation of Ti₂N begins at a temperature between 650°C and 690°C. At the final temperature of 730°C all TiN peaks have completely vanished and only Ti₂N peaks are observed besides the Ti-phases. From a plot of the integrated intensities for TiN and Ti₂N in Fig. 1 it can be seen, that this phase transformation is a continuous process.

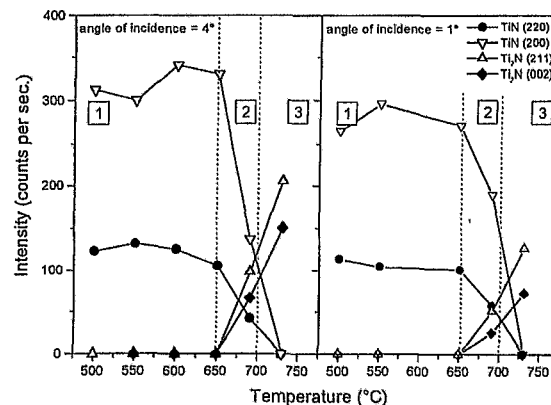


Fig. 1: Change of the integrated intensity of TiN and Ti₂N peaks during in-situ annealing of Ti6Al4V alloy

A further structural effect is the change in the lattice parameters in both the α -Ti and β -Ti phases, which is not conform with thermal expansion as shown in Fig.2. Especially, the lattice expansion of the β -Ti phase of 2% over a temperature range of 200K is remarkable. It is known, that V in Ti reduces the cubic lattice parameter significantly. From the behaviour shown in Fig. 2 one may conclude that the annealing is connected with a reduction of the V-content in the β -Ti. This is suggested as an additional process for hardness reduction besides the phase transformation.

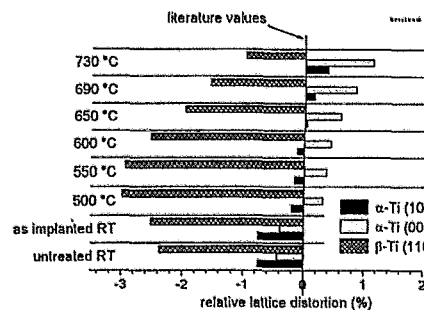
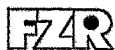


Fig. 2: Change of lattice constants of the Ti-phases during annealing



ROBL-CRG

Experiment title:*Characterization of waveguide-structures with single- / multimode-guiding-layers***Experiment number:**

20_02_021

Beamline:

BM 20

Date of experiment:

from: 17.05.1999 to: 18.05.1998

Date of report:

02.09.99

Shifts:

6

Local contact(s):

Dr. Norbert Schell

Received at ROBL:

02.09.99

Names and affiliations of applicants (* indicates experimentalists):

Franz Pfeiffer*, Tim Salditt*

Sektion für Physik und Center for NanoScience (CeNS)
LMU München, Geschwister-Scholl-Platz1, D-80539 München

Email: salditt@physik.uni-muenchen.de

Peter Høghøj*

ILL (DPT), Avenue des martyrs, B.P. 156, F-38042 Grenoble Cedex 9

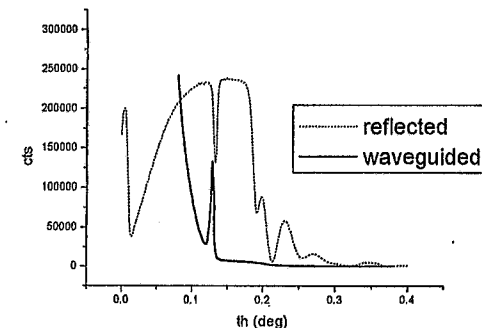
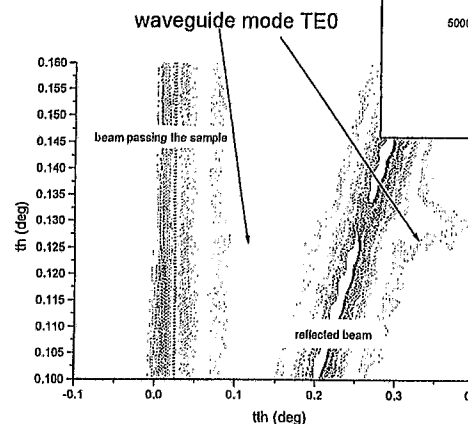
Report:

We have fabricated x-ray waveguides [1, 2] by different thin film deposition techniques, and characterized their x-ray optical properties by experiments using a 20 keV synchrotron beam at ROBL (BM20) [3]. A theory to describe the observed effects has been developed and compared to the experimental results. The good agreement confirmed our model and enabled us to design waveguides with several new features by simulating their guiding characteristics, and calculating the efficiencies.

A nearly perfect control of the automated sputter deposition process allowed us to design and study a series of sputtered Ni/C-waveguides varying different structural parameters, ranging from very thick (~ 1500 Å) to ultrathin guiding layers of 100 Å. Only a single mode can propagate in the ultrathin guiding layers, which has never before been observed. At the exit of the waveguide structure, a correspondingly small "nanobeam" is produced, to our knowledge the smallest beam ever reported.

The farfield patterns of many different waveguide devices have been characterized by two-dimensional mappings, which proved very useful to identify the resonances and to compare the results to multidimensional field simulations, see below. Furthermore, we have designed and characterized a new class of multiple guiding layer devices, with potential applications in interferometry.

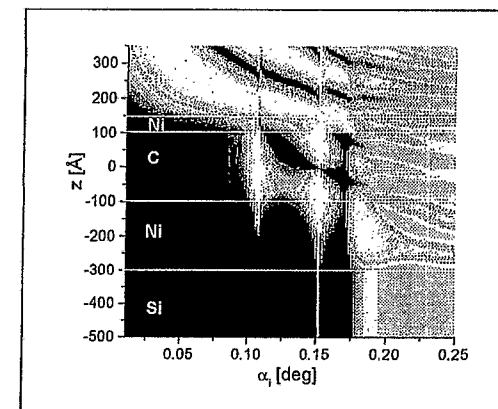
reflectivity and farfield pattern
single-mode waveguide
Ni[70Å]/C[100Å]/Ni[200Å]/Si



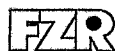
ROBL beamline 08.03.1999
 α_i / α_r - mapping, reflectivity and 1:1-scans
20 keV (4 GeV-Mode)

F. Pfeiffer, P. Hoghoj, T. Salditt,
N. Schell (ROBL)

A simulation of the field intensity distribution in a double mode waveguide structure as a function of the incidence angle. A resonant field enhancement of about two orders of magnitude is found in some structures and can be indirectly confirmed from a measurement of the farfield intensity of the exiting beam.



- [1] Y.P. Feng, S.K. Sinha, H.W. Deckmann, et al., Phys.Rev.Lett **71**, 537 (1993);
Y.P. Feng, S.K. Sinha, E.E. Fullerton, et al., Appl.Phys.Lett. **67**, 3657 (1995).
[2] S. Lagomarsino, W. Jark, S. Di Fonzo, et al., J. Appl.Phys. **79**, 4471 (1996);
S. Lagomarsino, A. Cedola, P. Cloetens, et al., Appl.Phys.Lett. **71**, 2557 (1997).
[3] F. Pfeiffer, P.H Høghøj, I. Anderson, T. Salditt, N. Schell, to be published.



ROBL-CRG

Experiment title:
*Stress Relaxation in CrN Layers***Experiment number:**
20_02_022**Beamline:**
BM 20**Date of experiment:**
from: 23.06.1999 to: 24.06.1999**Date of report:**
27.08.99**Shifts:**
6**Local contact(s):**
Dr. Norbert Schell*Received at ROBL:*
30.08.99**Names and affiliations of applicants (* indicates experimentalists):**

Prof. Dr. J. Bøttiger*, Dr. P. Kringhøj*
Dept. Physics and Astronomy
University of Aarhus
Ny Munkegade
DK - 8000 Aarhus

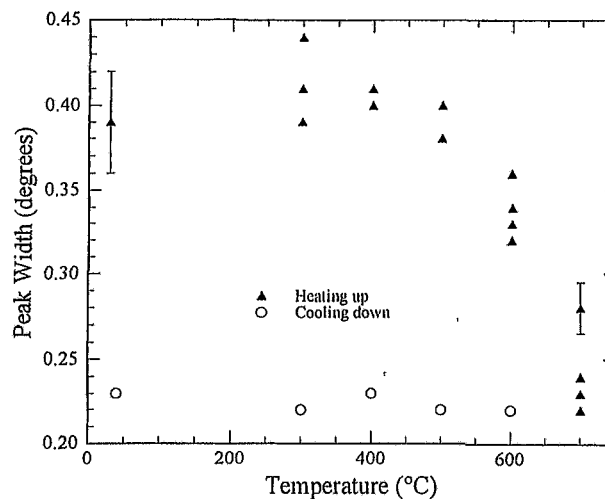
Report:

To get information on the high-temperature mechanical properties of magnetron-sputtered CrN hard coatings, the defect annealing and corresponding stress relaxation of the coatings were studied in the temperature interval from room temperature to 750 °C.

During *in-situ* X-ray diffraction experiments, the positions (planar distances) and widths (connected to inhomogeneous strain, i.e. defects) of two selected diffraction peaks, (111) and (200), were monitored as a function of time for various temperatures for two films with thicknesses of approximate 0.6 and 1.1 μm .

Some of the results are illustrated in the figure, where the width of the (111) peak of the thick sample is shown as a function of the annealing temperature. The triangles are data points taken as the temperature was changed in steps from the ambient temperature to the temperatures indicated. Data points lying on vertical lines reflect the change of the width with time at fixed temperatures. Defect annealing (a decrease in the width) is observed at temperatures of 500 °C and above. The circles are data points taken during the cooling-down cycle.

Further data are required for a detailed understanding of the kinetics of the process. For a characterisation of the defect structure before and after annealing, transmission-electron-microscopy studies are also required. In addition, hardness measurements have to be carried out to study the change in mechanical properties with the change in defect structure. Both electron-microscopy and hardness measurements are in progress in Aarhus.





Experiment title: Coordination sphere of the uranyl ion in solutions of perchloric and triflic acid		Experiment number: CH-618
Beamline: BM 20	Date of experiment: from: April 10, 1999 to: June 12, 1999	Date of report: August 26, 1999
Shifts: 21	Local contact(s): Dr. Tobias Reich, ROBL CRG	<i>Received at ESRF:</i>
Names and affiliations of applicants (* indicates experimentalists): Rémi Barillon, Isabelle Billard*, Jean-Marc Jung, Klaus Lützenkirchen*, Isabelle Rossini*, Laurent Sémon* Institut de Recherches Subatomiques Chimie Nucléaire F-67037 STRASBOURG Cedex 2		

Report (preliminary):

Highly acidic uranium(VI) solutions play an important role in the spent nuclear fuel cycle. In this context, the interaction of uranyl ions (UO_2^{2+}) with perchloric (HClO_4) and triflic acid ($\text{CF}_3\text{SO}_3\text{H}$) have previously been studied [1] with laser fluorescence spectroscopy. The fluorescence life times of uranium were found to generally increase with acidity. The effect is related to the number of H_3O^+ ions, but it remains largely unexplained on a molecular level. The aim of the present investigations is to determine the coordination sphere of uranyl ions in solutions of up to 12 M perchloric and 10 M triflic acid by extended X-ray absorption fine structure spectroscopy (EXAFS).

Uranium L_{III} -edge EXAFS spectra were measured in transmission mode at the Rossendorf beam line (ROBL) of the ESRF using a Si(111) double-crystal monochromator. The EXAFS spectra were analyzed according to standard procedures using the program EXAFSPAK and theoretical scattering phases and amplitudes calculated with the scattering code FEFF [2]. For the perchlorate solutions, uranium is found to be coordinated with two axial oxygen atoms (O_{ax} , at a distance $R=1.76 \text{ \AA}$) and a single shell of 4.8 ± 0.3 equatorial oxygen atoms (O_{eq} , at $R=2.41 \text{ \AA}$). No chlorine scattering contribution is observed at room temperature

EXAFS measurements. We conclude that UO_2^{2+} is coordinated with five water molecules and that the electrostatic interaction with the ClO_4^- ions takes place over longer distances. This is consistent with an EXAFS measurement of solid $\text{UO}_2(\text{ClO}_4)_2$, where chlorine scattering could neither be observed. Crystal structure data of this compound [3] show that the perchlorate tetrahedra are separated from uranium at U-Cl distances of $5.40 - 6.17 \text{ \AA}$. In the case of triflic acid uranium is again found to be coordinated with two O_{ax} and five O_{eq} atoms (four O_{eq} atoms for a concentration of 10 M). In addition, a contribution by sulphur atoms to the EXAFS signal was observed for acid concentrations larger than 6 M (Fig. 1). The U-S distance was determined as 3.59 \AA . The measured distances indicate that the triflate group is coordinated with uranium via one of its oxygen atoms in a monodentate fashion. The number of coordinated sulphur atoms could not yet be determined to better than 2 ± 1 . Additional information will be obtained from an X-ray diffraction measurement of solid $\text{UO}_2(\text{CF}_3\text{SO}_3)_2$.

At the highest acid concentration (10 M) uranium is coordinated with only four O_{eq} . One possible explanation is the formation of a UO_2^{2+} complex with four triflate ions and no water molecule for steric reasons. Again, more precise information on the number of coordinated sulphur atoms will help to elucidate this question. The coordination change at 10 M concentration is paralleled by a sharp increase of the uranium fluorescence life time from 5 μs (8 M) to 30 μs (10 M) [1]. Hence, the drastic life time variation would be related to a change in the coordination sphere of uranium.

[1] M. Bouby, I. Billard, A. Bonnenfant, G. Klein, Chem. Phys. 240 (1999) 353.

[2] S.I. Zabinsky et al, Phys. Rev. B 52 (1995) 2995.

[3] N.W. Alcock, F.F.S. Esperas, J. Chem. Soc. Dalton Trans. (1977) 893.

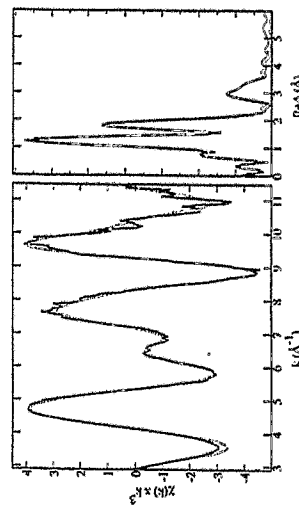


Fig. 1: k^2 -weighted uranium L_{III} -edge EXAFS spectrum (left) and its Fourier transform (right) of a 10^{-2} M U(VI) solution in 10 M triflic acid.



Experiment title: The influence of Pu local environment on the non ideality of (U,Pu)O ₂ solid solution		Experiment number: CH - 619
Beamline: BM 20	Date of experiment: from: 12/06 to 15/06 and from 07/07 to 11/07	Date of report: 30/08/1999
Shifts: 21	Local contact(s): Tobias Reich	<i>Received at ESRF:</i>
Names and affiliations of applicants (* indicates experimentalists): *RIPERT Michel CEA Cadarache DEC/SESC/LLCC Bat 315 13108 Saint Paul Lez Durance Cedex BEAUVY Michel CEA Cadarache DEC/SESC *DESGRANGES Lionel CEA Cadarache DEC/SECI/LECMI Bat 316 *PETIT Thierry CEA Cadarache DEC/SESC/LLCC Bat 315 *CARANONI Laurent CEA Cadarache DEC/SPUA *RUELLO Pascal CEA Cadarache DEC/SECI/LECMI Bat 316		

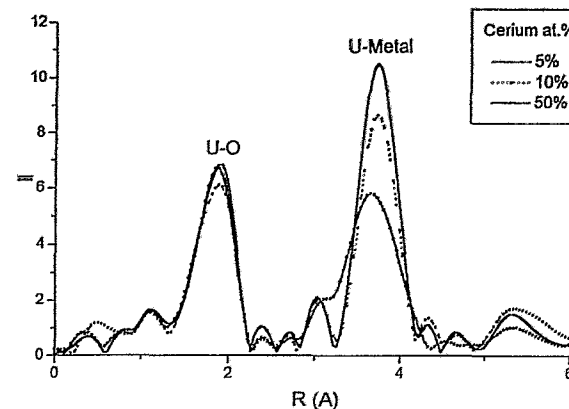
Report:

Some experimental results on unit cell parameter, electrical conductivity, specific heat and thermal conductivity show that (U,Pu)O₂ is not an ideal solid solution. M. Beauvy [1] notes that these anomalies occur when Pu concentration is around 3.1 and 12.5 at%. They respectively correspond to one Pu atom for 8 unit cells and one Pu atom for 2 unit cells. He supposed that these thresholds could correspond to different Pu local environments in UO₂ matrix.

Our aim was to see if Pu local environment is connected with Pu concentration in (U,Pu)O_{2+x} matrix. In other words, we wanted to check if any modification occurs when Pu content varies. However, because of the limitation in plutonium isotopes accepted on the beam line, we studied (U,Ce)O_{2+x} instead of (U,Pu)O_{2+x}. (U,Ce)O_{2+x} system is expected to show many similarities to (U,Pu)O_{2+x}, cerium is known to be a non active analogue of plutonium [2].

We thus used the 21 shifts allowed by the Review Committee to collect the EXAFS spectra of 5 (U,Ce)O_{2+x} pellets (with Ce amount of 0, 5, 10, 25 and 50 at%) in fluorescence detection mode.

In order to both probe U and Ce local environment, we worked at U L_{III} and Ce L_I edges (17.17 and 6.55 keV respectively). The following figure shows the Fourier transform moduli obtained at U L_{III} edge for the different cerium concentration.



Due to the high concentration of U and Ce, the amplitude of the XAFS spectra was corrected for self-absorption effects using the procedure of Tröger *et al.* [3]. To analyse our data we use the phase and amplitude calculated by the FEFF 7.02 program [4].

As a first result, the U-O coordination shell shows very low evolution with the amount of cerium. On the opposite, the intensity of the second peak, connected to metal-metal distances, decreases as increasing the cerium concentration.

The determination of metal-metal distance and coordination number is difficult because of the numerous multiple-scattering paths included in this contribution. Furthermore due to the nearness of the experiment we only deduced the parameters of the first coordination shell (U-O): uranium is coordinated with 8 oxygen atoms at 0.236 nm (the same as in UO₂). This first coordination shell remains the same whatever cerium concentration is.

Due to the complexity and low ratio signal over noise of the Ce L_I edge spectra, we could not have currently quantitative results on cerium environment, but work is still in progress.

References :

- [1] M. Beauvy J. Nucl. Mater. 188 (1992) 232-238.
- [2] D.J. Lones, J. Roziere, G.C. Allen and P.A. Tempest, Journal de Physique, Colloque C8, Tome 47, (1986) C8-745-C8-748.
- [3] L. Tröger, D. Arvanitis and K. Baberschke Phys.Rev. B 46 (1992) 3283-3289.
- [4] J. J. Rehr, S. I. Zabinsky, R. C. Albers, Phys.Rev.Lett. 69 (1992) 3397.



Experiment title: Local internal strains and stresses in coarse-grained and in ultrafine-grained nickel due to cyclic plastic deformation.		Experiment number: HS-897
Beamline: BM20	Date of experiment: from: 01. 03. 99 to: 06. 03. 99	Date of report: 07. 07. 99
Shifts: 15	Local contact(s): Dr. Norbert Schell	<i>Received at ESRF:</i>
Names and affiliations of applicants (* indicates experimentalists): Dr. Ellen Thiele *, Dr. Jörg Bretschneider *, Dr. Cesar Justino Buque * Institute of Physical Metallurgy, Technical University Dresden D-01062 Dresden Germany		

Report:

**INFLUENCE OF THERMAL TREATMENT AND
CYCLIC PLASTIC DEFORMATION
ON THE DEFECT STRUCTURE IN ULTRAFINE-GRAINED NICKEL**

Ellen Thiele and Jörg Bretschneider

Institut für Physikalische Metallkunde, Technische Universität Dresden

Because of their unusual physical properties polycrystals with a mean grain size of some 100nm, so called ultrafine-grained (UFG) materials, are of a great interest for both, theoretical and experimental investigations. Compared with conventional polycrystals the material shows a relatively high yield stress and microhardness combined with a sufficient ductility. However, the structure is non-stable against thermal treatment. Furthermore, it is still open, how a cyclic deformation at different temperatures changes the structure, i.e. the internal strains and the distribution of the grain size and orientation. In the present paper we intend to describe quantitatively the structure changes induced by thermal treatment and cyclic deformation.

In order to produce ultrafine-grained nickel, billets of 99.992% purity were prepared by equichannel angular pressing (EAP)¹. The thermal treatment experiments were carried out at different annealing temperatures on small blocks of the as produced UFG material. For the fatigue experiments samples with a rectangular cross section and with a loading axis parallel to EAP die axis were cut from the billets. The samples were cyclically deformed at room temperature and at 160°C at constant plastic strain amplitudes.

At room temperature deformation the stress amplitude didn't change significantly with the cycle number until macrocracks appeared. The mean stress always had a positive sign and decreased during cycling. As expected, the stress amplitude decreased with increasing deformation temperature.

The grain structure was observed using the orientation contrast in a scanning electron microscope. Recrystallization occurred even at temperatures significantly lower than that, usually required for recrystallization after cold rolling. The cyclic plastic deformation induced a slight grain coarsening already at room temperature.

To characterize the defect structure in the original UFG material as well as after thermal treatment and after fatigue, measurements of X-ray diffraction profiles were performed at the synchrotron radiation beamline ROBL of the Forschungszentrum Rossendorf at the European Synchrotron Facility in Grenoble². Diffraction profiles with a negligible instrumental broadening were measured for different {hkl}-types of lattices planes parallel to the sample surfaces. Using the Williamson-Hall and the Krivoglaз-Wilkens plots, the size of coherently scattering regions, the root mean square strain and the dislocation density were calculated from the profile shape. These parameters depend in a characteristic way on the deformation and annealing state of the samples.

Finally, conclusions were drawn concerning threshold values of the deformation temperature and of the deformation amplitude for the thermal and mechanical stability of the ultrafine grain structure.

¹The samples were delivered by the Advanced Materials and Technologies Foundation, St. Petersburg.

²The authors are obliged to N. Schell and C. Buque for their assistance in the synchrotron investigations at the ESRF. The invitation and financial support of the ESRF for the experiment HS-897 are also acknowledged.